PHYSICAL MODEL SIMULATIONS OF

SUPER-CRITICAL SUBSIDENCE

Chanodom Lertsuriyakul

A Thesis Submitted in Partial Fulfillment of the Requirements for the

Degree of Doctor of Philosophy of Engineering in Civil,

Transportation and Geo-resource Engineering

Suranaree University of Technology

Academic Year 2020
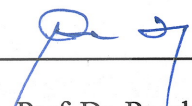
การจำลองเชิงกายภาพสำหรับการทรุดตัวที่เกินกว่าจุดวิกฤต

นายชโนดม เลิศสุริยะกุล

PHYSICAL MODEL SIMULATIONS OF

SUPER-CRITICAL SUBSIDENCE

Suranaree University of Technology has approved this thesis submitted in partial fulfillment of the requirements for the Degree of Doctor of Philosophy.

Thesis Examining Committee
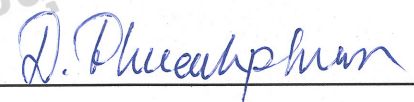
_____

(Assoc. Prof. Dr. Pornkasem Jongpradist)

Chairperson

_____

(Prof. Dr. Kittitep Fuenkajorn)
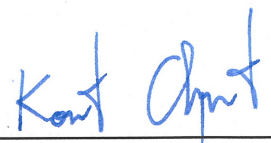
Member (Thesis Advisor)

_____

(Asst. Prof. Dr. Prachya Tepnarong)

Member (Thesis Advisor)

_____

(Asst. Prof. Dr. Decho Phueakphum)

Member

_____ _____

(Assoc. Prof. Flt. Lt. Dr. Kontorn Chamniprasart) (Assoc. Prof. Dr. Pornsiri Jongkol)

Vice Rector for Academic Affairs Dean of Institute of Engineering

and Internationalization

ชโนดม เลิศสุริยะกุล : การจำลองเชิงกายภาพสำหรับการทรุดตัวที่เกินกว่าจุดวิกฤต
(PHYSICAL MODEL SIMULATIONS OF SUPER-CRITICAL SUBSIDENCE)
อาจารย์ที่ปรึกษา : ศาสตราจารย์ ดร.กิตติเทพ เฟื่องขจร, 85 หน้า.

วัตถุประสงค์ของการศึกษาคือเพื่อจำลองการทรุดตัวของผิวดินที่เกิดจากโพรงเกลือระดับตื้น
ภายใต้สภาวะที่เกินกว่าจุดวิกฤตโดยใช้เครื่องจำลองการทรุดตัวเชิงกายภาพ การทดสอบได้ทำการผัน
แปรความกว้างและความสูงของโพรง เม็ดพลาสติก ABS ถูกใช้เพื่อจำลองอนุภาคเม็ดดินในชั้นดินปิด
ทับเหนือโพรง ผลการทดสอบแสดงให้เห็นว่ากรณีที่โพรงอยู่ในระดับตื้นการทรุดตัวสูงสุดจะเพิ่มขึ้นเมื่อ
ความสูงและความกว้างของโพรงเพิ่มขึ้น การทรุดตัวไม่อ่อนไหวต่อความสูงของโพรงสำหรับโพรงที่
แคบระดับลึกเมื่ออัตราส่วนของความลึกต่อความกว้างของโพรงเท่ากับ 7 ความกว้างของร่องการทรุดตัว
เพิ่มขึ้นตามความกว้างและความลึกของโพรง ผลการทดสอบจากแบบจำลองทางกายภาพให้ผล
สอดคล้องเป็นอย่างดีกับผลจากการจำลองโดยโปรแกรม PFC ผลกระทบของมุมเสียดทานของชั้นดินปิด
ทับต่อลักษณะของการทรุดตัวได้ถูกหาด้วยแบบจำลองทางคอมพิวเตอร์ ผลลัพธ์ระบุว่าขนาดของการ
ทรุดตัวจะลดลงเมื่อมุมเสียดทานเพิ่มขึ้น อย่างไรก็ตามความกว้างของร่องการทรุดตัวไม่อ่อนไหวต่อการ
เปลี่ยนแปลงของมุมเสียดทาน

สาขาวิชา เทคโนโลยีธรณี   ลายมือชื่อนักศึกษา _____
ปีการศึกษา 2563   ลายมือชื่ออาจารย์ที่ปรึกษา _____

CHANODOM LERTSURIYAKUL : PHYSICAL MODEL SIMULATIONS OF
SUPER-CRITICAL SUBSIDENCE. THESIS ADVISOR : PROF. KITTITEP
FUENKAJORN, Ph.D., P.E., 85 PP.

SUBSIDENCE TROUGH/ PFC MODEL/ FRICTION ANGLE/ ABS BALL/ CAVITY

The objective of this study is to simulate the surface subsidence induced by shallow salt cavities under super-critical condition using a trapdoor apparatus. Various widths and height of the cavities are assigned. ABS plastic balls are used to simulate soil particles in the overburden above the cavities. Results indicate that for shallow cavities, the maximum subsidence increases with increasing cavity height and width. The subsidence is insensitive to cavity height for narrows cavities at great depth when cavity depth and width ratio is 7. The subsidence trough width increases with cavity width and depth. The physical model results agree reasonably well with the PFC simulation results. The effects of overburden friction angles on the subsidence characteristics are determined by the computer simulations. The results suggest that the magnitude of subsidence decreases as the friction angle increases. The subsidence trough width is however insensitive to the changes of the friction angle.

School of Geotechnology   Student's Signature

Academic Year 2020   Advisor's Signature
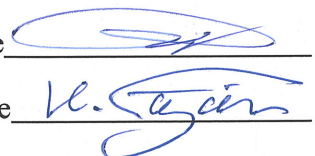
ACKNOWLEDGMENTS

I would like to express my sincere thanks to Prof. Dr. Kittitep Fuenkajorn for his valuable guidance and gave a critical review of this study. I appreciate his strong support, encouragement, suggestions, and comments during the research period. Many thanks to Assoc. Prof. Dr. Pornkasem Jongpradist, Asst. Prof. Dr. Decho Phueakphum, Asst. Prof. Dr. Prachya Tepnarong, and Asst. Prof. Dr. Akkhapun Wannakomol for their constructive advice, valuable suggestions, and comments on my study. Grateful thanks are given to all staffs of Geomechanics Research Unit, Institute of Engineering who supported my work.

Finally, I would like to thank my beloved parents for their love, support and encouragement.

Chanodom Lertsuriyakul

TABLE OF CONTENTS

Page

TABLE OF CONTENTS (Continued)

TABLE OF CONTENTS (Continued)

LIST OF TABLES

LIST OF FIGURES

LIST OF FIGURES (Continued)

LIST OF FIGURES (Continued)

LIST OF FIGURES (Continued)

LIST OF FIGURES (Continued)

SYMBOLS AND ABBREVIATIONS

α	=	Empirical constant
β	=	Empirical constant
γ	=	Empirical constant (for equation 5.8)
γ	=	Angle of draw
δ	=	Empirical constant
η	=	Empirical constant
κ	=	Empirical constant
λ	=	Empirical constant
ν	=	Empirical constant
ϕ	=	Friction angle
A	=	Empirical constant
ABS	=	Acrylonitrile butadiene styrene plastic
B	=	Empirical constant (for equation 5.6 and 5.8)
B	=	Width of trough
B_e	=	Equivalent trough width
B_s	=	Particle size
C	=	Empirical constant
D	=	Empirical constant
c	=	Cohesion
H	=	Opening height
H_e	=	Equivalent opening height

SYMBOLS AND ABBREVIATIONS (Continued)

K_n =   Normal stiffness

K_s =   Joint shear stiffness

L =   Length of

S_e =   Equivalent maximum subsidence

S_{max} =   Maximum magnitude of subsidence

W =   Opening width

W_e =   Equivalent cavity width

Z =   Overburden thickness

Z_e =   Equivalent cavity depth (or Equivalent overburden thickness)

CHAPTER I

INTRODUCTION

1.1　Background and rationale

Surface subsidence and sinkholes in the northeast of Thailand have long been problematic issues relevant to environmental impacts to farmland, agricultural areas, groundwater, and infrastructures. One of the primary causes has involved traditional salt production by using brine pumping technique. Saline groundwater is pumped through shallow boreholes (60-80 m) drilled directly on top of salt bed. The brine is left evaporate on ground surface. Through several years this practice has created cavities at the interface between topsoil and the underlying salt bed. Location and size of these cavities are often unpredictable. During dry season, the groundwater level is lower, and hence the cavities lose internal hydraulic pressure. This leads to the collapse of cavity roof. The failure propagates upward though the topsoil. Once the failure reaches the ground surface settlement will occur usually in the forms of surface subsidence. Large, tall and shallow cavities could induce sinkholes or pothole on the surface.

Several investigations have been made to correlate the subsidence configurations with the size and shape of cavity underneath. Numerical simulations are usually accomplished with scaled-down or physical modeling in an attempt to develop some mathematical relationships between these two phenomena. Results from the two approaches are compared to verify the correctness of the model prediction. One of the problems arises which involve the selection of materials used to simulate the behavior of the topsoil above the cavity. Sand, silt and gravel have long been selected for the physical model simulation. Due to the intrinsic variability of these natural materials in terms of

particle shape, size, uniformity and mechanical property consistency, discrepancies between the physical and numerical model results are commonly detected.

1.2   Research objectives

The objectives of this research are to develop the mathematical relationship between the subsidence components and characteristics of underground openings. ABS ball mass is used to simulate the overburden soil. The testing results are compared with those of the numerical simulation. The relation can be used as a predictive tool to determine the geometries of cavities from the corresponding subsidence components induced by the brine pumping.

1.3   Scope and limitations

The scope and limitations of the research include as follows.

1) Physical model testing in laboratory is performed by the trap door apparatus invented by Thongprapha et al. (2015).

2) Subsidence of the model is induced by real gravitational force.

3) Spherical acrylonitrile butadiene styrene plastic (ABS) balls with 6 mm in diameter are used to simulate the overburden.

4) The overburden thickness (Z) is varied from 120 mm to 300 mm.

5) The cavity height (H) and cavity width (W) are varied from 30, 60, 90 to 120 mm.

6) Cavity length is maintained constant at 200 mm.

7) All tests are made under dry condition.

8) The physical model results are compared with numerical analysis (using PFC 3.1 program).

1.4   Research methodology

Figure 1.1 shows the study plan to accomplish the objective. The main tasks involve literature review, material preparation, physical modelling method, computer simulations are using 2-dimension Particle Flow Code (PFC^{2D}), correlation between physical and numerical simulations, formulation of mathematical relationship, discussions and conclusions.
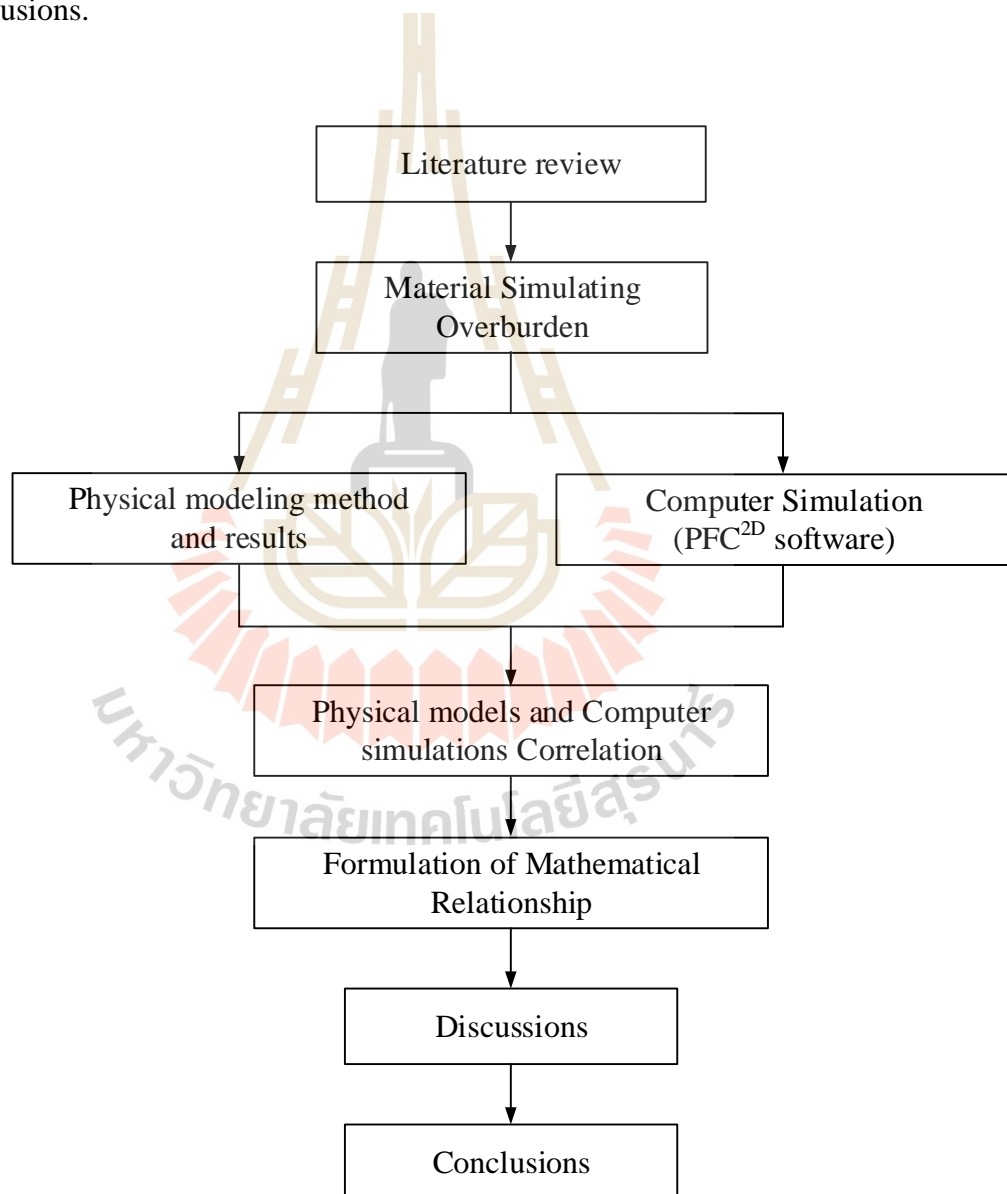
Figure 1.1 Research Methodology.

1.4.1 Literature review

Literature review is performed to study research on subsidence in northeastern region of Thailand, sources of information are from journals, reports, conference papers and books. A summary of literature reviews is given in this study.

1.4.2 Material simulating overburden

ABS balls with 6 mm are selected as the overburden material in the physical model. The material is subjected to two tests: bulk density test and direct shear test.

1.4.3 Physical modeling methods and results

A test frame for physical model developed by Thongprapha et al. (2015) is used to perform ground movement of overburden in two-dimension. The laboratory testing gives maximum surface subsidence (S_{max}) and width of subsidence trough under different cavity geometries. The model testing is simulated for the cavity width (W) from 30 mm to 120 mm with and increment of 30 mm. The cavity length (L) is 200 mm all cases. The cavity height (H) is from 30 mm to 120 mm, with 30 mm increment. In this study, overburden thickness (Z) is varied from 120 mm to 300 mm. A laser scanner is used to measure surface profile of the ABS ball mass before and after the subsidence is induced under each set of variables.

1.4.4 Computer simulations

The physical model testing in this study is to assess the effects of the cavity geometry and depth on the surface subsidence. PFC^{2D} can simulate the movement and interaction of circular particles. The mechanical and physical properties of the ABS ball and the cavity geometries are correlated with the overburden and geometry of actual mines in Maha Sarakham formation. The cavity width and height are simulated from 30, 60, 90 to 120 mm. The overburden thickness or depth is varied from 120, 150, 180, 210, 240, 270 to 300 mm.

1.4.5 Correlation between physical and computer simulations

Results obtained from physical model in laboratory tests is used to correlate with the computer simulation from the Particles Flow in 2 dimensions code. The material properties used in the computer simulations are same with those of the physical model.

1.4.6 Formulation of mathematical relationships

The results from the simulations are used to develop mathematic relationships between the maximum surface subsidence (S_{max}) and width of trough (B) and overburden thickness (Z). Such relationships are later used to predict cavern configuration (cavern size, opening width, opening height and depth).

1.4.7 Discussions and conclusions

Discussions are on the reliability and adequacies of the approaches used here. All research activities, methods, and results are documented and complied in the thesis. The findings are published in the journals.

1.5 Thesis contents

This research thesis is divided into six chapters. **Chapter I** explains the objectives, problems and rationale, and methodology or thesis. **Chapter II** includes background and rationale, research objectives, scope and limitations and research methodology. **Chapter III** presents results of the literature review to improve an understanding of surface subsidence knowledge. **Chapter III** describes materials simulating overburden and physical model simulations. Computer Simulations by PFC^{2D} software and comparison between the results obtained from physical model computer simulation are described in **Chapter IV**. **Chapter V** describes formulation and mathematical relationships. **Chapter VI** presents discussions, conclusions, and recommendation for future studies.

CHAPTER II

LITERATURE REVIEW

2.1   Introduction

In this chapter the relevant research and information about previous studies related to surface subsidence due to man-induced process are received. These include the effects of underground opening geometries and overburden properties on surface subsidence, surface subsidence prediction, physical modeling, empirical subsidence calculation and numerical simulations. The review results are summarized below.

2.2   Subsidence (Sinkholes) in Thailand

The northeastern Thailand is in the Khorat Plateau and separated to the northern Sakhon Nakhon Basin and the southern Khorat Basin. Two basins contain claystone and rock salt layers of Maha Sarakham Formation. Under the Khorat Plateau is consist with mudstone, shale, siltstone, sandstone and conglomerate, these sediments have been continuously deposited by wind and sand. under a semi-arid to arid climate. A hundred of meters salt beds thick were left behind after the seawater transgression dried out by the aridity at the end of the Era. The salt layer was deposited with very fine-grained overburden by wind and water transportation. Under huge overburden pressure, the rock salt mass flows raise up through the fractured cap rocks in the upper layer to form salt domes as a plastic body. The rock salt underneath subsurface in the Sakon Nakhon Basin has an area approximately 20,323 km^2, covering the area of Udon Thani, Nong Khai, Sakon Nakhon, Mukdahan, Nakhon Phanom, and some part of Laos, and the Khorat Basin has an area about 25,620 km^2, covering the province of Khon Kaen, Nakhon Ratchasima,

Chaiyaphum, Kalasin, Roi Et, Maha Sarakham, Ubon Ratchathani, Burirum, Yasothon, Sisaket and Surin (Satarugsa et al., 2005). Warren (1999) gives detailed explanation of geology and salt basins. Figure 2.1a. shows the geological sequence of the Maha Sarakham formation.

Solar salt production representing old fashioned technique (brine pumping) is practiced in the Khorat and Sakhon Nakhon Basin. This technique has been widely performed at the end of both basins boundary where well depth is about 60 to 100 meters. (Figure. 2.1b and 2.1c). Boreholes are drilled through the topsoil directly into above the layer of salt . Saline groundwater (brine) is brought over the pumping well and bared on land field for evaporation. The contact of a salt bed with flowing water or unsaturated brine produces cavities in the salt through the leaching of soluble minerals. This process is simple and inexpensive however it has caused an environment impact in the forms of unpredictable surface contamination, ground movement and sinkholes (Wannakao et al. 2005) . The subsidence trough and sinkhole, or pot-hole can be caused by brine pumping (Lokhande et al. 2014), are affected from a cavity roof collapse of the unsupported span and propagates through soil formation to the ground surface. Some of the land subsidence caused by brine pumping are shown in Figure 2.2. This always occurs during low rainfall period when the cavity roofs loss the brine saturated groundwater support. Several methods have often been used to estimate the geometry and shape of the cavities to minimizes the harmful effects to property and augmentation damages.

2.3   Theory and Criteria

Underground excavation is significantly created void causes changes in the magnitude and orientation of in-situ stress and results in deformations both in the remaining and surrounding salt.   Singh (1992) describes mine subsidence as ground

movements that arise due to the formation collapse over opening voids. Ground subsidence is the lowering or collapse of the ground surface. The problems correlated with ground subsidence have long been recognized. The early to mid‑20th century showed many developments in the understanding and prediction of subsidence, which was motivated by legal action resulting from severe damage to surface structures, communications, and agricultural resources due to underground mining. It was the defense against unjustified claims that required improved understanding of subsidence phenomena.

Subsidence engineering have three main objectives as

1) To predict ground movement.

2) To determine the effects of such movements on structures and resource.

3) To reduce damage due to land subsidence.

The creation of any subsurface opening perturbs the stress state in the surrounding material. This perturbation produces displacements and deformations of the material, the magnitudes of which depend on the degree of the stress change, the spatial extent over which it occurs, and the nature of any rock support or reinforcement. If sufficiently large, these even can cause the rock mass around an excavated section breakdown into caving (Figure 2.3). The ground movements related with such collapse and distributed onto the overburden, with the displacements and deformations occurred. Surface subsidence mainly procures both lateral and vertical movements, which are continuous (the surface deforms smoothly) and/or discontinuous processes (cracks, steps, or cavities from at the ground surface). This leads to the concepts of subcritical, critical, and supercritical conditions. Figures 2.4 to 2.6 show the coal seam under the horizontal ground surface. When coal seam portion has been extracted, ground surface subsidence is occurred. For clarity, h and m parameters (and therefore the parameters B and S_{max}) are set as constants in the figure.

The subsidence factor (a) is taken to be 1.0 then that calculated maximum surface subsidence (S_{max}) is equal to the overburden depth or thickness (m) (Hawkes, 2010).

Figure 2.4 represents a subcritical subsidence where the width of extraction area is less than 2·B, Figure 2.5 represents a critical subsidence, where the width of extraction area is equal to 2·B and Figure 2.6 represents a super-critical subsidence, where the width of extraction area is greater than 2·B. The salt layer subsidence covered by a thin layer of granular soil is different from a coal mine. It generally occurs in silt and sand areas where they are not knitted or bonded well together (Waltham et al., 2005). When the overburden loses hydraulic pressure from groundwater declining, the void cavity is created and leads to a collapse of the cavity roof. The collapse of the cavern roof touches the cavern floor that the vertical movement of the ground does not continue. Failure of the cavern roof can occur under super-critical conditions (Fuenkajorn and Archeeploha, 2010; Thongprapha et al., 2015; Saoanunt et al., 2019).
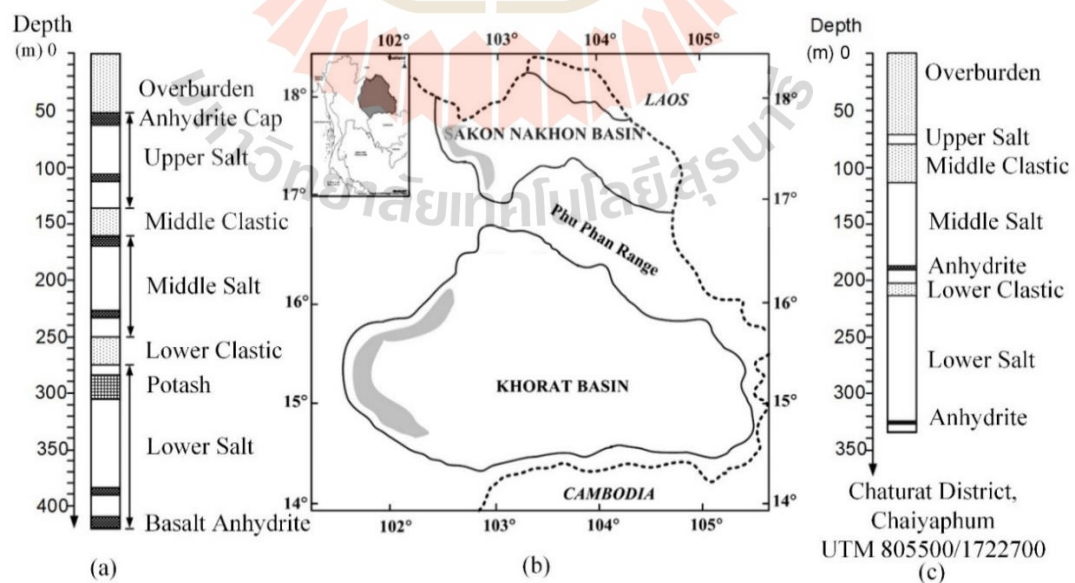
Figure 2.1 Geological borehole of Khorat basin (a), Saline pumping area has been practiced (b), and borehole logging nearby the end of basin boundary (c). (Saoanunt et al., 2019)

Figure 2.2 Brine pumping operation cause the sinkhole in Sakon Nakhon basin

(Wannakao et al., 2005).
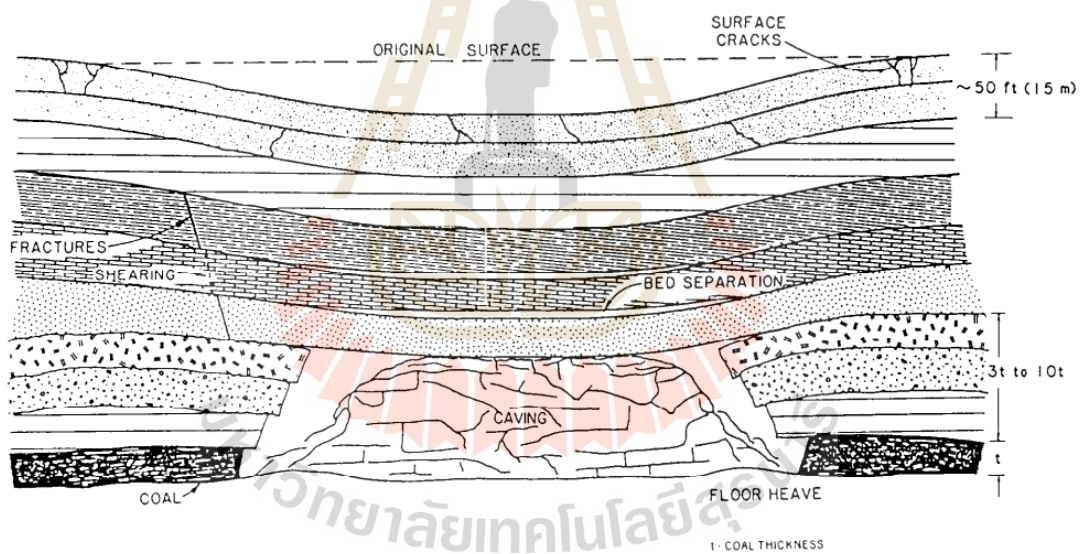
Figure 2.3 Mining subsidence and strata disturbance (Singh and Kendorski, 1981).

Figure 2.4 Sub-critical extraction (Hawkes, 2010).

Figure 2.5 Critical extraction (Hawkes, 2010).
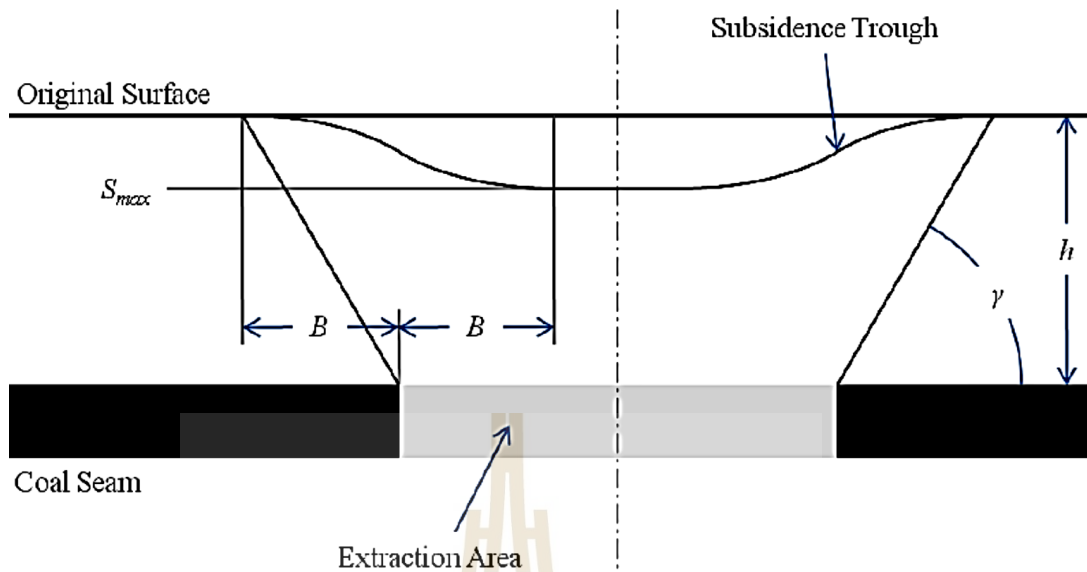
Figure 2.6 Super-critical extraction (Hawkes, 2010).

2.4   The estimation of subsidence

Subsidence predictions from several researchers (Nieland, 1991; Asadi et al., 2005). Many techniques have been presented for estimating the surface subsidence induced by underground mining, such as physical models, empirical methods, analytical methods, and numerical modeling. (Terzaghi, 1936; Adachi et al., 2003; Thongprapha et al., 2015; Ghabraie et al., 2015).

2.4.1   Physical models

Physical modeling is performed to study the behavior of prototypes. Most physical model tests are established at much smaller than the prototype models because the test results are expected to obtain more comfortably and avoid uncontrollable factors than the full-scale testing.

Thongprapha et al. (2015) study the effects of opening geometry on surface subsidence under super-critical conditions. Trap door device are used to operate the scaled-down 3-D testing of ground subsidence opening width (W) is maintained constant

at 5 cm.   Clean gravels are used to form represent of the overburden with the purpose of simulate a cohesionless subsidence behavior.   The influences of opening length (L) and opening height (H) are assessed by normalizing the L/W from 1 to 5 and H/W from 0.2 to 1, where W = 50 mm. The effect of overlying thickness (Z) is examined by Z/W carrying from 1, 3 and 4. It is observed that the angle of draw, the maximum subsidence, and the volume of trough are regulated by the opening arrangements (e.g., height, width, and depth of the openings)   The maximum subsidence and angle of draw increase with increasing L/W ratio and tends to approach a limit when L/W equals 3. For the same L/W ratio and H/W ratio, increasing the Z/W ratio reduces the angle of draw and maximum subsidence. The volume of subsidence trough noted from the physical model is regularly lower than the opening volume (Figure 2.7). The subsidence trough volume tends to decrease with opening depth increasing. The finding can be used to evaluate the subsidence profile for void cavity under soft surface and fractured rock mass by various geometry of void opening.
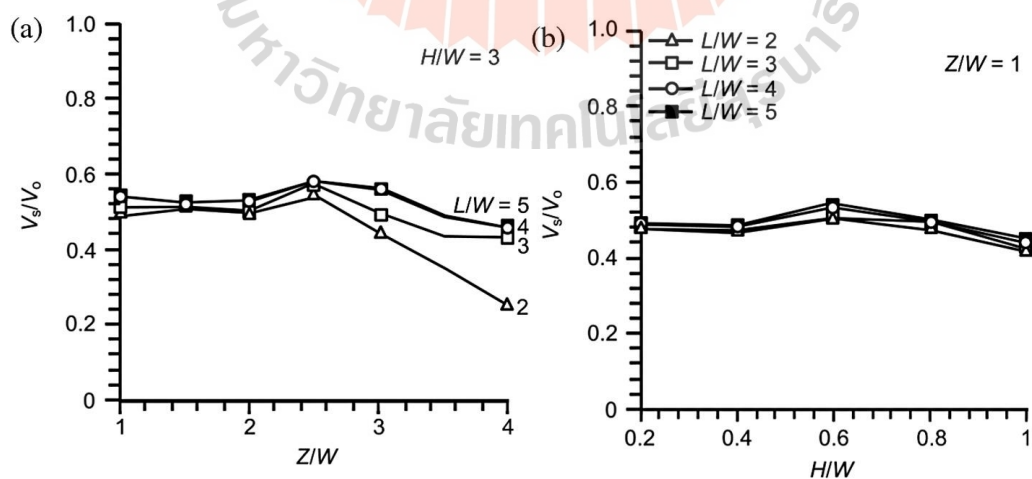
Figure 2.7   Relationship between surface trough volume-to-opening volume (V_s/V_o) and opening depth ratio Z/W (a) and opening height ratio H/W (b) (Thongprapha et al., 2015).

Sartkaew and Fuenkajorn (2019) perform physical models to verify and testify the accuracy of the hyperbolic, trigonometric and exponential profile functions that have been mainly using determine the ground subsidence in sub-critical to critical situation induced by salt or soluble underground mining. The physical models use synthetic paraffin gel to represent the overburden. A modified trap door device (Thongprapha et al., 2015) is performed to demonstrate the ground surface movement and to evaluate the consequence of mining geometry and mining depth . Figure 2.7 illustrates the trap door apparatus for physical simulation. The opening widths (W) are varied from 100 mm to 250 mm. The overburden thickness (Z) is varied from 40 to 100 mm. The opening height and length are 10 and 200 mm. The results from both methods show that the angle of draw (γ) increases with increasing opening width. For each depth when the opening becomes wider the maximum subsidence increases more rapidly. The angle of draw is more sensitive to W than Z. For sub-critical to critical situation, application of the hyperbolic function would be most suitable for estimation the surface subsidence size and curvature.
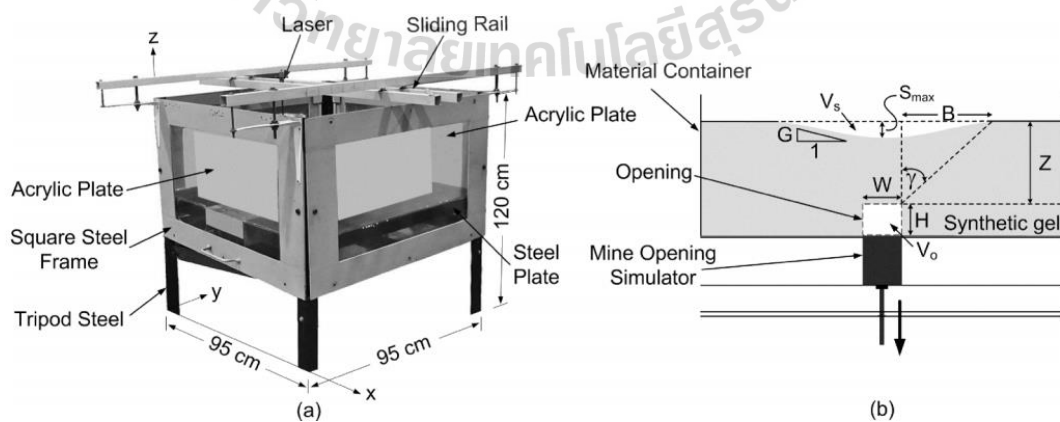
Figure 2.8 (a) Detail of trap door device testing (Sartkaew and Fuenkajorn 2019)

(b) Mine opening is simulated by plastic blocks.

Saoanunt and Fuenkajorn (2015) present the effects of the mining sequences, overburden slope and excavation rates on super critical subsidence by using trap door apparatus. They find that the angle of draw and S_{max}/H ratios decrease with increasing Z/H ratios when the mining height (H) is maintained constant at 50 mm and the mining depth (Z) varies from 50 mm to 200 mm. To mining sequence from the center of panel gives the lowest angle of draw and highest settlements while excavation from the edge to center of panel is causing the highest angle of draw and the lowest subsidence. Under various overburden slopes, the angle of draw on up slope and down slope increases with increasing slope angles. The S_{max}/H ratios decrease with increasing Z/H ratios and slope angles. The results can be used to estimate the surface profile for various underground excavation methods as affected by excavation sequence, overburden slope and extraction rate in a heavily fractured rock mass.

Meguid et al. (2008) review a variety of soft ground tunneling technology in physical model testing. The model is an essential part of the analysis and design of tunnels. Physical models can procure data that can verify and calibrate numerical models. Several researchers around the world have developed and implemented a variety of techniques to simulate the tunnel excavation process. Small-scale physical tests under 1g model provide full control over the excavation method. However, they unutilized basic properties from field stress interaction. The development of centrifuge modeling made a simulation of in-situ stresses condition more realistic, but the tunnel excavation procedure needs to no longer be complicated. Several applications have been developed to simulate the procedure of tunnel excavation in unconsolidated ground. Soil arching around excavated tunnels has been efficiently simulated applying by trap door apparatus. Both of 2-D and 3-D conditions, vertical stresses such as surface settlement can be recognized after a trap door mechanism is pulled down. The tunnel face stability can be determined using rigid

tube represent excavated tunnel line and removal/flexible face (rubber, membrane, air bag) in excavated zone. Tunnel excavation is simulated by monitoring a soil movement and reducing pressure inside ductile fabric. Different methods such as the dissolvable polystyrene stud show some success, but the tunnel excavation caused ground subsidence is non-uniform. Furthermore, the excavation under saturated condition indicate test results are dissatisfied. Mechanical augering techniques to perform ground response to tunnel excavation and state-of-the-art make the test result closer a realistic but automated test 1g physical models come at a high cost.

Saoanunt et al. (2019) present a study for prediction of shallow salt cavity geometry from surface subsidence configurations by obtaining the physical model test using trap door apparatus. Clean uniform sand dropped into test box without compaction to represent the overburden material. The physical model supposes the use of Mohr-Coulomb failure criteria with sand properties of bulk-density, cohesion and friction angle. They are varied width and hight of cavity or overburdence thickness caused settlement using 3-D laser scanner. For super-critical condition, the test results show that the increase of maximum subsidence closely relates to cavity height increasing, while the increase of trough widths is correlated to the increase of cavity width. The maximum subsidence values is not depend on overburden thickness. The trough width however is more sensitive to the overburden thickness. The test results are plotted to empirical equations which can be used as a predictive tool to estimate width and hight of shallow cavity.

Asadi et al. (2005) suggest a new profile function for subsidence analysis. It is formed from the sum of two exponential functions that have been modified to three survey lines in the case study in the Negin coalmine, east of Iran. Because of simplicity of profile function, the using new model reduces the calculation time for predicting the land

surface subsidence and improves the precision of subsidence prediction. The results obtained from ground movement measurements at Negin coalmine show a good correlation between the predicted and measured the ground subsidence by using the new model. The coefficient of correlation is 0.99, that is extremely high. In the empirical relationships, different tables and graphs are given for different geometrical shapes and conditions. It is possible to predict amount of the subsidence using these tables and graphs. The National Coal Board (NCB) has recommended one of the most well-known graphs for the prediction of surface subsidence (Figure 2.9). By clear monitoring and processing of data, the amount of ground surface movement in a real condition is calculated. The example of the physical model, as shown in Figure 2.10. In numerical model methods, subsidence and movements of ground surface can be calculated by using boundary elements, finite elements, finite difference, and distinct elements methods. Computer application for solved complex of equations in differing initial and boundary conditions with different material behavior made the numerical model methods more popular in the surface subsidence prediction. Other program has been developed to consider anisotropic and inhomogeneous behavior of rock mass worldwide.
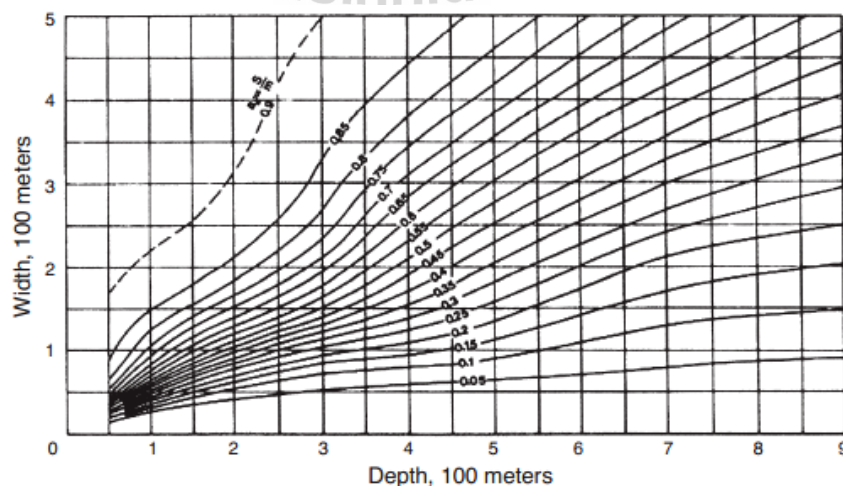
Figure 2.9 Graph suggested by NCB (Asadi et al., 2005).
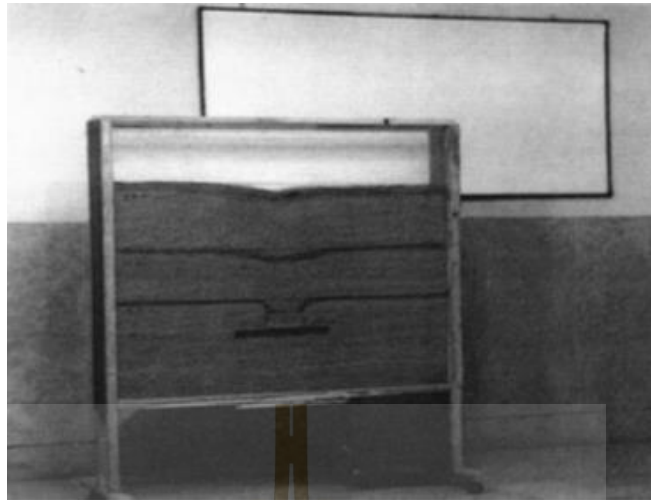
Figure 2.10 A physical model for prediction of subsidence (Asadi et al., 2005).

Caudron et al. (2006) developed a physical small-scale model and Schneebeli steel rods to present case study and define it with contained set of parameters. They study interaction of soil in a sinkhole spectacle using cohesionless material and analog 2D physical apparatus (Figure 2.11) Particle image velocimetry (PIV) and digital image correlation (DIC) is used to observe the material movement. Three sizes of steel rods are collected to represent the different cohesive frictional properties. The results are compared with previous empirical formula and numerical simulation. The results between subsidence curve of physical model and previous empirical formula are significantly close.

Park and Li (2004) conclude that surface movement cause damage, deterioration and failure of infrastructures, building, underground utility lines, dams, etc., resulting in environmental hazards and severe economic loss. The principal cause of subsidence is underground mining. In order to prevent or minimize damage due to subsidence, understanding to subsidence phenomenon is important. It is difficult to predict or model subsidence evolution because of the complication in physical simulation for instance yield behavior and rock failure, time dependent behavior and geometry differentiation. In this study a new physical simulation method is represent. The method

utilizes laser optical triangulation distance measurement devices, which can measure the surface of various material, including viscous materials or granular, and digitally measure vertical distances with a high resolution and extreme accuracy. With this new technique, the effect of material parameters, shape, size and cavity depth can be explored. Using this method of analysis and unique technology, significant results are produced. Subsidence factors, angles of draw, and subsidence profiles are analyzed. This research is being continued using the same technique for modelling subsidence with different simulate materials for various cavity geometry phenomena, and underground tunneling.
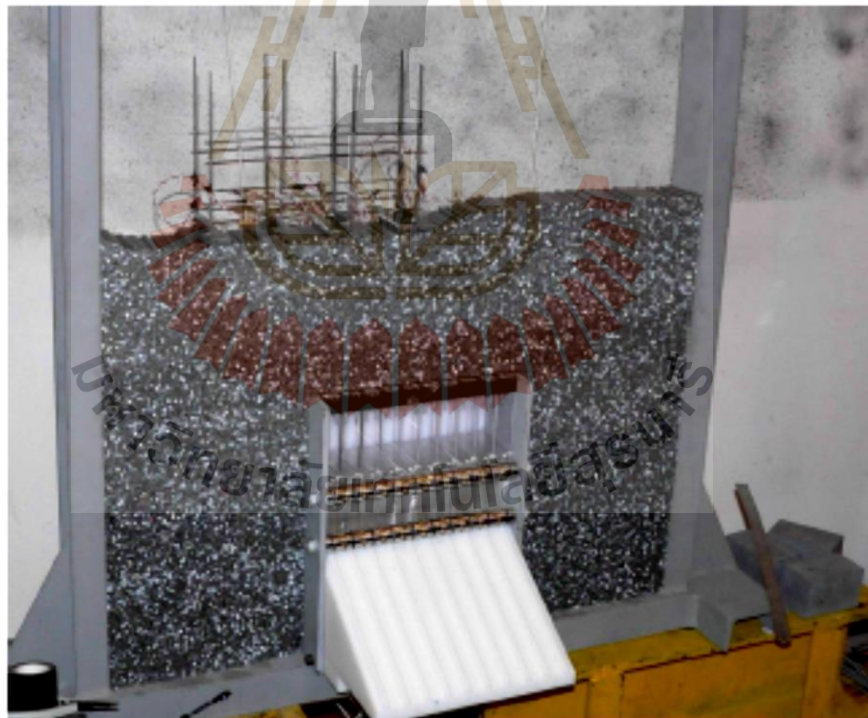
Figure 2.11 Small-scale experimental model (Caudron et al., 2006).

2.4.2 Empirical methods

Empirical method offers uncomplicated calculation, and thus has widely been used in workable applications. The most common and generally used empirical method in engineering work caused by underground tunnel is the Peck's formula (Peck, 1969) (Equation 2.1). preliminary equation is useful for investigate and first concept to determine surface settlement. The formula is as follows:

$$S_v(y) = S_{v\,max} \cdot e^{\frac{-y^2}{2i^2}} \qquad (2.1)$$

where $S_v(y)$ is the surface settlement.

$S_{v\,max}$ is the maximum settlement above tunnel axis.

i is the horizontal distance from the tunnel axis to the point of inflection of the settlement trough.

y is the horizontal distance from the tunnel axis.

Peck (1969) describe the shape of subsidence examples for more than 20 cases by the Gaussian curve, shown in Figure 2.12. The researcher presents equation to find shape of trough using subsidence maximum (S_{max}), distance from middle of opening (x) and width of trough (i).

$$i = k \cdot Z_0 \qquad (2.2)$$

Several researchers are employed actual surveying investigation and tests regarding evaluating i. The prediction of i values is based on various studies. The evaluation of maximum settlement can be done by Equation 2.3 (Mair, 1993), where V_L is ground loss (ratio of ground loss volume/tunnel volume per meter length) and D is the diameter of tunnel.

$$S_{max} = \frac{0.313 V_L \cdot D^2}{i} \qquad (2.3)$$
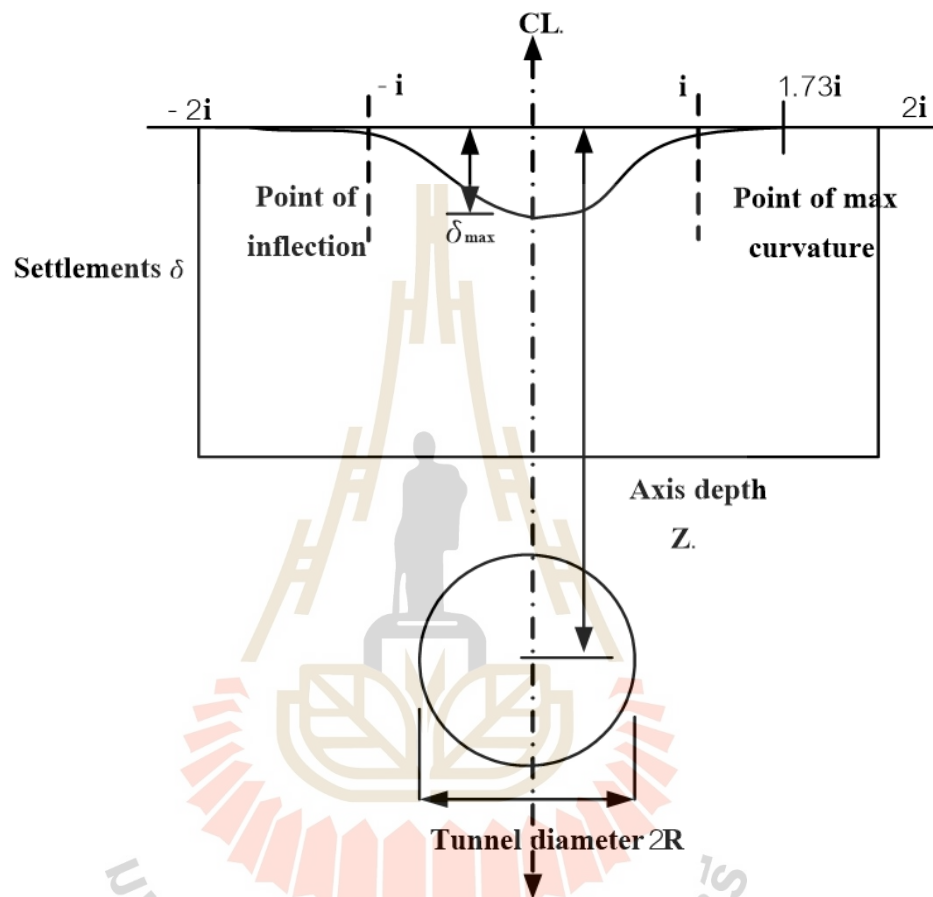
Figure 2.12 Properties of error function curve to represent cross-section settlement trough

above tunnel (Peck 1969).

McCay et al. (2018) present a new method to estimate maximum subsidence from coal mining. Pooling and meta-analysis which widely used in the medical research are adapted in this study. More than 70 publications with subsidence data from different region are required. Main factors that determine in this study consist of maximum subsidence (S_{max}), width of void (W) and depth of void (D). They develop and analyze data from those previous empirical about the relationship between S_{max} and ratio of W/D. The formula is as follows:

$$S_{max} = \left[\frac{c}{1+10^{-a\left(\frac{W}{D}\right)-b}}\right] m \tag{2.4}$$

where m is the effective void thickness. Parameters a, b and c are constant values governing a resistance of overburden. The validation of S_{max} value from empirical estimation has a good correlation with historical underground coal mine data from Australia and United Kingdom. The results indicated that maximum subsidence increase as W/D increasing. For the same void width, the shallow one will lead to more subsidence. The overburden resistance affects surface subsidence, lower resistance overburden shows more subsidence than higher one.

Many researchers (Chi et al., 2001; González and Sagaseta, 2001) revealed limited applicability of empirical solution, such as unadaptable to modify ground conditions, excavation sequence, horizontal and subsurface movements. They cannot adequately simulated excavation with tunnel support configuration. Numerical method provides better solution to overcome these problems. However, the empirical method is useful for comparing the results with the numerical method for validation purpose of a model.

2.4.3 Analytical methods

Profile functions are mathematical equations used to represent the subsidence profile at the surface along a traverse either parallel or perpendicular to the face of a longwall panel. Although they are, in effect, integration of an influence function along a particular traverse, profile functions are nonetheless selected empirically, and the controlling constants determined from subsidence observations. Provided that sufficient suitable observation data exist to allow calculation of the constants, this method can be applied to a wide range of geological conditions, and profile functions have a history of application in several countries (Hood et al., 1983). A major limitation of profile functions is that they are applicable only to simple mine geometries, such as longwall panels.

Subsidence consists of five major components: vertical movement, lateral movement, slope, vertical strain, and curvature, as follows;

Vertical movement:

$$S(x) = \frac{1}{2}S_{max}\left[1 - \tanh\left(\frac{cx}{B}\right)\right] \tag{2.5}$$

Slope (or tilt):

$$G(x) = S'(x) = -\frac{1}{2}S_{max}\frac{c}{B}\operatorname{sech}^2\left(\frac{cx}{B}\right) \tag{2.6}$$

Vertical curvature:

$$\rho(x) = S''(x) = S_{max}\frac{c^2}{B^2}\left[\operatorname{sech}^2\left(\frac{cx}{B}\right)\tanh\left(\frac{cx}{B}\right)\right] \tag{2.7}$$

Lateral movement (horizontal displacement):

$$u(x) = -\frac{1}{2} S_{max} \frac{bc}{B} \text{sech}^2 \left(\frac{cx}{B}\right) \tag{2.8}$$

Lateral strain:

$$\varepsilon(x) = S_{max} \frac{bc^2}{B^2} \left[\text{sech}^2 \left(\frac{cx}{B}\right) \tanh \left(\frac{cx}{B}\right)\right] \tag{2.9}$$

where S_{max} is the maximum subsidence,

D is the opening or cavern depth,

γ is angle of draw,

x is horizontal distance,

c is constant,

b is constant, and

B is cavern maximum area.

Fuenkajorn and Archeeploha (2010) develop an analytical method to evaluate the location, size and depth of the caverns occurred near a contact between salt layer and overburden strata. The hyperbolic function is performed in the actual survey data to investigate the cavern location, ground settlement, tilt or slope, and curvature under subcritical and critical conditions. The analytical method is developed to execute the regression and produce a set of surface subsidence components and a representative profile of the surface subsidence. Finite difference analyses (FDM) correlate the surface subsidence components with the cavern size and depth under the variety of overburden strengths and deformation moduli (Figure 2.13). The empirical equations correlate subsidence components with the cavern configurations and overburden properties. For the

super-critical condition, a discrete element method (DEM) is employed to simulate the uncertainties of the sinkhole development and ground movement resulting from the joint movement complexity and overburden post-failure deformation. The correlations of the subsidence configurations with the cavern geometries and overburden characteristics are applicable to the range of actual conditions (e.g., half oval-shaped cavern created in overburden-salt interface, flat ground surface, saturated condition, and horizontal rock units).
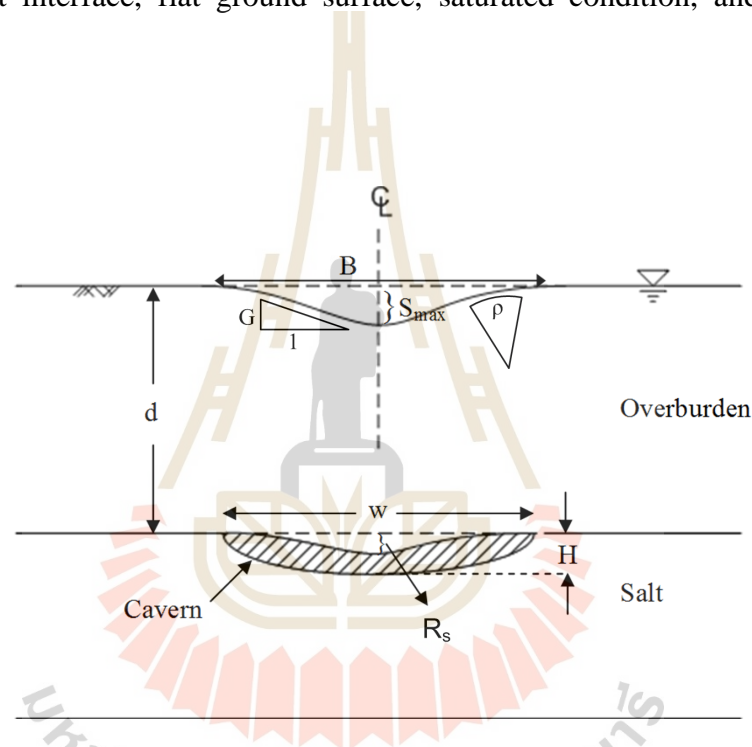
Figure 2.13 Variables used by Fuenkajorn and Aracheeploha (2010)

Bobet (2001) develops an analytical solution from Einstein and Schwartz (1979) to estimate ground movement from shallow circular tunnel in dry and saturated ground under limited condition as isotropic soil, homogeneous tunnel and not have extensive yielding. He finds a good agreement comparison between actual tunnel and data prediction along with correlation of soil tunnel, liner and sequence of construction. The gap parameter and small soil yielding are mostly responsible for the maximum surface settlements. The distances of ground movement occur within 3 to 4 times of tunnel radius.

The obstacle of this method is that it gives reasonable for preliminary design of shield driven tunnels in medium to stiff clays, or in soils and soft rocks where plastic deformations around the tunnel are small. The results indicate that the tunnel in dry ground shows the largest settlement (without buoyancy from water). The settlement trough increases with tunnel depth increasing.

Singh and Dhar. (1997) reviews sinkhole subsidence mechanism due to shallow mining in India. Shallow mining reports are collected from 14 coalfields. Cover collapse, overburden properties and too excavation are main causes. When subterranean voids are occurred by excavation and then surrounding strata fail down into the void, the ground movement spreads upward through the overburden strata, to the surface unless it is arrested by more competent roof layers. Maximum depth, overburden thickness and mechanical properties are the issues that has been discussed. The review shows that the shape of sinkholes is governed by their origin, overburden thickness and mining height. When overburden thickness to mining height ratio less than 5, there is an opportunity of sinkholes occurring. Most sinkholes occur where the range of mining depth is about 50 m. to 100 m. The occurring of sinkhole tends to be decrease with increasing overburden thickness. However, surface settlement characteristics are governed by the physical properties and thickness of overburden. Ground improvement and engineering constructions can be chosen to minimize the damage from sinkhole hazard.

2.4.4 Numerical methods

Application of numerical methods has more useful than physical method in terms of time and cost. Several researchers used numerical modelling to verify test result from physical modelling. in other words, the numerical model is a high precise reflection of physical actuality.

Guo et al. (2021) investigate of surface subsidence subjected to overburden strata. It also focuses on mechanism, deformation and properties of overburden due to long wall mining. The trapezoid area method and numerical simulation are performed to understand effect of alluvium strata and mechanical parameters. The field measurements are validating to verify numerical simulation. Different alluvium thickness (150 m – 450 m), cohesion (23 kPa – 133 kPa) and friction angles of overburden (10° - 25°) are conducted in experimentation. The result indicates that the maximum subsidence is clearly governed by overburden strata properties. The effect of surface subsidence increases with weak overburden ratio increasing. The friction angle affects the subsidence, surface subsidence exponentially and logarithmically decreasing while friction angle and cohesion increases, respectively. Furthermore, the observed subsidence profile from field measurements reasonably agrees well with the result from numerical simulation.

Al-Halbounil et al. (2018) perform numerical modelling to understand the cavity growth and sinkhole hazard for single void space and application to the Dead Sea. Discrete element method use to simulate sinkhole development under various condition: geometry and depth of cavities, effect of material properties and laid sequence of overburden layers. Figure 2.14 shows the setup for DEM modelling and material parameters as used in PFC^{2D}. They calibrate actual parameter for the three main material types from Dead Sea region: mud, alluvium and salt (weak to strong material respectively). The result shows a good agreement of sinkhole geometry with actual topography. The stability of cavities is clearly related to the mechanical properties of overburden and depth of dissolution. When ratio of cavity depth to cavity width decreases until strength of cavern roof cannot support its (shallow cavity), cavern roof will collapse into the cavity. Weak material does not support huge cavities. Multiple overburden layers are more sensitive to subsidence than uniform materials not only due to a lower integrated strength

of the overburden, but also due to the expansion of collapse zone in weak materials that unsettle the overburden. The model results suggest that the observed distribution of sinkhole depth / diameter values in each material type partly reflect sinkhole growth trends.
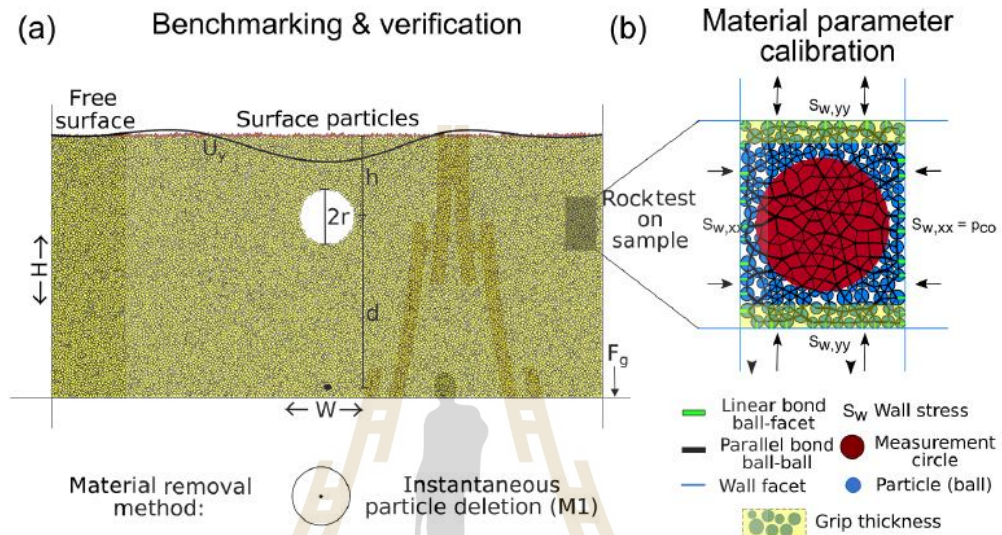
Figure 2.14 Setup for numerical sinkhole modelling. (a) benchmarking and model verification (b) material parameter calibration.

Zhang et al. (2018) study tunnel failure mechanism by using transparent soil model test and DEM simulation. They investigate the effect of overburden strength and cavity depths on deformation and failure process. Table 2.1 shows the three model tests for different material properties used in PFC^{3D}. Peck's settlement formula from (Equation 2.1-2.3) are used to compare surface settlement. The result from Figure 2.15 shows that the maximum subsidence is occurring over the tunnel axis for each method. The settlement trough of higher friction angle is smaller than the lower ones. Maximum subsidence of dense sand is lower than loose sand due to the effect of friction angle. Numerical result curves agree well with physical model. The result clearly shows the settlement value by Peck formula is often underestimate (too small) for granular soil. Peck's method was not suitable for shallow overburden tunnels, and the calculation

process of the stochastic medium theory are complicated. This observation agrees with reported by New and O'Reilly (1991) and Song (2019). The stress field and the displacement field derived from the numerical results can help interpret the tunnel failure mechanism. It is obvious from the results that the Peck formula (1969) is less applicable for the surrounding materials with low strength.

Table 2.1 Physical and mechanical properties for three tests (Zhang et al., 2018)

Test No.	Relative density (%)	Buried depth (mm)	Friction Angle (°)	Minimum density (g/cm³)	Maximum density (g/cm³)	Dry density (g/cm³)
1	30	60	21	0.970	1.274	1.045
2	70	60	34	0.970	1.274	1.161
3	70	120	34	0.970	1.274	1.161
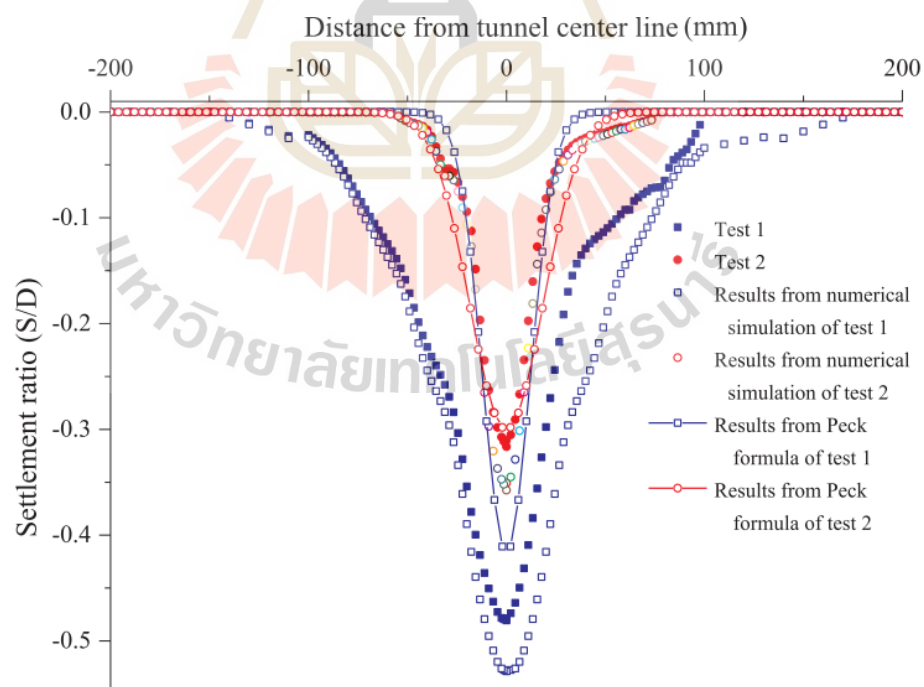
Figure 2.15 Comparison of numerical and physical test results with Peck 's formula

(Zhang et al., 2018)

Tao (2015) establishes physical and numerical modeling to understanding the processes, development, and collapse of sinkhole formation. Sandbox 150 x 120 x 20cm with three layers material materials are filled to represent karst environment. Water tanks are conducted to observe the impacts of groundwater pumping on sinkhole. Particle Flow Code (PFC) and Fast Lagrangian Analysis of Continua code (FLAC) are coupled to verify tested result base on the sandbox apparatus. PFC is used to simulate part of particle flow into the cavity, and other areas used FLAC. The data exchange between two codes running via I/O socket. For the flow simulation, sand and clay particles start flow down to void cavity when seepage force increases with increasing hydraulic gradient. The results of the numerical modeling are similar to the phenomena observed in the physical experiment, which have a good reasonableness in comparison with the physical experiment. The expansion of the cavity due to particle movement caused by the increase of seepage force after hydraulic head in the clay layer drops.

Shahriar et al. (2009) presented a study for the two shallow panel subsidence due to longwall mining of inclined coal seam in Parvadeh (Tabas) coalfield, easten part of Iran. Coal mine subsidence data has been collected by surveying. FLAC^{3D} software which founded on finite difference method (FDM) is chosen for subsidence prediction without including residual subsidence behavior (creep). Material properties of coal seam and rock formation are used from collected data from Fernandez et al. (2005). FLAC^{3D} results are compared with measured surveying and empirical profile function method provided by Asadi et al (2005). Predicted maximum subsidence from FLAC^{3D} underestimated up to 3% in comparison with profile function and surveying. The profile function method predicts final subsidence trough but the time dependent in shallow depth is neglected in this study. However, FLAC^{3D} results show some different predicted subsidence profiles from survey monitoring and measured profile function method.

Maximum subsidence in shallow coal seams uplift over the panels rise side at the surface. The reason that no uplift at surface with measured profile by Asadi et al (2005) is due to their neglect on measuring upwards subsidence. However, it has not obviously contrast with deep coal seam mining. Sensitivity analysis showed that by increasing the depth, this point gradually shifts toward the panel dip side. The range of critical width to depth ratio (W/H) is between 1.0 and 1.4 (observed for both panels). This range is a lower than the range of critical from previously research. It is expected that a very shallow depth of coal seam of both panels. The results showed that numerical modeling is truly responsive to variation of input parameter. It can represent stage of mine subsidence better than profile function due to considering the mechanism of geological properties. It can rarely be use empirical profile function which customized from local site to another. The most advantage of empirical method are simple and affordable process.

Rawal et al. (2017) study complex multi-physics involved in the processes of sinkhole development using hydro-mechanical simulations. FLAC is used simulate to compare the influence of rapid and slow drawdown of water situations and its influence on the subsidence or cavity deformation. Figure 2.16 shows the geometry and conceptual model that bottom layer is limestone rock and upper layer is clay overlaying. The material thickness is 5 m for each layer. A circular cavity with 1 m diameter is perform in between a both layers. Plasticity simulation is used and typical range of soil or rock properties as shown in the Table 2.2. The results show that the vertical displacement increases with increasing the rate of head drop. It is obvious that if the water is withdrawn from the ground model which higher rate (rapid drawdown), the deformation become more significant and lead to fast develop of sinkhole.
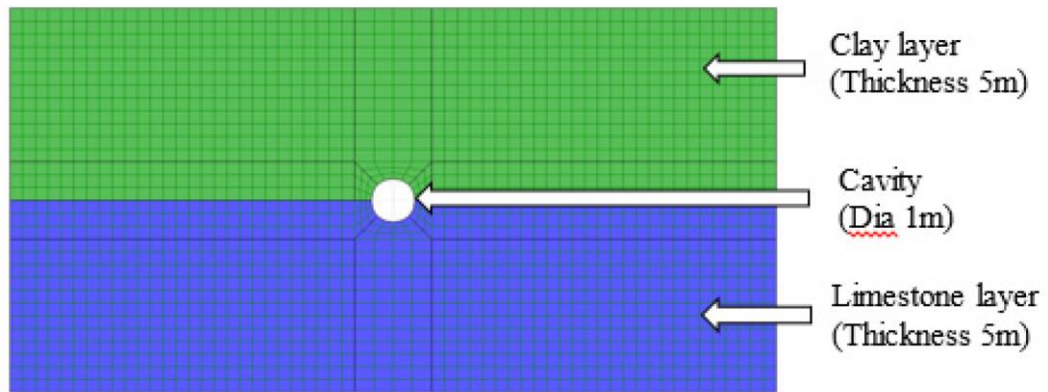
Figure 2.16 Geometry of FLAC model Rawal et al. (2017)

Table 2.2 Strength parameters used in simulation (Rawal et al., 2017).

Parameters	**Clay layer**	**Limestone layer**
Mass Density (ρ)	2000 kg/m^3	2700 kg/m^3
Cohesion (c)	15 kPa	1 kPa
Friction Angle (ϕ)	27	30
Tension (*T*)	0 – 10 kPa	100 kPa
Elastic Modulus (E)	30 MPa	5000 MPa
Poisson's Ratio (υ)	0.3	0.3

Li and Wang (2011) use Particle Flow Code to simulate the collapse consequence of case study. Collected survey subsidence data in Shandong province, east China is investigated to observe the interaction of contact force and displacement of ore particles. Mine situation and rocks parameter are established to simulate actual data with PFC model (Figure 2.17). The PFC^{2D} well simulates the ground movement caused by underground mining. Particle flow method has more advantages in the simulation of mechanical behavior of overburden lowering , in the mechanical analysis of collapse process and in the collapse displacement of ores. The result of

discrete element modeling is employed for this study show the good consistency in comparison with actual field survey.
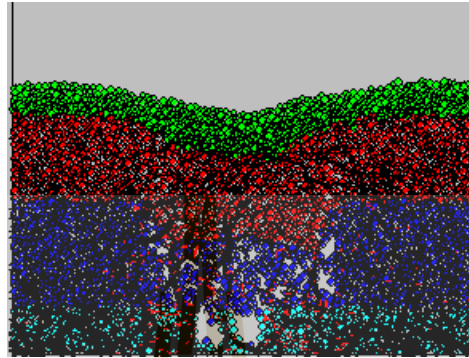
Figure 2.17 Particle flow simulation model of mine (Li and Wang, 2011)

Mcnearny and Barker (1998) compare physical and numerical models of the block-caving mining methods. PFC^{2D} program is made an effort to better realize the deformations and flow within each of the physical models during the draw procedure. Bridging and interlocking of the blocks occurred in approximately the same places and similar times during the draw sequence. The results show that the draw down patterns and the rate of draw generated within the numerical models are very similar in development of the physical models. For the given cases of the physical model, the numerical model simulated the behavior of the physical model quite well. The only constraints that are placed on the numerical models are the initial boundary conditions of the physical models. By inspection, the overall shape and flow lines of both the numerical and physical models are extremely close in area removed and flow characteristics. The numerical results as reported in this study are the result of the internal algorithms of the PFC^{2D}software.

Singh and Yadav (1995) predict and compare the surface subsidence by using a visco-elastic modeling from two shallow coal mines in India (weak and hard overburden). The important parameters are input, such as overburden thickness, width

working, extraction thickness and rock mass properties. The seam thickness and room width are about 3.3 m and 4.5 m, respectively. The results show that subsidence decreases with increasing overburden thickness. The strength of overburden clearly affects the surface subsidence, weak overburden shows more subsidence value than those of hard overburden. The results of subsidence from computer are larger than the observed profile. Subsidence profile due to coal mining in hard overburden has been correlated with observed data better than weak overburden. This may be governed by site factors which are not incorporated in the theoretical model. The proposed model will be more accurate if other factors or physical rock properties are considered in model.

Numerical methods have more advantage than other methods such that the geotechnical aspects of the mine working can be considered. Among numerical techniques, Particle Flow Code (PFC) may be most suitable for solving highly non-linear and large strain problems like subsidence phenomena, as compared to the laboratory-scale models and the actual survey data (Li and Wang, 2011; Lisjak and Grasselli, 2014).

CHAPTER III

PHYSICAL MODEL SIMULATIONS

3.1 Introduction

The objective of the physical model simulations in this study is to determine the maximum subsidence and trough width as a function of cavern width and height under super-critical condition. This chapter describes the material, equipment, method, and results of the simulations. The varied parameters are widths, depths, and heights of cavity.

3.2 Material property

The types of overburden material used in this study are uniform spherical acrylonitrile butadiene styrene plastic (ABS) balls (cohesionless medium). The ABS balls are used to simulate the settlement of overburden under super-critical condition. ABS balls (Figure 3.1) are used here because of their extremely uniform regarding the mechanical and physical properties. Consistency of weight density is obtained as shown in Figure 3.2. Estimation of roundness and sphericity of granular particles are compared with the Power (1953) classification system (Figure 3.3), which is classified as high spherical and well round. The cohesion and friction of ABS balls are obtained by ASTM D3080/D3080M standard practice. The bulk density of ABS balls is 582 kg/m^3. A relation between shear strengths and the normal stress are shown in Figure 3.5. The friction angle is 15 degrees. The cohesion is effectively zero. The normal (K_n) and shear (K_s) stiffness values are 20 GPa/m and 1 GPa/m. The properties of ABS balls are summarized in Table 3.1.

Figure 3.1 ABS balls with uniform sizes of 6 mm used to simulate cavern roof and overburden.

$y = 0.1093x - 0.0099$

$R^2 = 1$
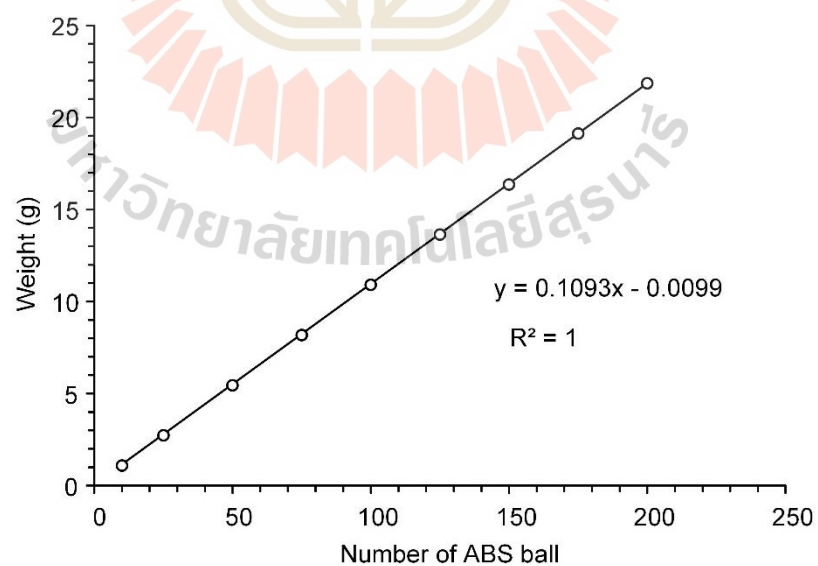
Figure 3.2 Weight of ABS ball as a function of particle number.
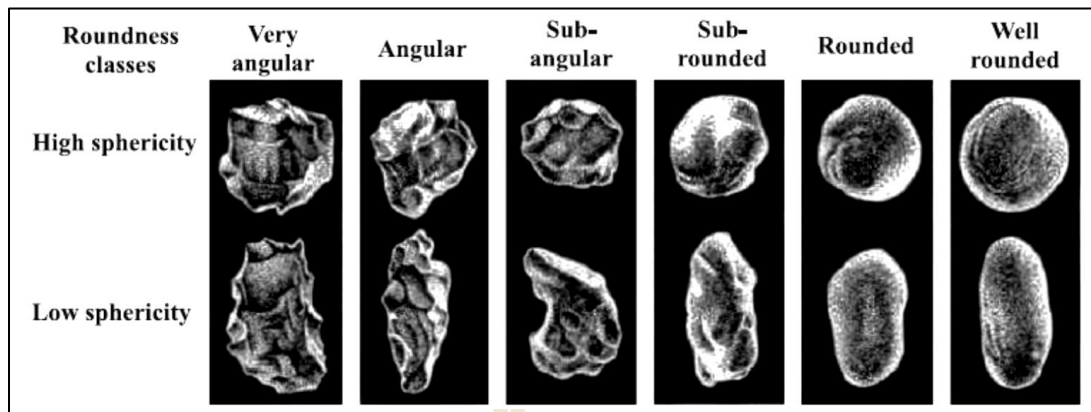
Figure 3.3 Chart for estimation of roundness and sphericity (Powers, 1953).
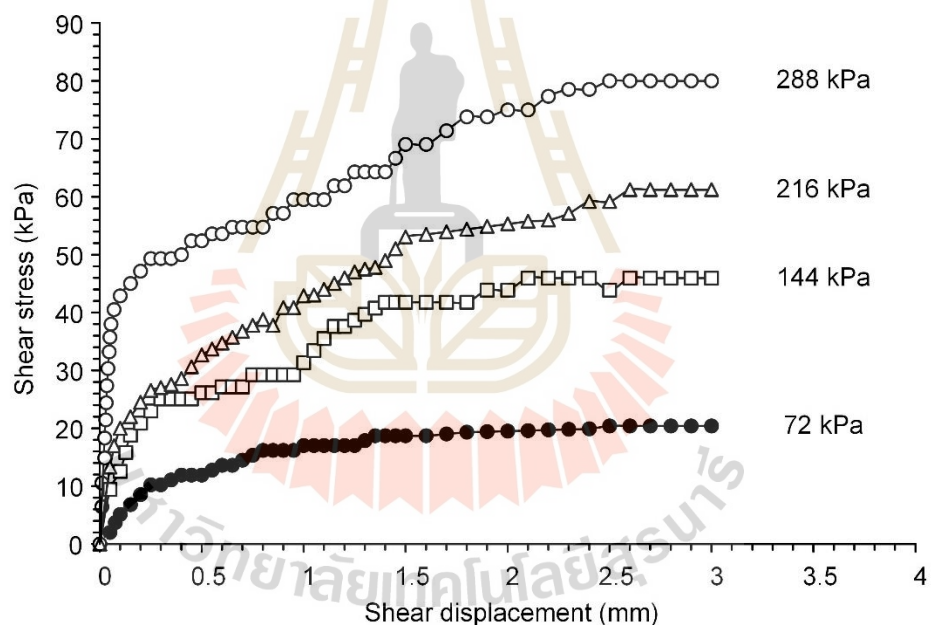
Figure 3.4 Direct shear test results.
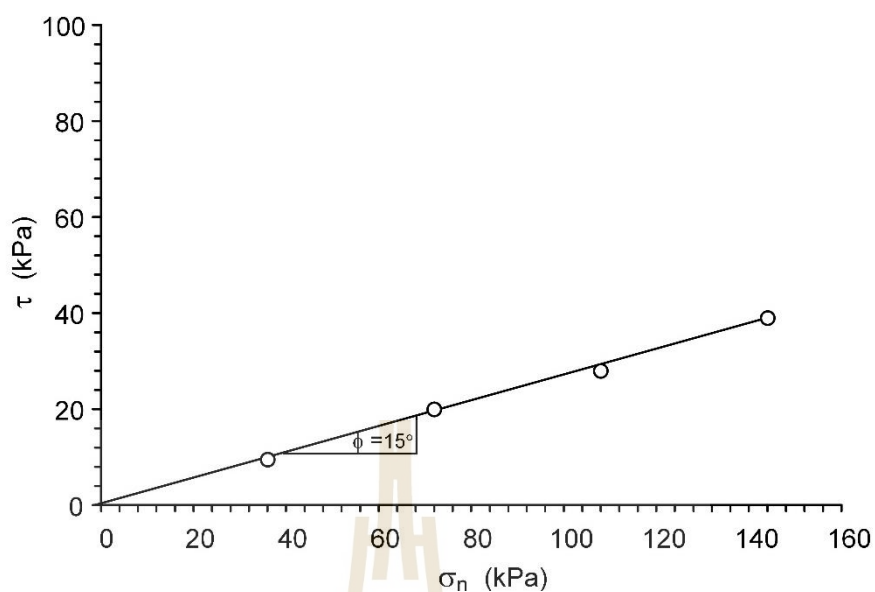
Figure 3.5 Coulomb criterion fitted to test results.

Table 3.1 Physical and mechanical properties of ABS balls.

Test method	Soil properties	Values
Grain Shape	Sphericity	High sphericity
	Roundness	Well rounded
Direct shear test	Bulk density (kg/m^3)	582
	Cohesion, c (kPa)	0
	Friction angle, ϕ (degree)	15.0
	Normal stiffness, K_n (GPa/m)	20.0
	Shear stiffness, K_s (GPa/m)	1.0

3.3 Physical model testing

The physical model test here uses a trap door apparatus developed by Thongprapha *et al.* (2015), as shown in Figure 3.6. The trap door consists of 3 main functions: (1) to establish surface subsidence process in two-dimension, (2) to assesses the effect of overburden properties and geometries of cavity on the surface settlement, and (3) to induce subsidence of overburden. The testing space inside the custom-made acrylic container is $75 \times 25 \times 30$ cm^3. The experiments are measured with laser scanner with a precision of 0.001 mm mounted on X-Y sliding rails. For each subsidence test, acrylic container is filled with ABS balls to represent overburden layer over the simulated cavity.
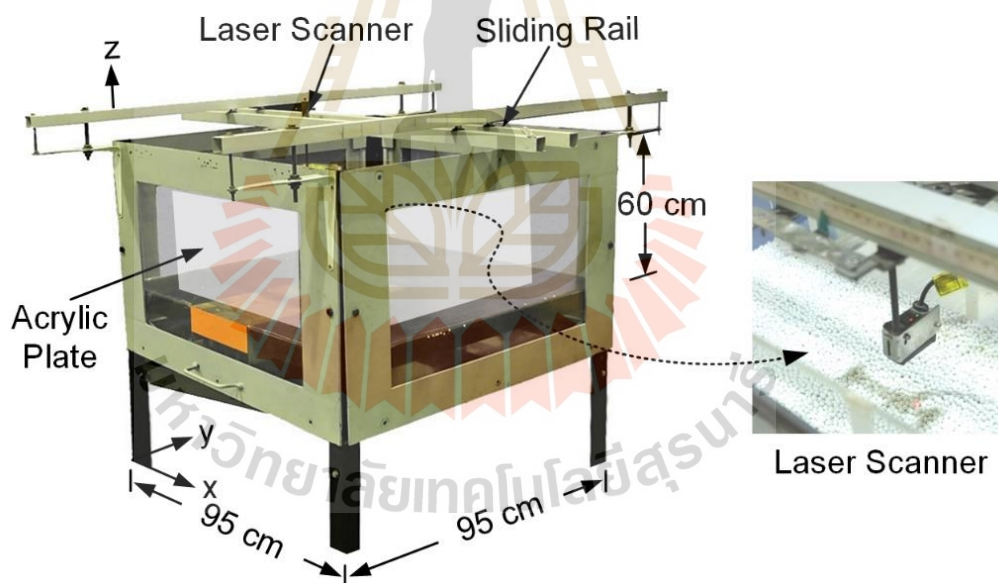
Figure 3.6 Trap door device and measure system (adapted from Thongpraoha et al., 2015).

The ABS balls are gently dropped into the test box without compaction, and the top surface is even flattened before scanning. The cavity shape simulations are formed by series of plastic blocks with 25 cm in length, 3 cm in width and 12 cm in height. They are placed underneath the container. Combination of these blocks can represent various widths and heights of the cavity. For this study, the cavity width (W) is varied from 30 mm to 120 mm.

The cavity length is maintained at 250 mm. The cavity height (H) is simulated from 30, 60, 90 to 120 mm. The cavity depth (Z) is simulated between 120 and 300 mm with 30 mm increment. Trap door parameters model and measuring devices are shown in Figure 3.7.
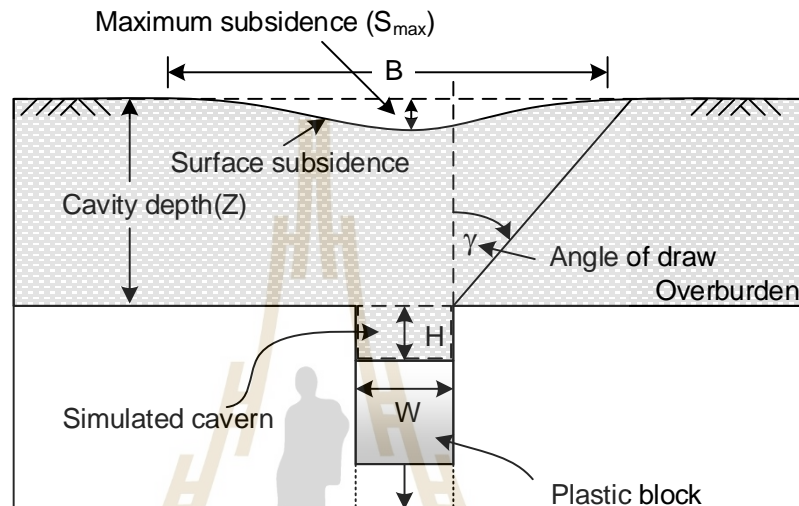
Figure 3.7 Detail view of variables cavity configurations in physical model.

For each combination of variables, the subsurface void is simulated by pulling the plastic blocks down gently. The ABS balls flowed into the cavity, and settlement of the ground surface is induced subsequently. The laser scanner (KEYENCE, CMOS Multi-function laser sensor, Model IL-030) measures the surface profile before and after the settlement occurred. The measurement interval is to the nearest 1 mm. The vertical measurements were read to the nearest 0.1 mm. Each cavity configuration is simulated 3 times to verify test results. The laboratory testing gives the maximum subsidence (S_{max}) and the trough width (B). Maximum subsidence is measured at the peak point of maximum subsidence trough. The trough width is measured from limited edge to edge of surface subsidence.

Figure 3.8 illustrates an example of a full surface in three-dimension scanning and its cross-section. The physical model results are focused on the variation of the maximum subsidence and subsidence trough width as affected by the opening geometry, and block size under super-critical condition. All opening configurations are repeated at least 3 times to verify the trends and reliability test results.
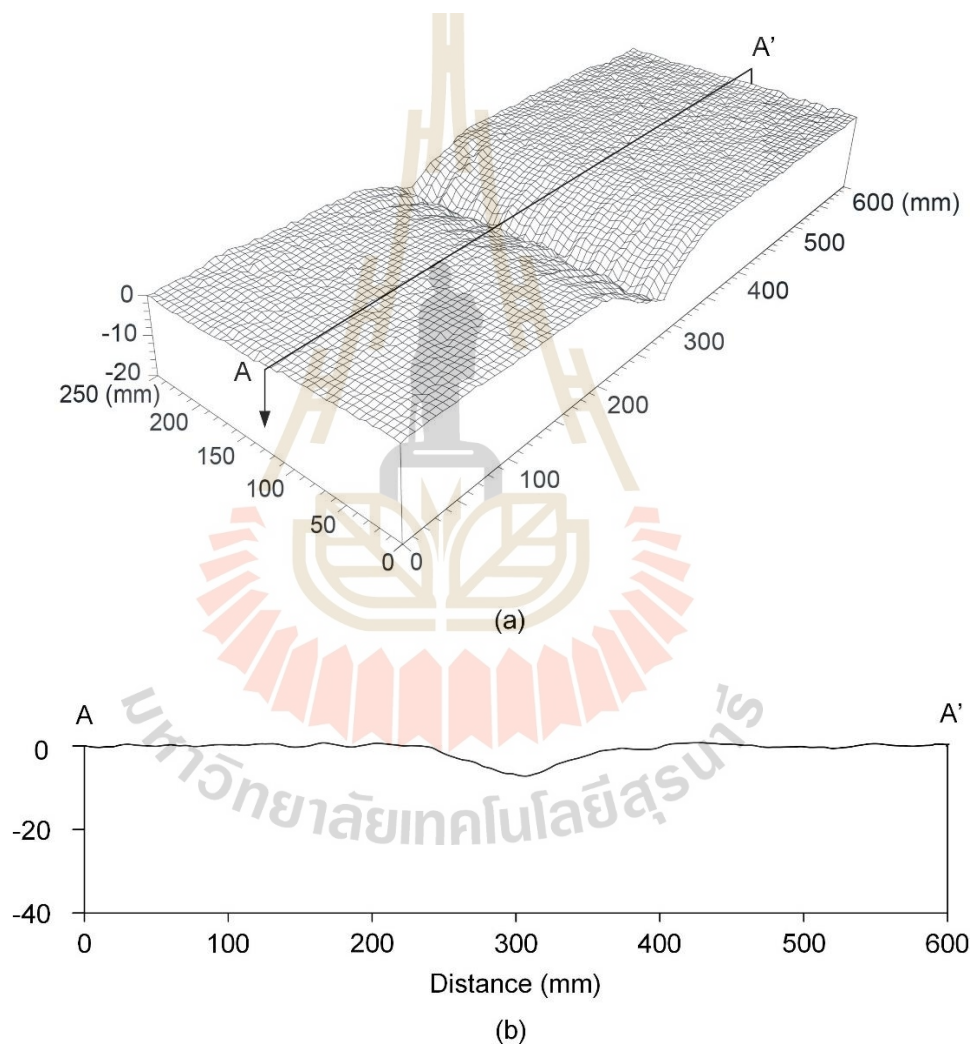
Figure 3.8 Example of three-dimensional image of physical subsidence (a) and cross-section (b) with vertical exaggeration scale

3.4   Test results

The collapse of cavern roof and overburden results obtained here are shown in Table 3.2, in term of the maximum subsidence (S_{max}), trough width (B) and angle of draw (γ). Several scanned subsidence profiles are presented in Figures 3.9 through 3.15. The maximum subsidence as a function of the cavity height (H) for each cavity width (W) are shown in Figure 3.16. The results clearly indicate that the maximum subsidence increases with increasing cavity height and width. This is because the particles can collapse into the cavity more easily when the volume of opening is larger. The maximum subsidence tends to decrease slightly as the cavity depth increases. This is due to the inter–locking of ABS balls above the void area (Meguid et al., 2008). This observation agrees well with those of Thongprapha et al. (2015) who study the surface subsidence above underground opening using gravel in order to exhibit a cohesionless frictional behavior of the overburden material. Note that the S_{max} values are more sensitive to the cavity height for the wider openings than for the narrower ones (Figure 3.16). Under the same cavity geometry, deep cavities showed shallower and wider trough than shallower ones. As the cavity height increase, the maximum subsidence increases.

Relationship between the trough width (B) and cavity width (W) are plotted in Figure 3.17. The results suggest that depth and width of subsidence trough increase with increasing of cavity height and width. This test results are based on super-critical condition, ABS balls can flow into the cavity more easily when cavity expanding, and hence induced deeper and wider subsidence trough. The trough depth decreases as the cavity depth (Z) increases. This is again probably due to the inter-locking of the ABS balls above the cavity. This observation agrees with those reported by Kim and Ha (2014) and He and Xu (2018) who conclude that the maximum subsidence tends to be sensitive to the cavity height only for the wide cavities at shallow depth. The trough depth is not sensitive to the height of deep cavities.

Table 3.2 Physical model test variables and subsidence results.

Test variable			Results		
Z (mm)	W (mm)	H (mm)	S_{max} (mm)	B (mm)	γ (degrees)
120	30	30	2.91	131.80	23.50
		60	10.57	164.17	30.00
		90	19.90	194.98	31.80
		120	27.85	222.98	39.00
	60	30	10.49	197.00	30.20
		60	26.14	244.00	37.80
		90	38.46	254.10	39.40
		120	44.30	270.00	45.00
	90	30	16.84	230.00	30.30
		60	37.19	281.00	38.70
		90	49.16	293.28	40.70
		120	60.42	321.32	44.50
	120	30	25.74	280.00	33.30
		60	44.11	300.85	37.00
		90	56.14	328.00	41.00
		120	72.73	350.00	49.50
150	30	30	2.51	110.40	14.80
		60	8.00	191.60	28.40
		90	13.57	217.11	31.80
		120	20.01	225.00	33.00
	60	30	9.79	216.00	27.60
		60	23.48	273.00	35.50
		90	35.64	287.00	37.30
		120	44.00	300.00	43.50
	90	30	15.53	260.00	29.50
		60	34.47	306.00	36.60
		90	45.86	340.00	39.70
		120	56.90	359.00	41.80
	120	30	21.71	290.00	29.60
		60	42.00	346.20	36.80
		90	53.05	373.00	40.00
		120	69.60	417.00	44.20

Table 3.2 Physical model test variables and subsidence results (Cont.).

Test variable			Results		
Z (mm)	W (mm)	H (mm)	S_{max} (mm)	B (mm)	γ (degrees)
180	30	30	2.50	155.00	10.20
		60	5.50	195.78	24.80
		90	12.60	224.00	28.50
		120	19.84	242.00	32.70
	60	30	8.55	230.00	26.00
		60	19.10	300.00	34.50
		90	28.56	327.50	37.00
		120	39.19	360.00	40.20
	90	30	13.35	279.00	27.80
		60	29.91	354.00	36.00
		90	40.67	380.00	38.90
		120	53.57	408.00	41.50
	120	30	17.69	314.00	28.00
		60	37.89	386.24	36.00
		90	51.72	410.00	39.20
		120	64.54	428.00	41.80
210	30	30	0	0	0
		60	4.30	199.50	20.20
		90	7.23	227.50	25.50
		120	11.85	290.00	31.80
	60	30	7.12	250.00	24.30
		60	15.57	318.40	31.60
		90	24.00	366.00	37.00
		120	36.60	386.72	38.30
	90	30	10.53	284.00	24.00
		60	28.23	361.00	33.10
		90	40.03	398.00	34.00
		120	49.37	420.00	40.00
	120	30	17.66	344.00	27.50
		60	36.04	398.00	34.00
		90	51.19	413.00	35.00
		120	63.89	454.00	38.40

Table 3.2 Physical model test variables and subsidence results (Cont.).

Test variable			Results		
Z (mm)	W (mm)	H (mm)	S_{max} (mm)	B (mm)	γ (degrees)
240	30	30	0	0	0
		60	3.22	266.00	26.30
		90	7.00	280.00	27.70
		120	11.28	288.60	28.30
	60	30	5.94	250.00	26.20
		60	14.27	310.00	27.50
		90	23.15	390.00	38.00
		120	35.66	415.00	38.50
	90	30	9.00	288.50	22.60
		60	21.00	366.00	30.00
		90	32.84	422.00	34.00
		120	44.69	444.00	36.00
	120	30	15.24	358.13	26.20
		60	34.15	430.50	33.10
		90	48.27	457.00	35.00
		120	58.58	499.00	38.20
270	30	30	0	0	0
		60	3.22	223.00	20.00
		90	6.32	290.00	25.80
		120	9.35	319.60	28.00
	60	30	3.24	248.40	19.30
		60	9.71	340.00	27.70
		90	18.69	400.00	36.50
		120	23.69	430.00	37.50
	90	30	7.09	310.00	22.30
		60	16.08	378.00	29.00
		90	28.80	432.00	32.60
		120	42.01	505.00	37.70
	120	30	12.00	383.24	26.00
		60	29.08	481.73	34.00
		90	44.24	512.00	35.00
		120	55.49	530.00	36.00

Table 3.2 Physical model test variables and subsidence results (Cont.).

Test variable			Results		
Z (mm)	W (mm)	H (mm)	S_{max} (mm)	B (mm)	γ (degrees)
300	30	30	0	0	0
		60	2.84	277.00	20.00
		90	6.30	320.00	26.00
		120	9.34	345.00	28.00
	60	30	2.55	285.00	17.70
		60	8.29	350.00	27.00
		90	17.50	400.00	34.60
		120	23.00	430.00	35.60
	90	30	6.50	381.00	22.00
		60	13.34	440.00	33.50
		90	25.44	470.00	31.60
		120	36.84	500.00	35.50
	120	30	8.94	450.00	26.00
		60	26.07	516.89	33.60
		90	33.82	522.00	33.90
		120	46.66	560.00	34.00
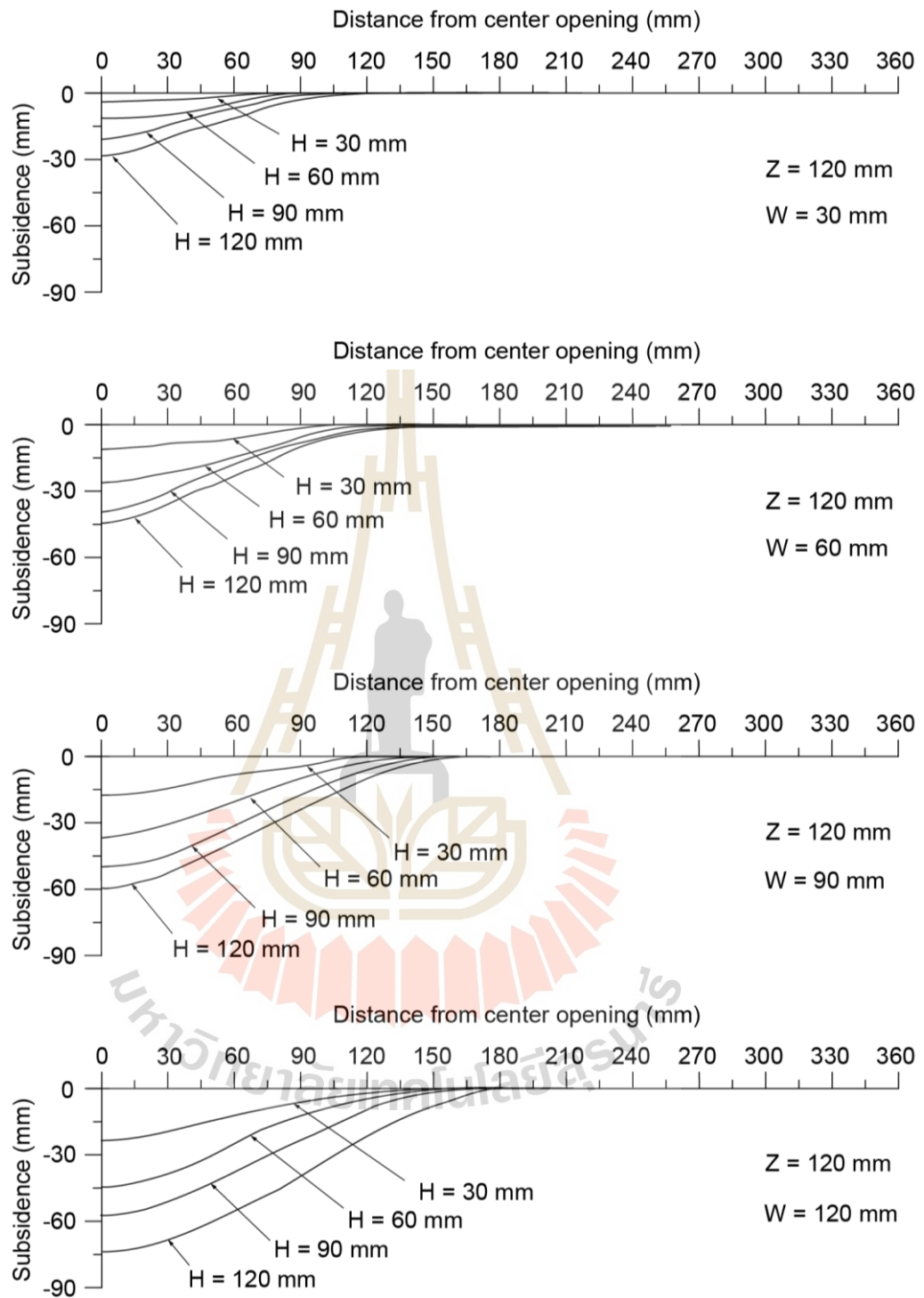
Figure 3.9 Line scanned profile of surface subsidence for cavity depth (Z) 120 mm in each

cavity height (H) and cavity width (W).
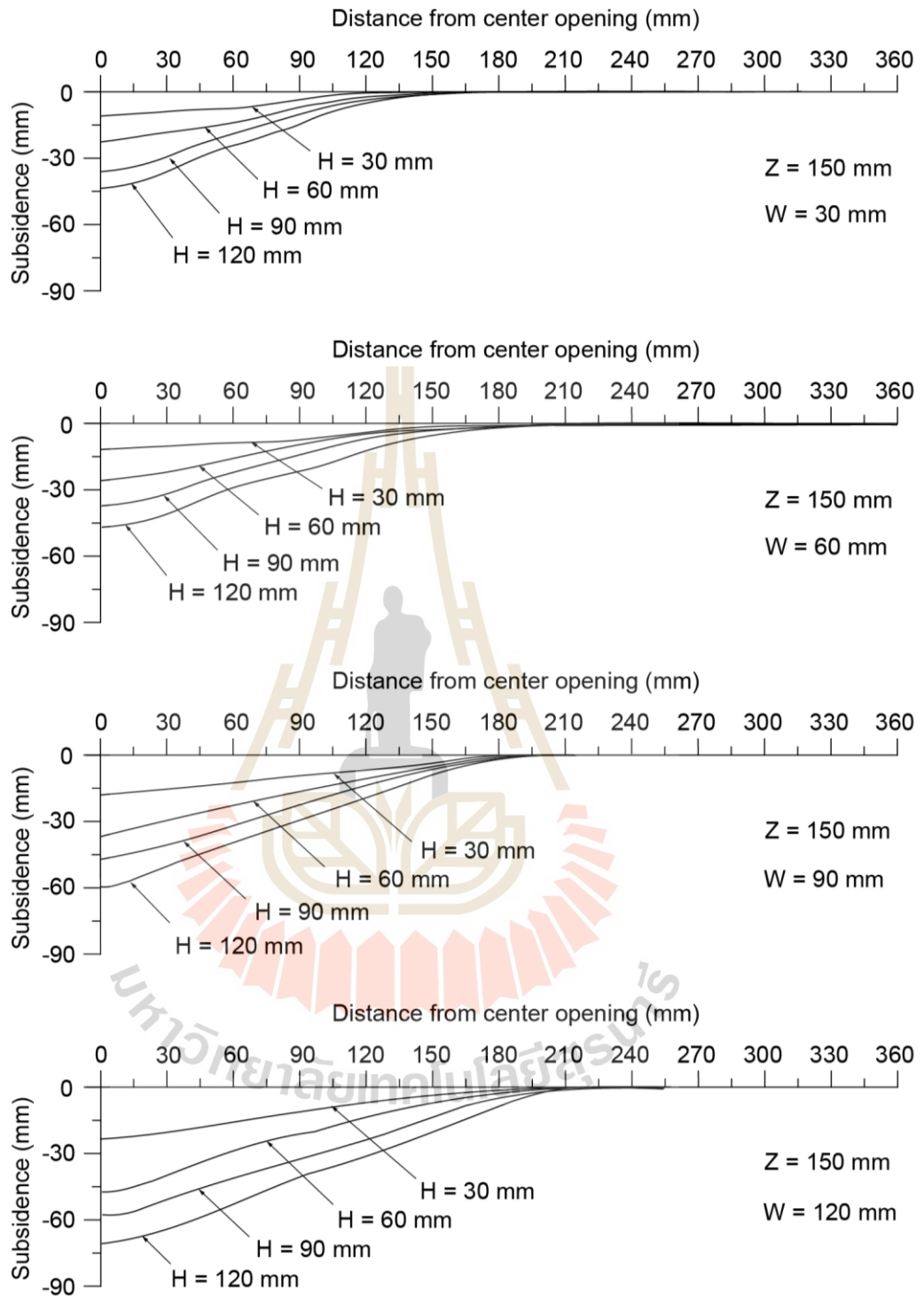
Figure 3.10 Line scanned profile of surface subsidence for cavity depth (Z) 150 mm in each

cavity height (H) and cavity width (W).
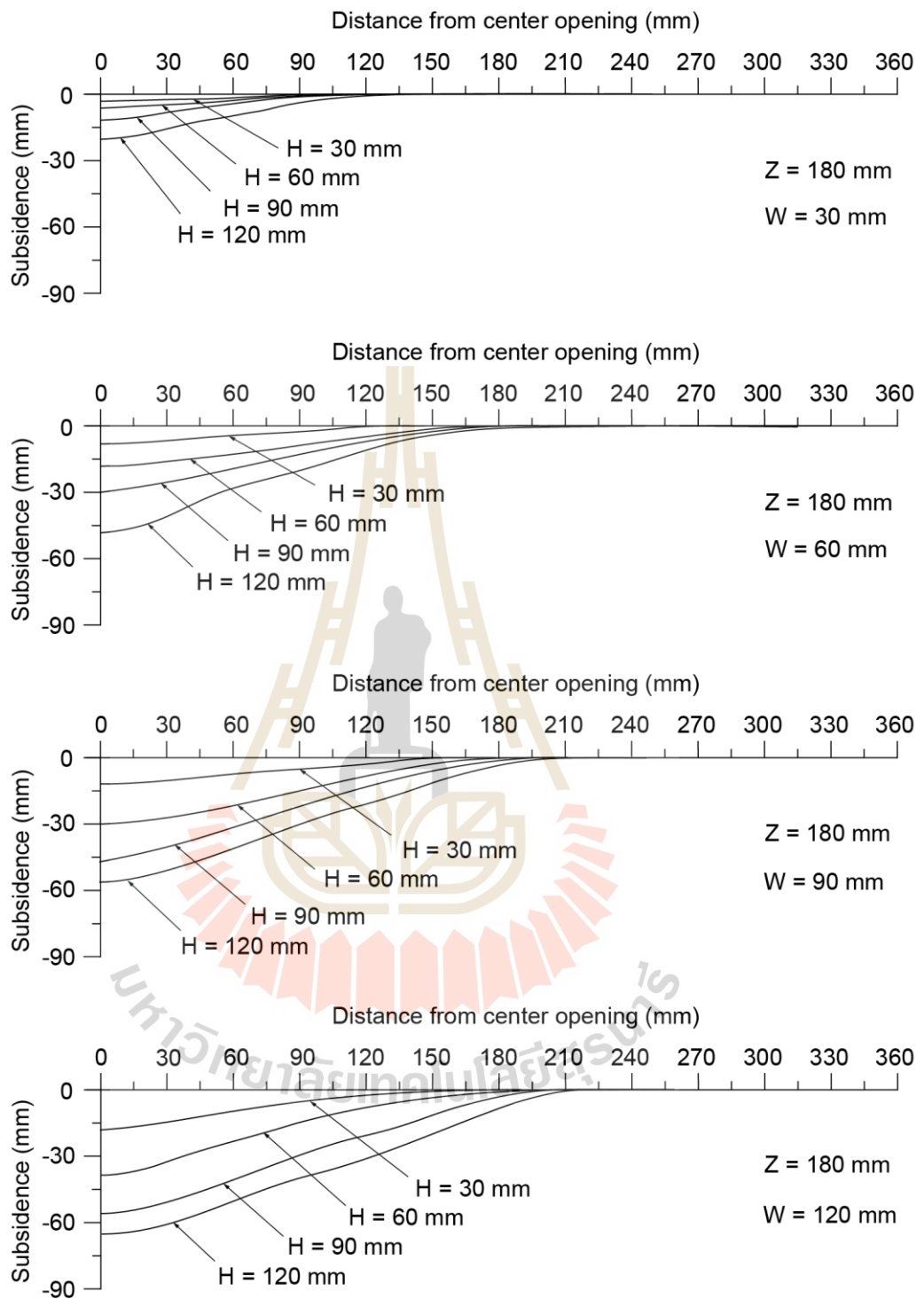
Figure 3.11 Line scanned profile of surface subsidence for cavity depth (Z) 180 mm in each

cavity height (H) and cavity width (W).
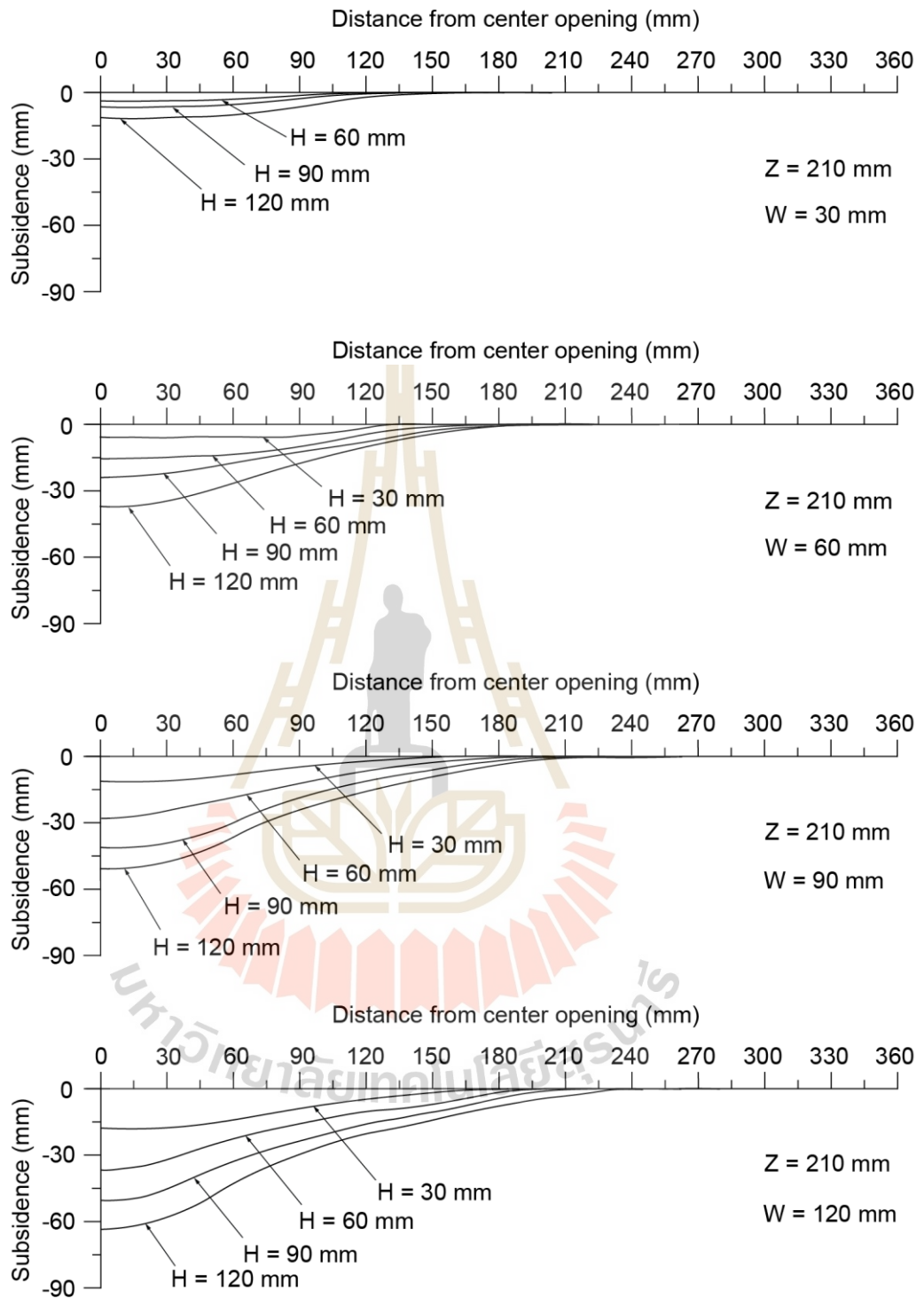
Figure 3.12 Line scanned profile of surface subsidence for cavity depth (Z) 210 mm in each

cavity height (H) and cavity width (W).
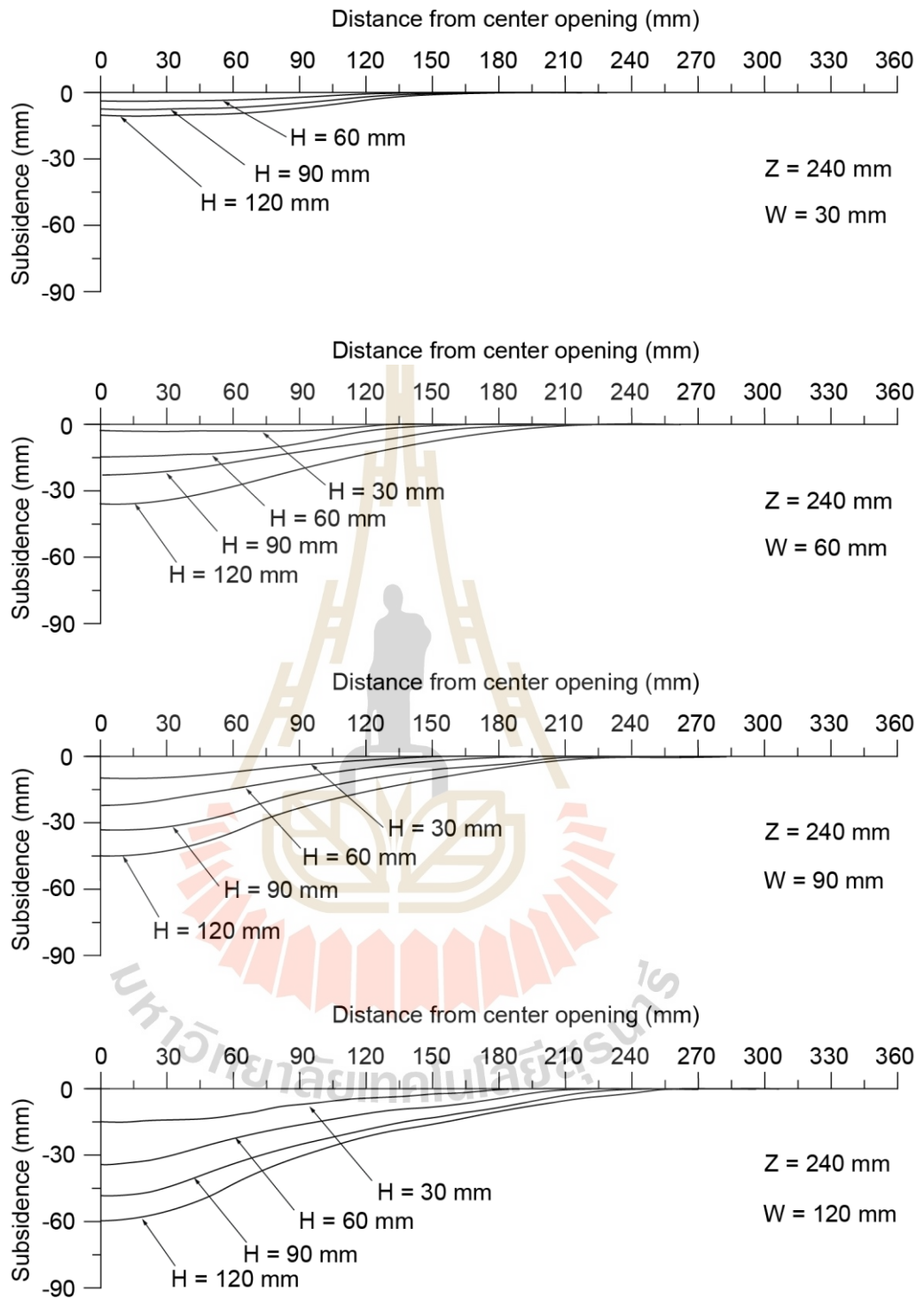
Figure 3.13 Line scanned profile of surface subsidence for cavity depth (Z) 240 mm in each cavity height (H) and cavity width (W).
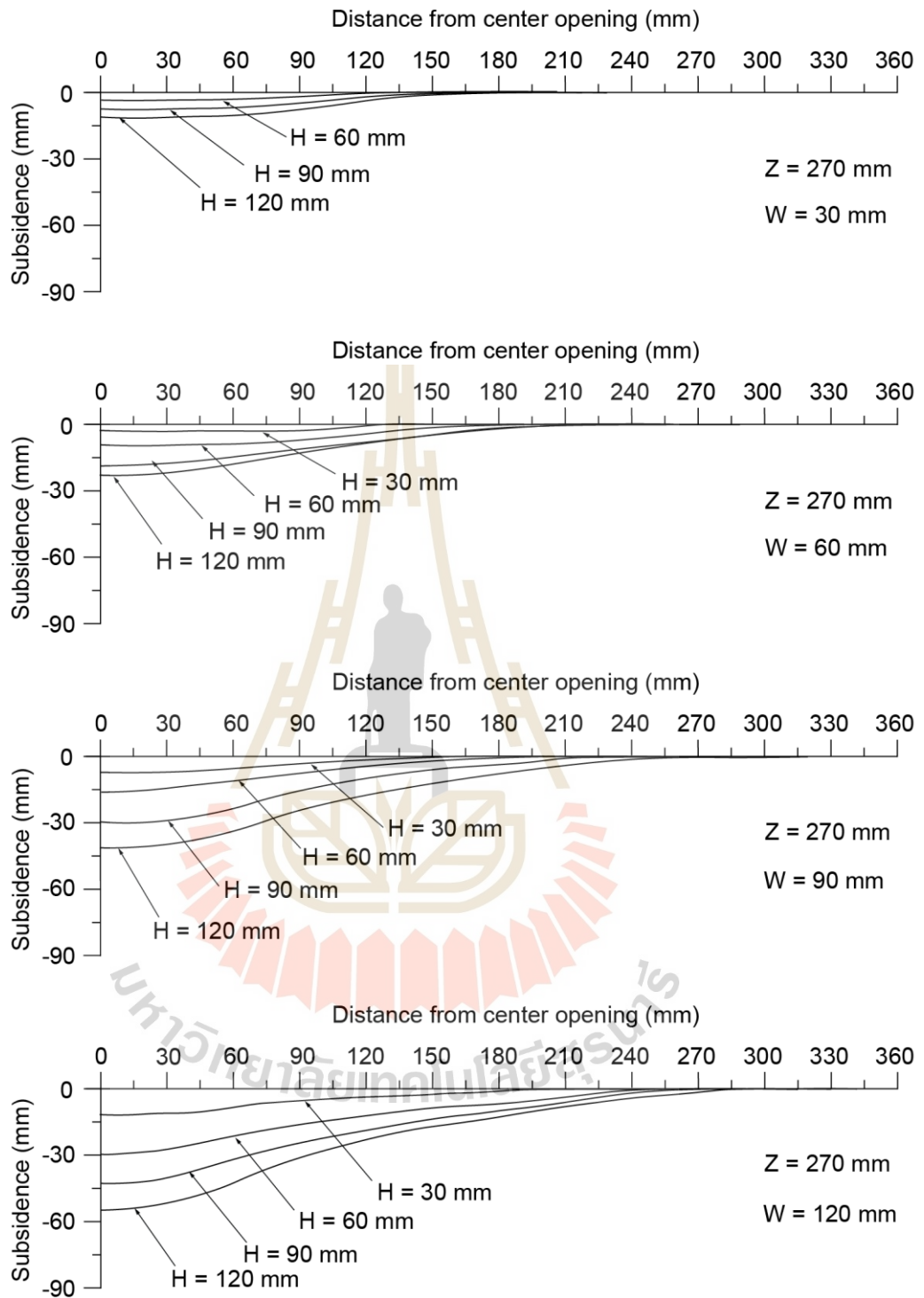
Figure 3.14 Line scanned profile of surface subsidence for cavity depth (Z) 270 mm in each

cavity height (H) and cavity width (W).
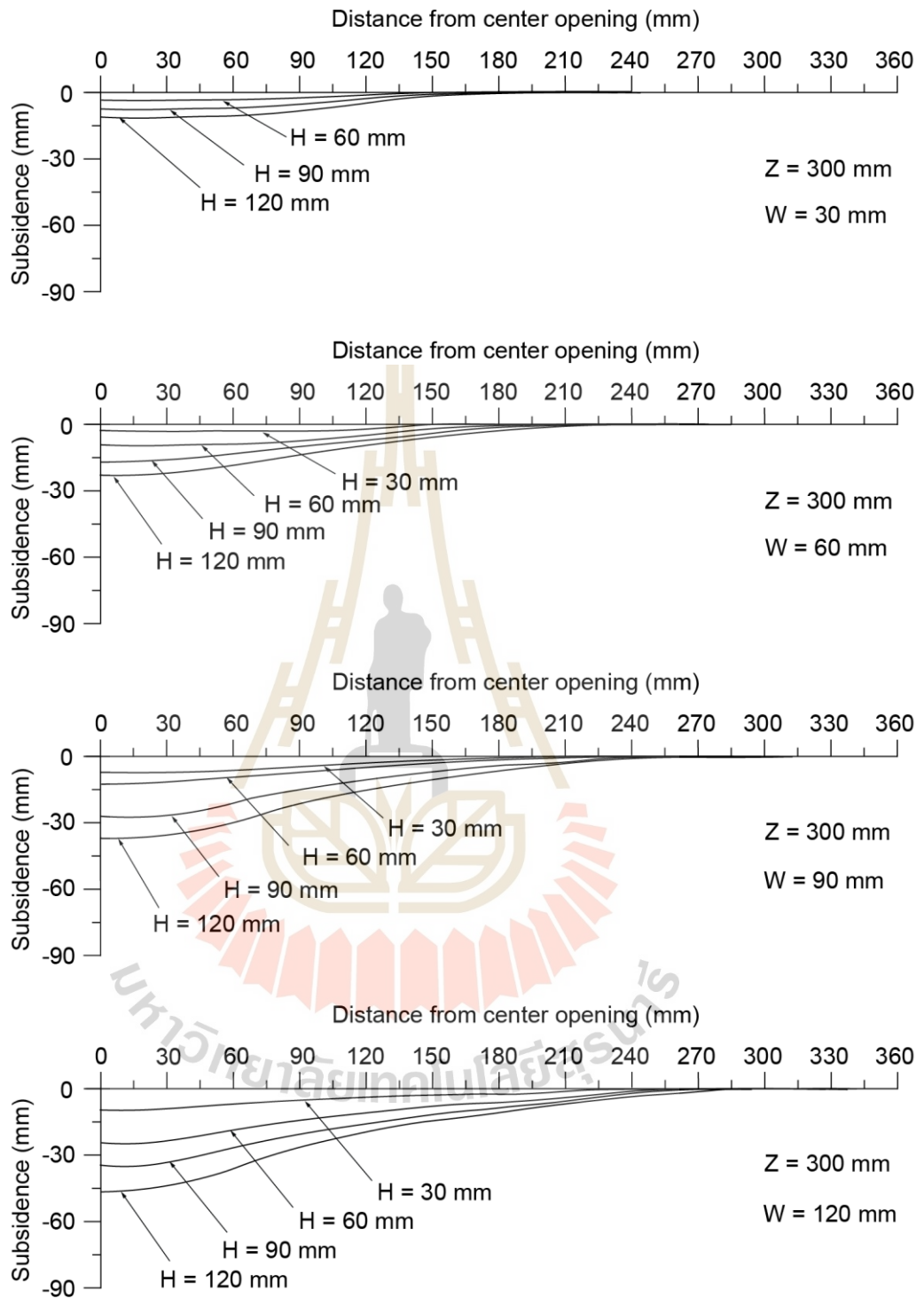
Figure 3.15 Line scanned profile of surface subsidence for cavity depth (Z) 300 mm in each

cavity height (H) and cavity width (W).
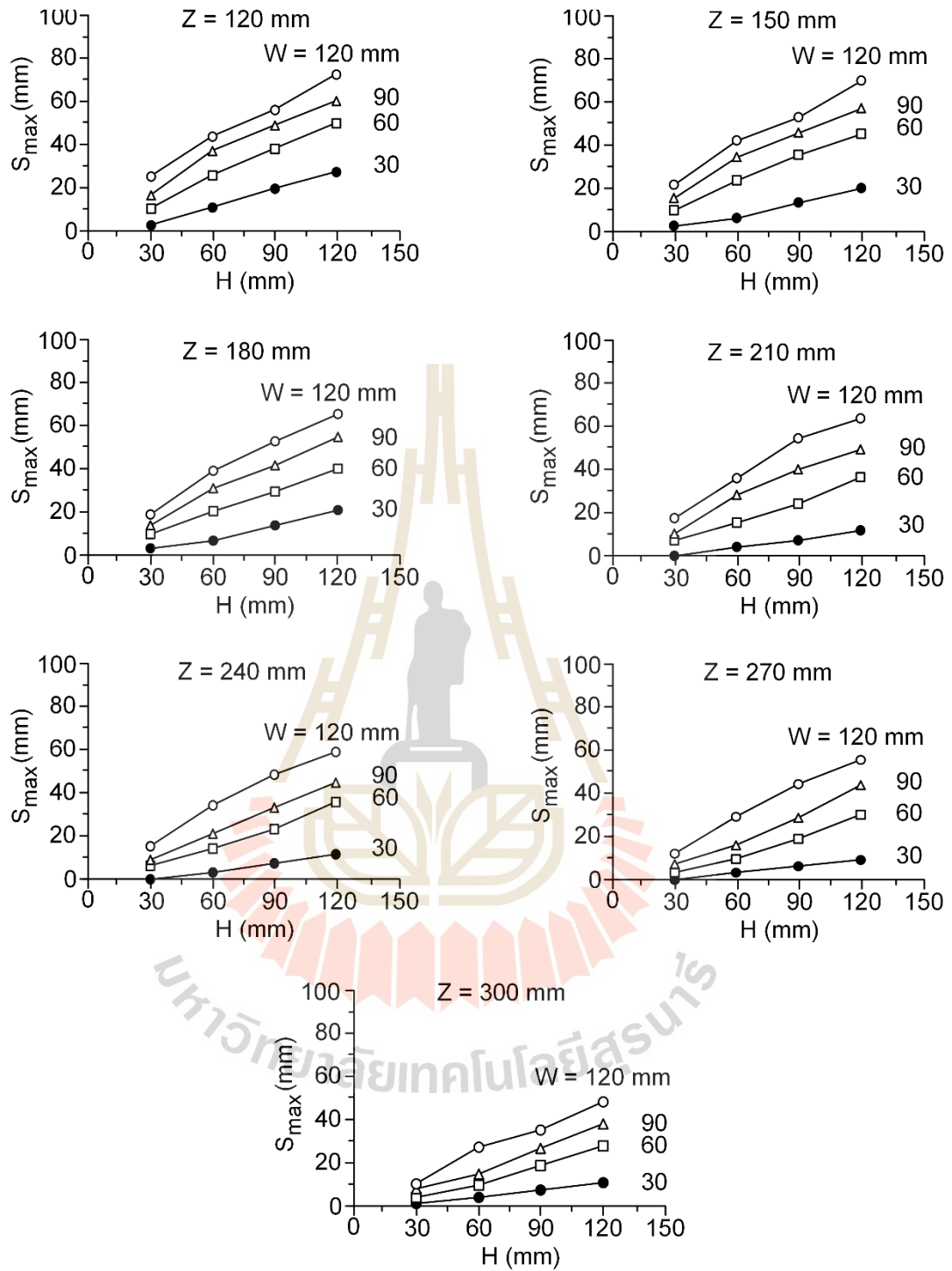
Figure 3.16 Maximum subsidence (S_{max}) as a function of cavity height (H).
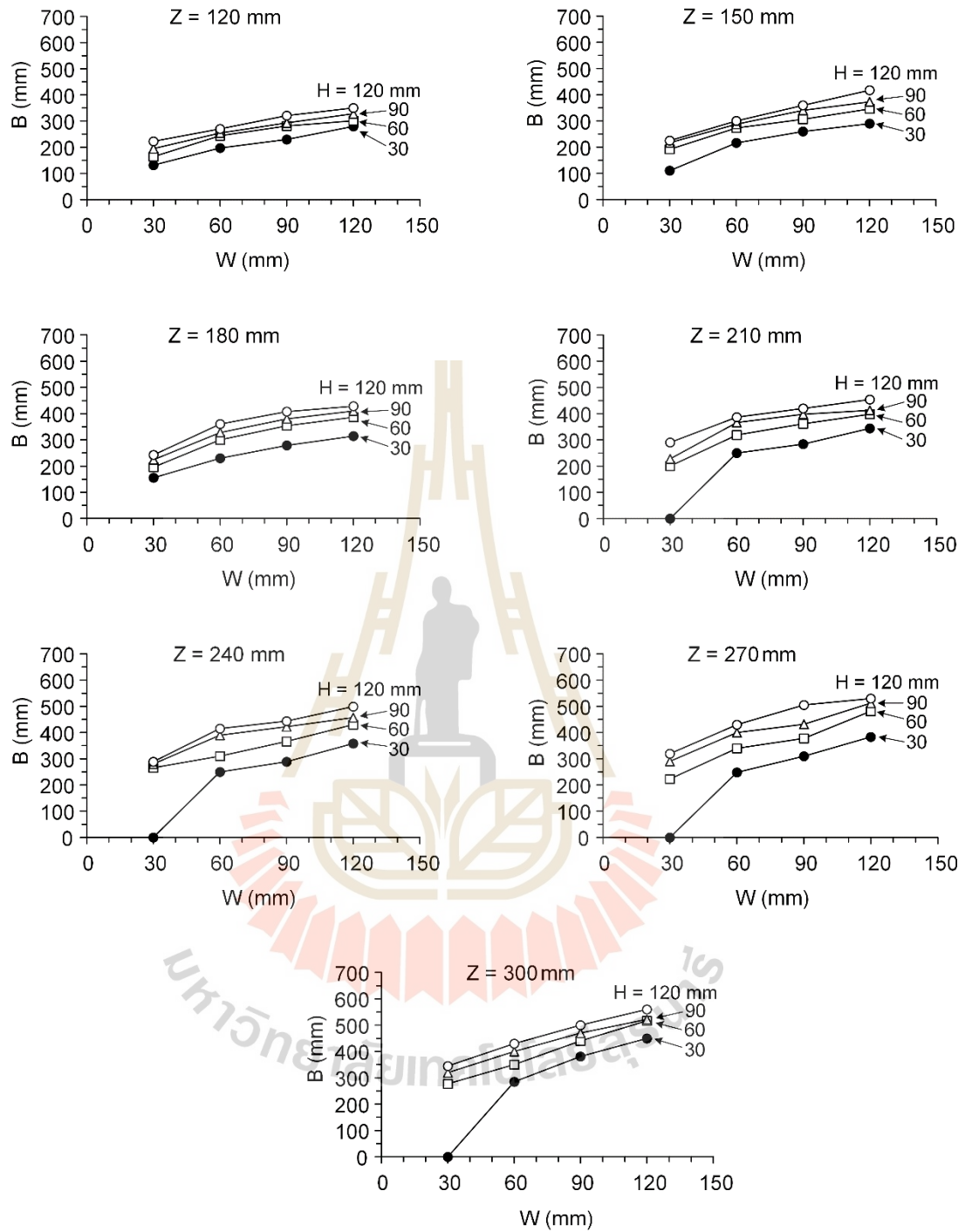
Figure 3.17 Relationship between trough width (B) and cavity width (W).

CHAPTER IV

NUMERICAL SIMULATIONS

4.1   Introduction

Physical model simulation results in the previous chapter suggest the presence of relationship between cavity configurations and subsidence profiles. In order to verify the test results and to allow extrapolating the results beyond the test conditions used in the laboratory, discrete element analysis is performed. This chapter presents the method and results of the numerical analysis using PFC code (Itasca, 2008).

4.2   Discrete Element Analysis

Discrete element model (DEM) using PFC^{2D} (Itasca, 2008) are developed simulate the physical model results. PFC^{2D} is based on the static and dynamic processes and on their internal or contact force (simulated by ABS balls). The particle elements are represented in spherical rigid balls. The contact forces and displacements of the balls are obtained by recognizing the ball movement. Based on a force-displacement law and Newton's law of motion, the forces and displacements are computed for each contact. The propagation movement depends on material properties which is obtained from laboratory testing.

4.2.1   Model Parameters

The input parameters used in the PFC^{2D} model are obtained from those of the physical model tests.   The characteristics of the underground opening and ABS balls overburden are given in Chapter III.   Some important parameters for the simulations of subsidence are described as follows:

- The particle radius is 3 mm,

- The friction angle is 15 degrees,

- The bulk density is 582 kg/m^3,

- The friction coefficient between the balls is 0,

- The normal stiffness (K_n) is 20 GPa/m,

- The shear stiffness (K_s) is 1 GPa/m, and

- The cohesion is effectively zero.

Several friction angles are later assumed varying from 15, 20, 25, 30 to 35 degrees. This is to allow correlating with the actual overburden properties. The assumption of zero cohesion used here is also supported by the experimental results of Barton (1974), Crosby (2007) and Grøneng et al. (2009) who find the cohesion of rock mass comprising claystone, mudstone and siltstone is zero or negligible.

4.2.2 Discrete Element Analyses

The boundaries of the models are simulated based on the boundary conditions of the overburden and the underground opening. All boundaries are smooth and nonrestrictive with regards to material movement. The generated command places particles within the boundary specified such that no overlap occurs. The trials are specified 500,000 – 1,500,000 attempts to add the desired number of particles within the defined area. This method is to achieve the initial equilibrium state, since particles move to large distances to come to rest. Once all of the particles are at rest and the model is at equilibrium, the top of the particle assembly is leveled by deleting all particles above a specified thickness of overburden (Figure 4.1). The command codes define the generation of the overburden model and the boundaries, as well as perform the extraction operations similar to those in the physical models.

After the particles are at rest and the model is at equilibrium as predefined overburden thickness, the wall above the cavity (roof) is deleted to simulate the solution cavern (extraction) of material from each case using the same procedures used in the physical model. The particles continuously flow into the opening floor until the opening completely fill, and hence the surface subsidence is induced. Image overlay techniques are used here to compare the surface profile before and after the subsidence occurs. The trough width is measured at the lateral line detectable subsidence (Figure 4.2). The subsidence of the overburden for both physical and numerical approaches, is governed by gravity. No lateral pressure is applied.
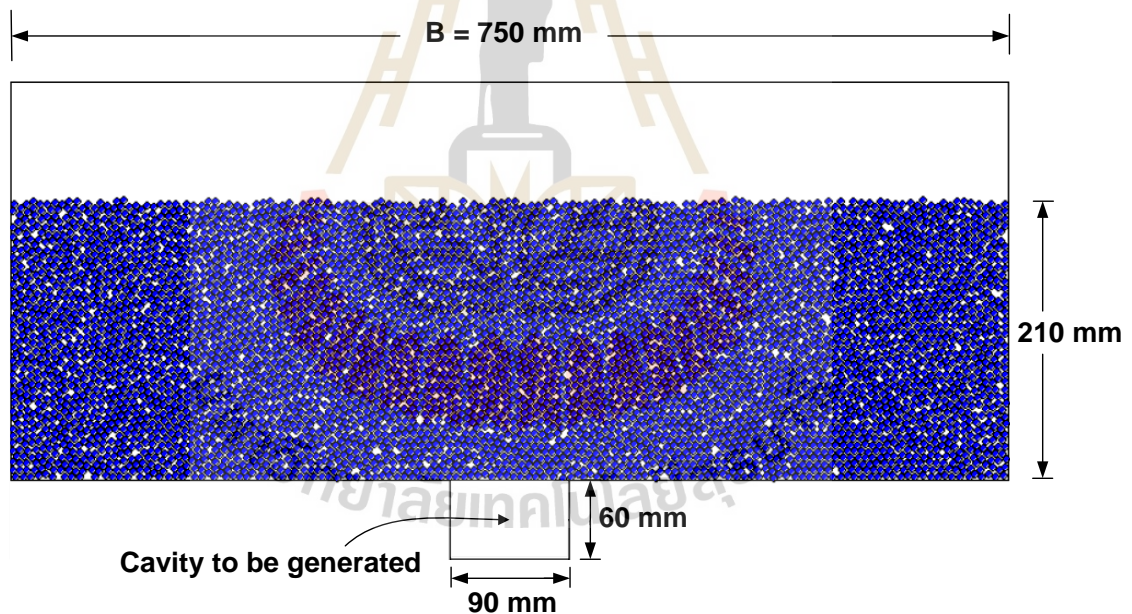
Figure 4.1 Example of PFC2D surface subsidence before cavity is created.
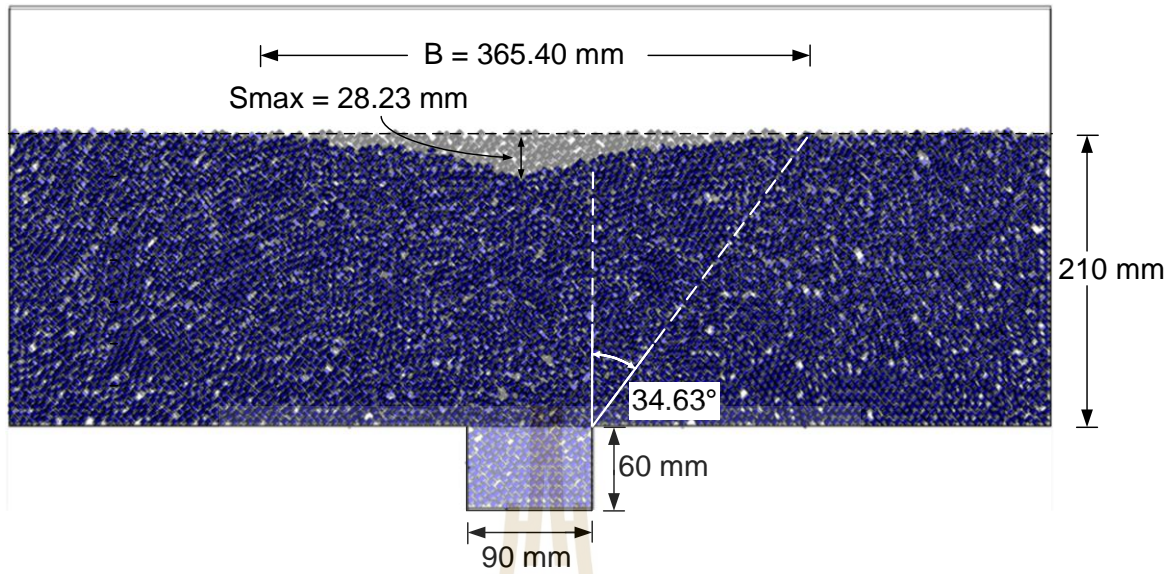
Figure 4.2 Example of PFC^{2D} surface subsidence after cavity has been created.

4.3   Results

Figures 4.3 and 4.4 compare the physical model results with the PFC^{2D} simulations for friction angle of overburden equal to 15 degrees under different cavity depths, height, and width. The maximum subsidence (S_{max}) as a function of cavity height (H) is given in Figure 4.3, and the trough width (B) as a function of cavity width (W) is given in Figure 4.4. Both relations indicate that the S_{max} values tend to be independent of the opening depths. The trough width, however, is dependent of the overburden thickness. The increase of the maximum subsidence closely relates to the increase of cavity height, while the increase of trough width is related to the increase of opening width. The results from PFC^{2D} simulations agree well with those observed from the physical model testing. The close agreement between the numerical simulations and the physical model measurements suggests that the procedure and results of the physical modelling are sufficiently accurate and reliable. The diagrams in Figures 4.3 show that the maximum subsidence is sensitive to cavity height only

for the case of large cavity width (e.g., here W = 120 mm). For narrow cavities, the maximum subsidence is not that sensitive to the cavity height. The effect of cavity width, W, on the trough width, B, tends to act equally among all room height, as suggested by the slope of B-W curves obtained for all depths. Increasing the cavity height induces small increase of the trough width.

The results of varied friction angles from 15,20, 25, 30 to 35 degrees are shown in Figures 4.5 and 4.6 for the depth of 180 mm. The simulation results indicate that the maximum subsidence and trough width decrease with increasing friction angles of overburden material. The effect of friction angle acts more for wide rooms. (e.g., = 120 mm) than for the narrower ones. (Figure 4.5 (a)). Increasing of the overburden friction slightly decreases the trough width, regardless of the room height (H), as shown in Figure 4.5 (b).

Under low friction angles, the maximum subsidence is highly sensitive to the room height (Figure 4.6 (a)). As the friction of the overburden increases, the room height effect reduces. The trough width (B) slightly decreases as the friction angle of the overburden material increases (Figure 4.6 (b)). Such slight reduction of the trough width is observed for all room width. This suggest that the effect of the overburden friction acts more on the magnitude of the maximum subsidence than on the trough width. The effect of the friction angle descended above is also true for all cavity depths as shown in Figure 4.7.
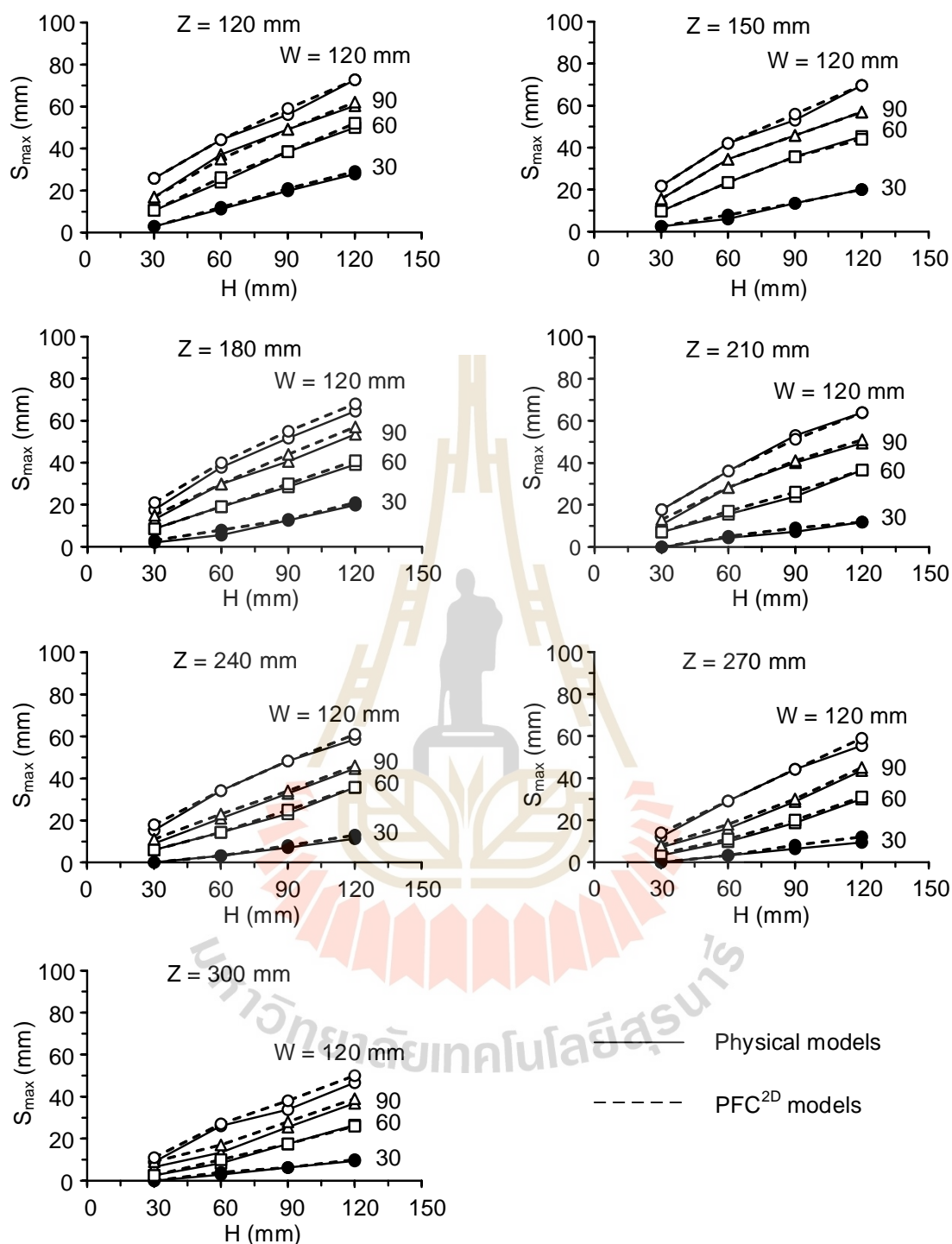
Figure 4.3 Comparisons of maximum subsidence (S_{max}) between physical model results

(solid lines) and PFC model simulations (dash lines).
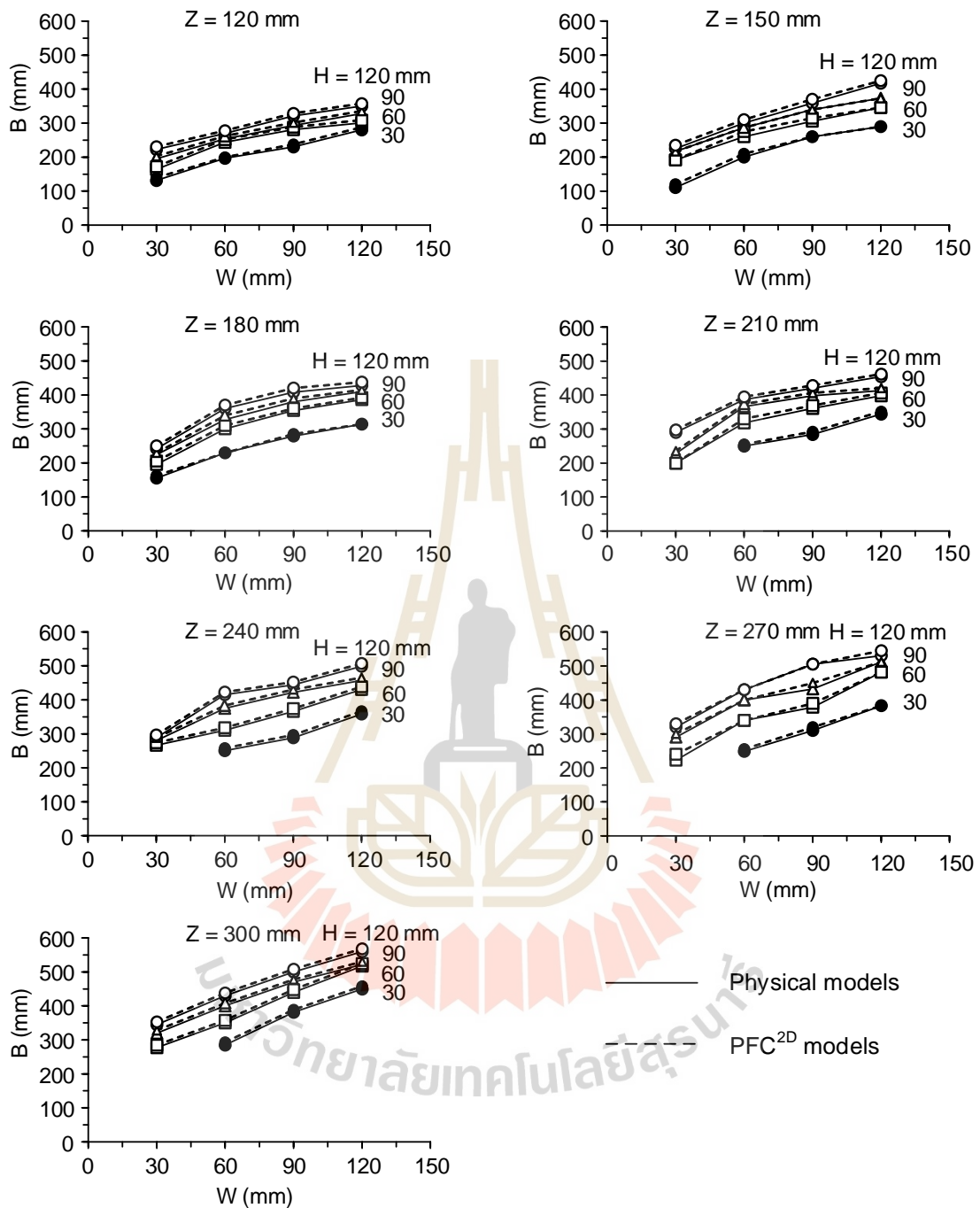
Figure 4.4 Comparisons of trough (B) between physical model results (solid lines) and

PFC model simulations (dash lines).
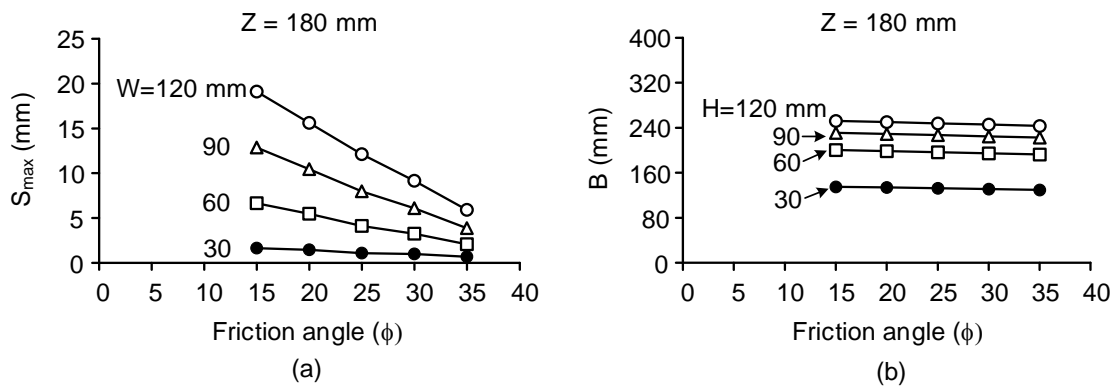
Figure 4.5 Example of the maximum subsidence (S_{max}) as function of friction angle (ϕ) for

cavity height (H) is 30 mm (a), and trough width (B) as function of friction

angle (ϕ) for cavity width (W) is 30 mm (b).
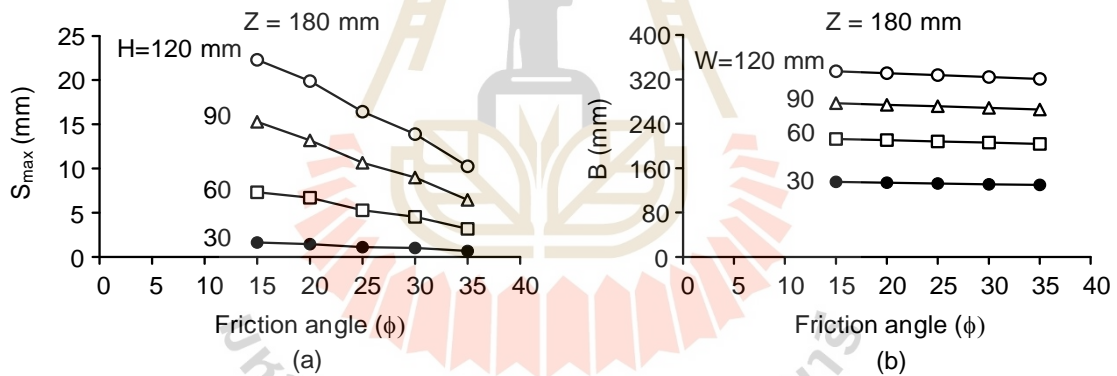
Figure 4.6 Example of the maximum subsidence (S_{max}) as function of friction angle (ϕ) for

cavity height (H) is 30 mm (a), and trough width (B) as function of friction

angle (ϕ) for cavity width (W) is 30 mm (b).
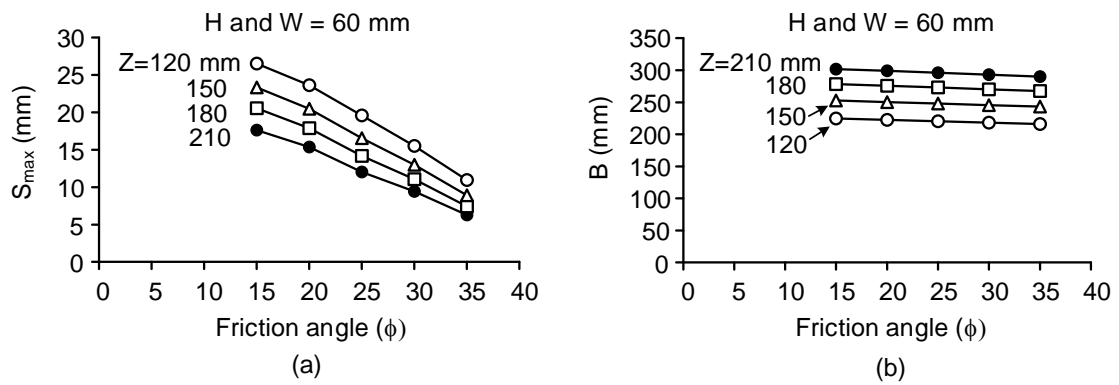
Figure 4.7 Example of the maximum subsidence (S_{max}) as function of friction angle (ϕ) for

cavity height (H) and cavity width (W) is 60 mm.
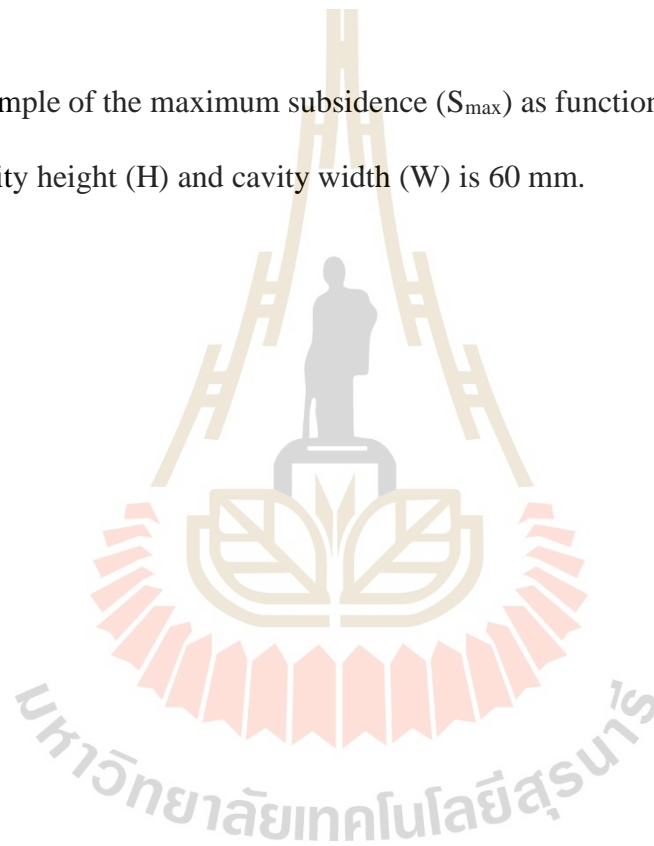
CHAPTER V

MATHEMATICAL RELATIONSHIPS

5.1 Introduction

This chapter describes a method to estimate the geometry of established cavern from subsidence trough configuration. The results from the physical model and numerical simulation are used to derive from subsidence of mathematical relationships between the surface subsidence component and the cavern configurations and overburden properties. The considered variables are the cavity height (H), cavity width (W), maximum subsidence (S_{max}), trough width (B), overburden thickness or cavity depth (Z), and friction angle (ϕ) of overburden material. The empirical equations are developed for the surface subsidence under super-critical conditions.

5.2 Empirical equations

The cavity height (H), cavity width (W), maximum subsidence (S_{max}), trough width (B) and cavity depth (Z) are first equivalented by size of ABS balls (B_s), as shown in Figures 5.1 and 5.2. This approach can isolate the particle size effect, and hence allows us to correlate the modeling results with the actual field condition where the particle sizes of the overburden may be smaller. Table 5.1 shows the equivalent subsidence components with 6 mm particle size. The equivalent cavity height (H_e), cavity width (W_e), maximum subsidence (S_e), trough width (B_e), and cavity depth (Z_e) can be expressed as:

$$H_e = H/B_s \qquad\qquad (5.1)$$

$$W_e = W/B_s \tag{5.2}$$

$$S_e = S_{max}/B_s \tag{5.3}$$

$$B_e = B/B_s \tag{5.4}$$

$$Z_e = Z/B_s \tag{5.5}$$

where B_s is particles size of ABS balls with nominal size 6 mm.

Table 5.1 Equivalent subsidence component.

Z_e	W_e	H_e	S_e	B_e
20	5	5	0.49	21.97
		10	1.76	27.36
		15	3.32	32.50
		20	4.64	37.16
	10	5	1.75	32.83
		10	4.36	40.67
		15	6.41	42.35
		20	7.38	45.00
	15	5	2.81	38.33
		10	6.20	46.83
		15	8.19	48.88
		20	10.07	53.55
	20	5	4.29	46.67
		10	7.35	50.14
		15	9.36	54.67
		20	12.12	58.33

Table 5.1 Equivalent subsidence component (Cont.).

Z_e	W_e	H_e	S_e	B_e
25	5	5	0.42	18.40
		10	1.33	31.93
		15	2.26	36.19
		20	3.33	37.50
	10	5	1.63	36.00
		10	3.91	45.50
		15	5.94	47.83
		20	7.33	50.00
	15	5	2.59	43.33
		10	5.74	51.00
		15	7.64	56.67
		20	9.48	59.83
	20	5	3.62	48.33
		10	7.00	57.70
		15	8.84	62.17
		20	11.60	69.50
30	5	5	0.42	25.83
		10	0.92	32.63
		15	2.10	37.33
		20	3.31	40.33
	10	5	1.42	38.33
		10	3.18	50.00
		15	4.76	54.58
		20	6.53	60.00
	15	5	2.22	46.50
		10	4.99	59.00
		15	6.78	63.33
		20	8.93	68.00
	20	5	2.95	52.33
		10	6.32	64.37
		15	8.62	68.33
		20	10.76	71.33

Table 5.1 Equivalent subsidence component (Cont.).

Z_e	W_e	H_e	S_e	B_e
35	5	5	0	0
		10	0.72	33.25
		15	1.20	37.92
		20	1.98	48.33
	10	5	1.19	41.67
		10	2.59	53.07
		15	4.00	61.00
		20	6.10	64.45
	15	5	1.75	47.33
		10	4.70	60.17
		15	6.67	66.33
		20	8.23	70.00
	20	5	2.94	57.33
		10	6.01	66.33
		15	8.53	68.83
		20	10.65	75.67
40	5	5	0	0
		10	0.54	44.33
		15	1.17	46.67
		20	1.88	48.10
	10	5	0.99	41.67
		10	2.38	51.67
		15	3.86	65.00
		20	5.94	69.17
	15	5	1.50	48.08
		10	3.50	61.00
		15	5.47	70.33
		20	7.45	74.00
	20	5	2.54	59.69
		10	5.69	71.75
		15	8.04	76.17
		20	9.76	83.17

Table 5.1 Equivalent subsidence component (Cont.).

Z_e	W_e	H_e	S_e	B_e
45	5	5	0	0
		10	0.54	37.17
		15	1.05	48.33
		20	1.56	53.27
	10	5	0.54	41.40
		10	1.62	56.67
		15	3.11	66.67
		20	3.95	71.67
	15	5	1.18	51.67
		10	2.68	63.00
		15	4.80	72.00
		20	7.00	84.17
	20	5	2.00	63.87
		10	4.85	80.29
		15	7.37	85.33
		20	9.25	88.33
50	5	5	0	0
		10	0.47	46.17
		15	1.05	53.33
		20	1.56	57.50
	10	5	0.43	47.50
		10	1.38	58.33
		15	2.92	66.67
		20	3.83	71.67
	15	5	1.08	63.50
		10	2.22	73.33
		15	4.24	78.33
		20	6.14	83.33
	20	5	1.49	75.00
		10	4.34	86.15
		15	5.64	87.00
		20	7.78	93.33
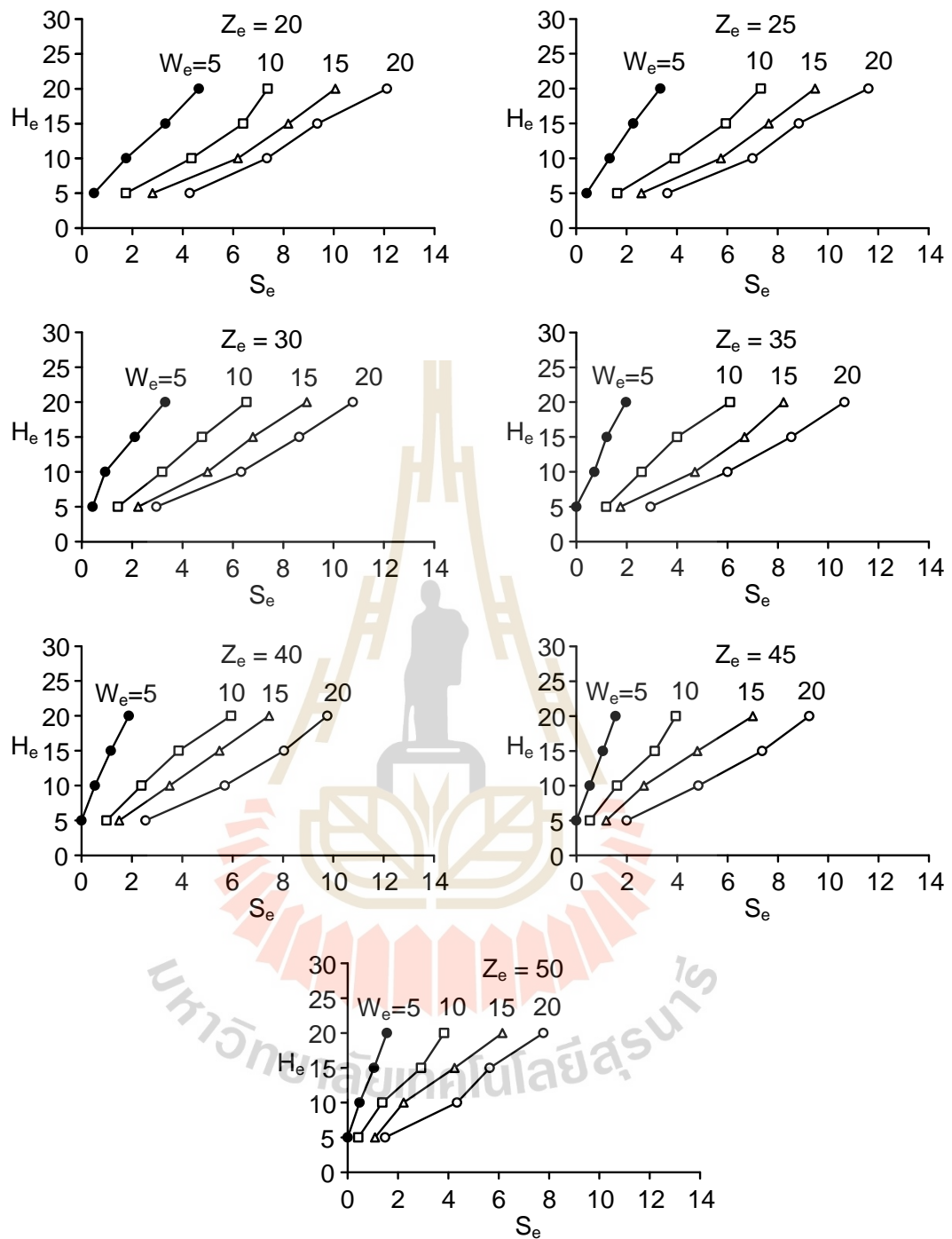
Figure 5.1 Relations of equivalent cavity height (H_e) along with equivalent maximum subsidence (S_e) for different equivalent depth (Z_e).
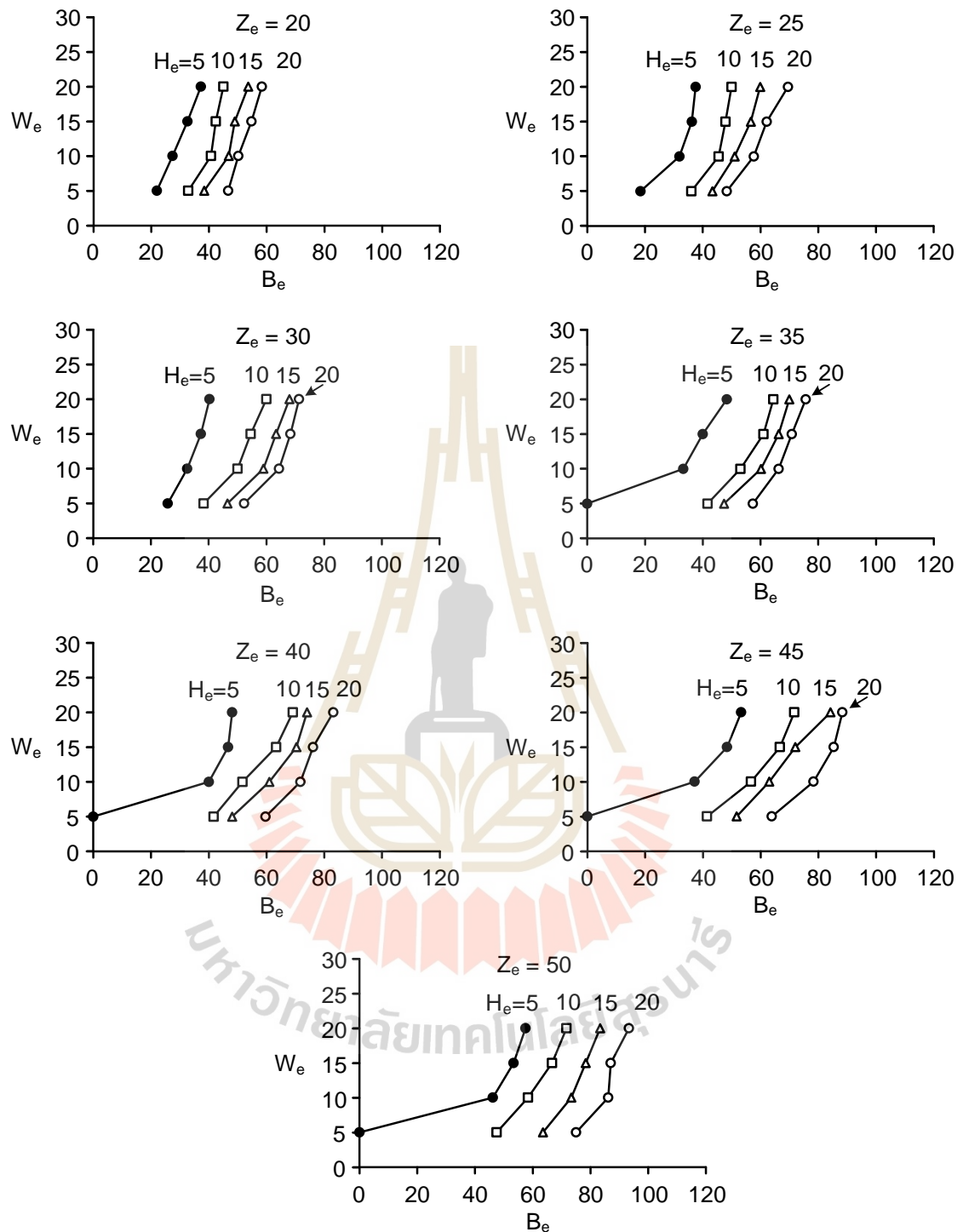
Figure 5.2 Relations of equivalent cavity width (W_e) as a function of equivalent trough width (B_e) for different equivalent depth (Z_e).

Figure 5.3 plots the equivalent cavity height (H_e) as a function of equivalent subsidence which is normalized by the equivalent cavity depth (S_e/Z_e). Empirical equation is proposed to represent the equivalent cavity height as a function of normalized subsidence, as follows:

$$H_e = A \cdot S_e/Z_e{}^B \tag{5.6}$$

where A and B are empirical constants. Regression analyses using SPSS statistical software (Colin and Paul, 2012) are performed to determine these constants. The constant A represents the ultimate slope of the H_e-S_e/Ze relations while B defines their curvatures. It was found that the A and B values could be defined in terms of cavity depth and trough width, as follows:

$$A = \alpha Z_e \cdot (B_e/Z_e)^{\beta} \tag{5.7}$$

$$B = \gamma \cdot (B_e/Z_e) + \delta \tag{5.8}$$

where α, β, γ and δ are empirical constants equal to 32.16, -2.13, 0.53 and 0.69 respectively. Based on linear regression analyses, B parameter is related to the variation of H_e-S_e/Z_e relation, the constants γ and δ are likely depend on the friction angle of the simulated overburden material.

Figure 5.4 shows the equivalent cavity width (W_e) as a function of equivalent trough width that is normalized by the equivalent cavity depth (B_e/Z_e). Similar to the equivalent height in equation (5.6) above, an empirical equation can be proposed to represent the cavity width as a function of normalized subsidence obtained from the physical model results, as follows:

$$W_e = C \cdot (B_e/Z_e)^D \tag{5.9}$$

$$C = \eta Z e \cdot (S_e/Z_e)^\kappa \tag{5.10}$$

$$D = \lambda \cdot \ln (S_e/Z_e) + \nu \tag{5.11}$$

where η, κ, λ and ν are empirical constants, equal to .01, -0.52, -0.19 and 3.45, respectively. The proposed equation can be applied only for large W_e values (overburden particles are much smaller than cavity width).
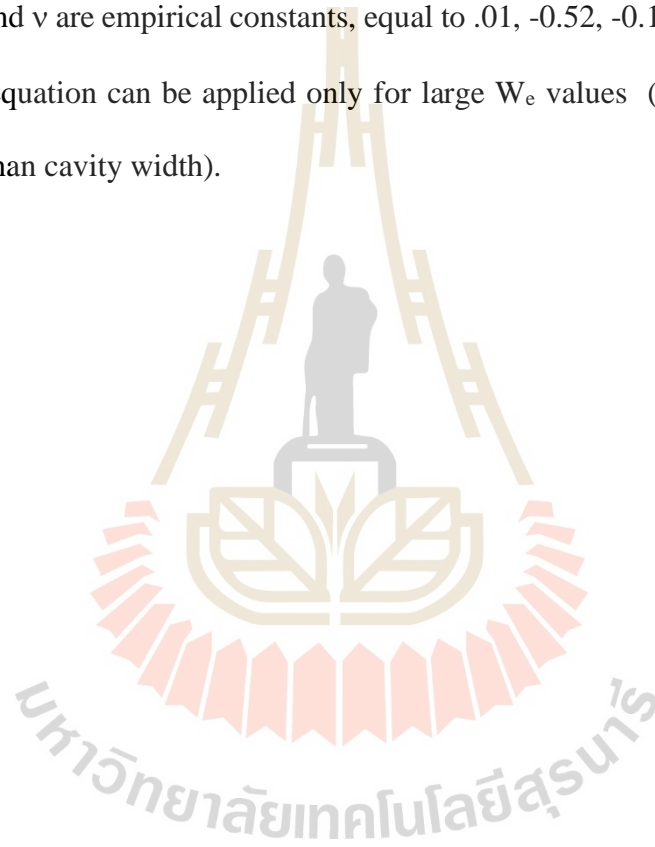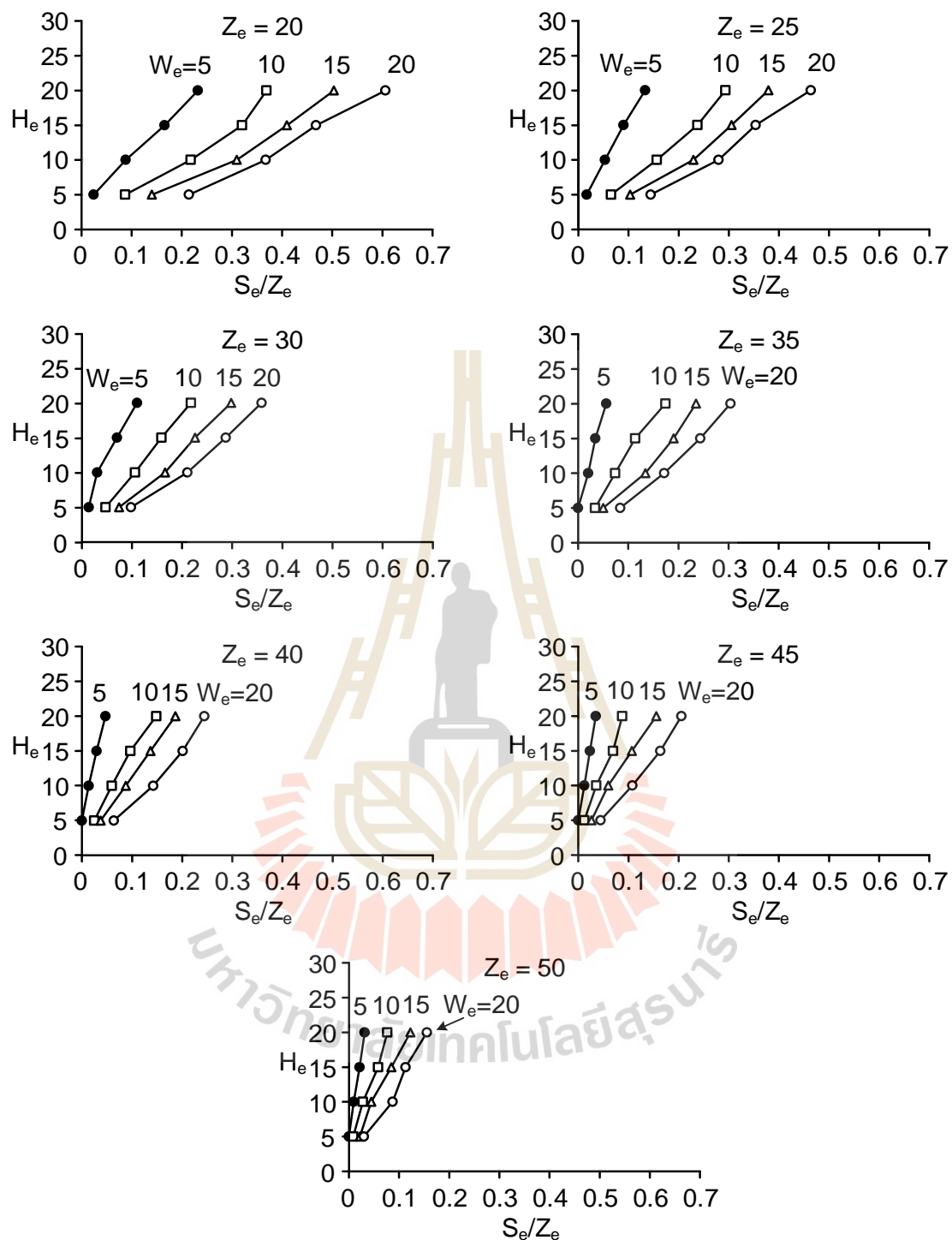
Figure 5.3 Equivalent cavity height (H_e) as a function of normalized maximum subsidence

(S_e/Z_e).
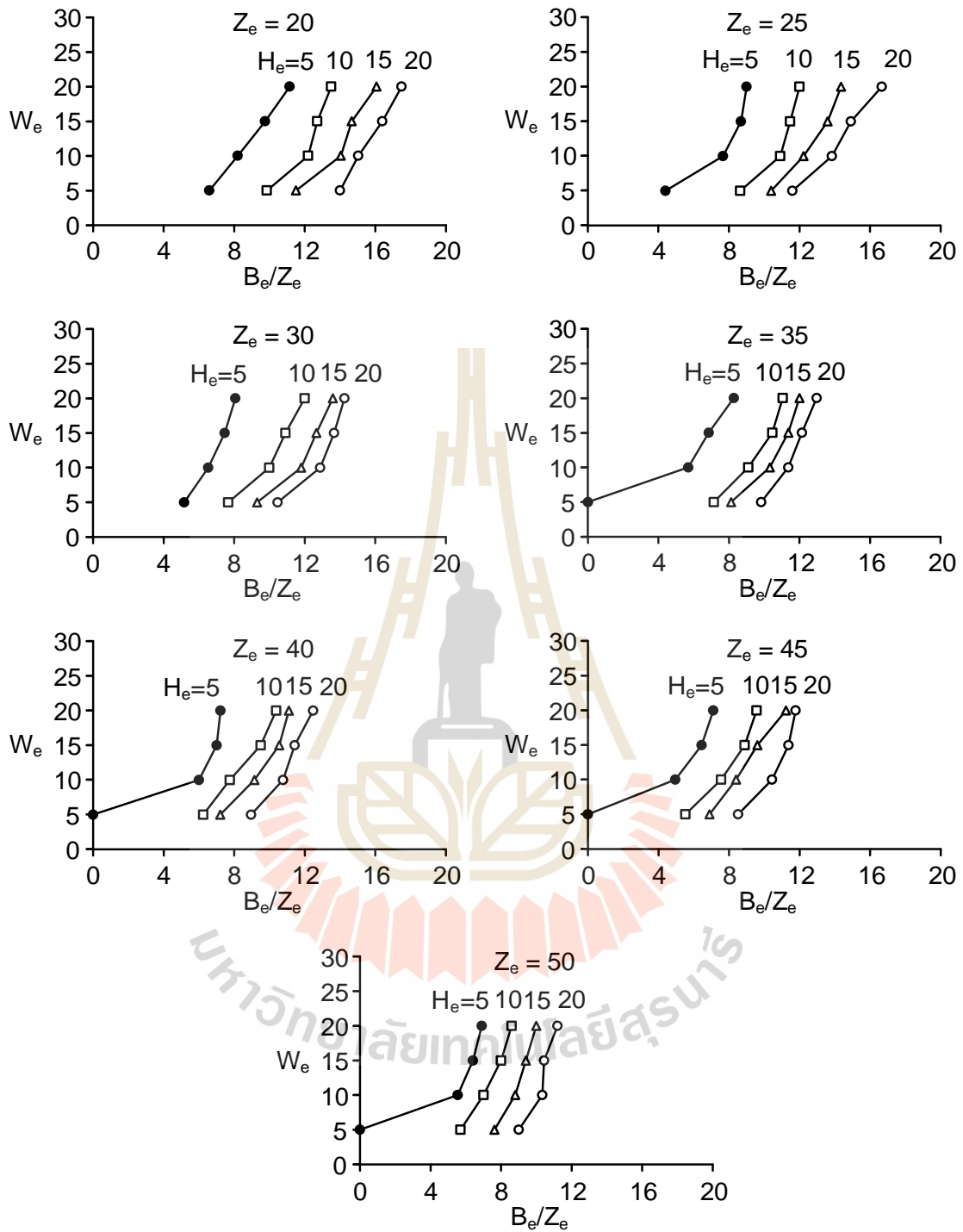
Figure 5.4 Equivalent cavity width (W_e) as a function of normalized trough width (B_e/Z_e).

5.3   Overburden Properties Considerations

To find the relationship between the empirical constants in the equations above and the overburden properties, series of numerical simulations are performed using the particle friction angles varying from 15,20, 25, 30 to 35 degrees. Figure 5.5 compares the numerical model results with the predictions given by equations (5.6) to (5.7). The equivalent cavity height (H_e) as a function of normalized maximum subsidence (S_e/Z_e) for various normalized cavity widths (B_e/Z_e) obtained from the equations agrees well with those numerical simulations. For each width, the cavity height increases with the maximum subsidence S_e/Z_e, which can be described by the power equation. Figures 5.6 and 5.7 show the constants γ and δ from equation (5.7) as a function of friction angles. It is found that the empirical constants γ and δ depend on the friction angles (ϕ) of the overburden which can be described by a linear equation:

$$\gamma = -0.0194(\phi) + 0.815 \tag{5.12}$$

$$\delta = 0.0104(\phi) + 0.538 \tag{5.13}$$

where ϕ used in the computer simulations are 15,20, 25, 30, and 35 degrees. Figures 5.8 and 5.9 show the equivalent cavity height as a function of normalized maximum subsidence for various normalized cavity widths at friction angles of 15 and 30 degrees. The diagrams show that under same cavity, higher friction angle of overburden will result in a lower maximum subsidence on ground surface.

The equivalent cavity width (W_e) increases with increasing normalized trough width (B_e/Z_e) based on the results of physical models for overburden friction angle of 15 degrees, as shown in Figure 5.10. Similar to the equivalent cavity width equations above, the

equivalent cavity height can be expressed as a function of S_e/Z_e. The friction angle of the overburden would affect the trough width only when the equivalent cavity width is small.

It should be noted that the maximum subsidence and trough width in the equations above are normalized by the equivalent cavity depth. The depth of the solutioned cavities is usually known from the depth of the pumping wells used to draw the brine directly above the salt bed.
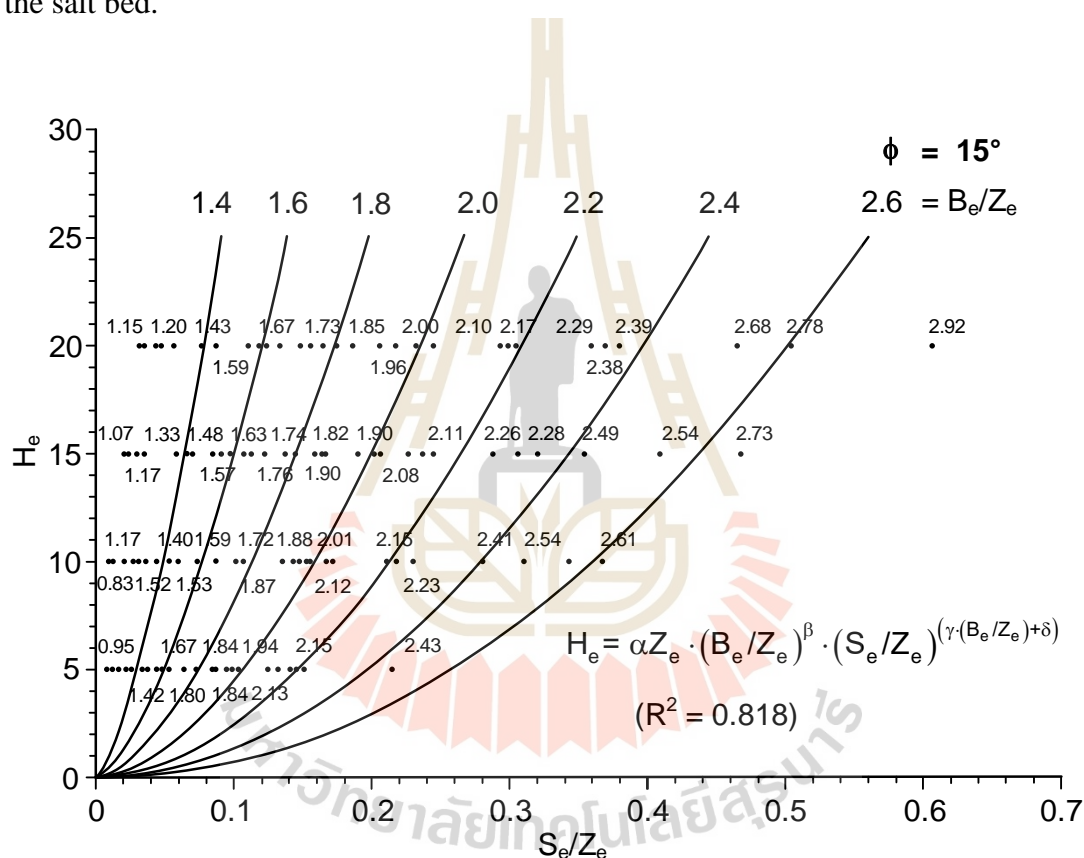
Figure 5.5 Curve fits for equivalent cavity height (H_e) compared with results of physical models.

ϕ	γ
15°	0.53
20°	0.41
25°	0.34
30°	0.24
35°	0.13

$\gamma = -0.0194(\phi) + 0.815$

$(R^2 = 0.994)$

Figure 5.6 Constant γ as a function of friction angle (ϕ).

ϕ	δ
15°	0.69
20°	0.76
25°	0.78
30°	0.86
35°	0.90

$\delta = 0.0104(\phi) + 0.538$

$(R^2 = 0.976)$
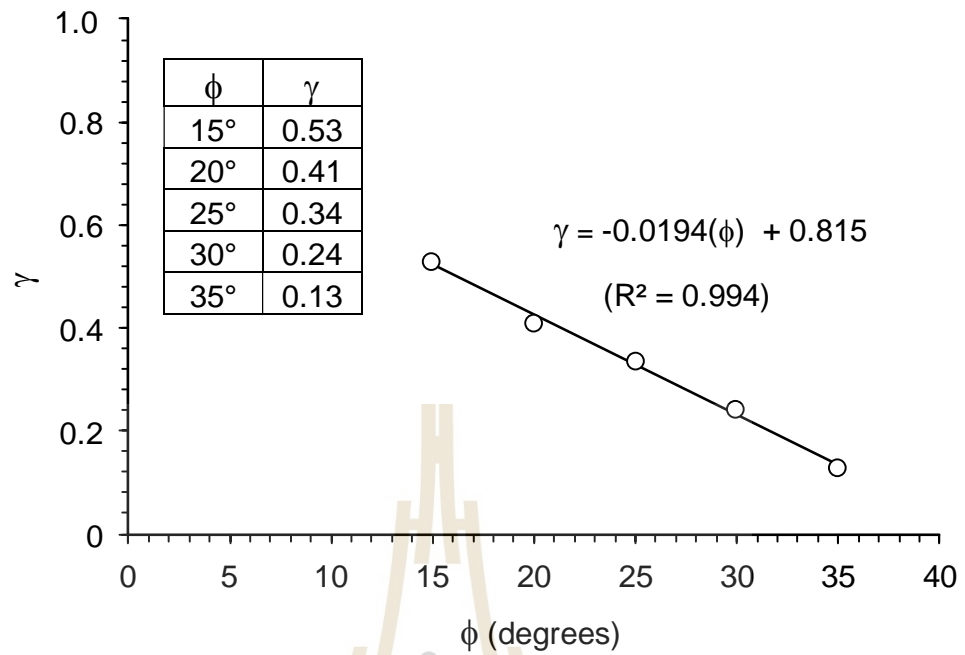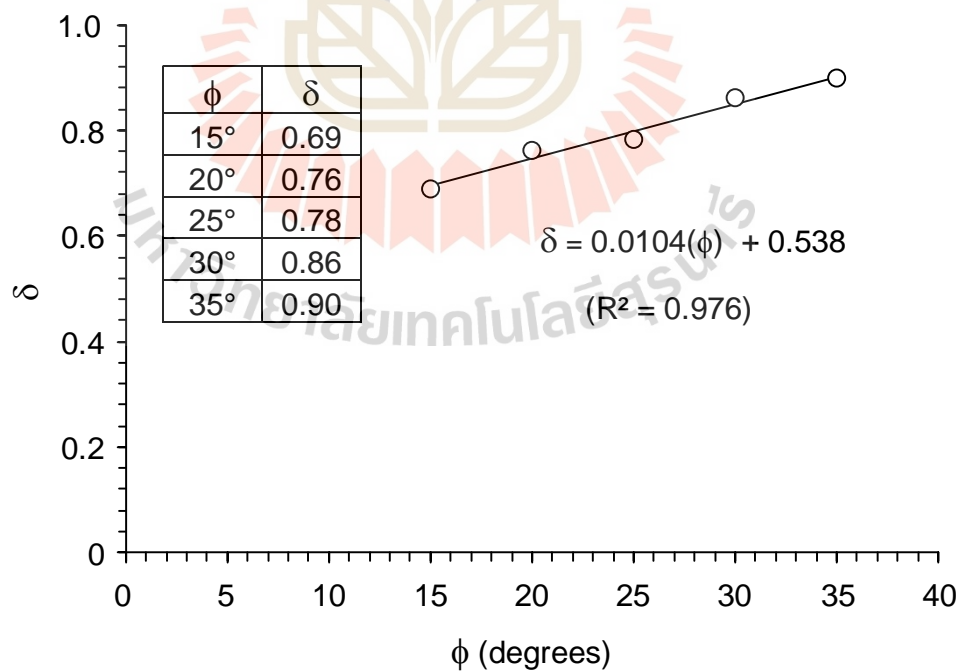
Figure 5.7 Constant δ as a function of friction angle (ϕ).
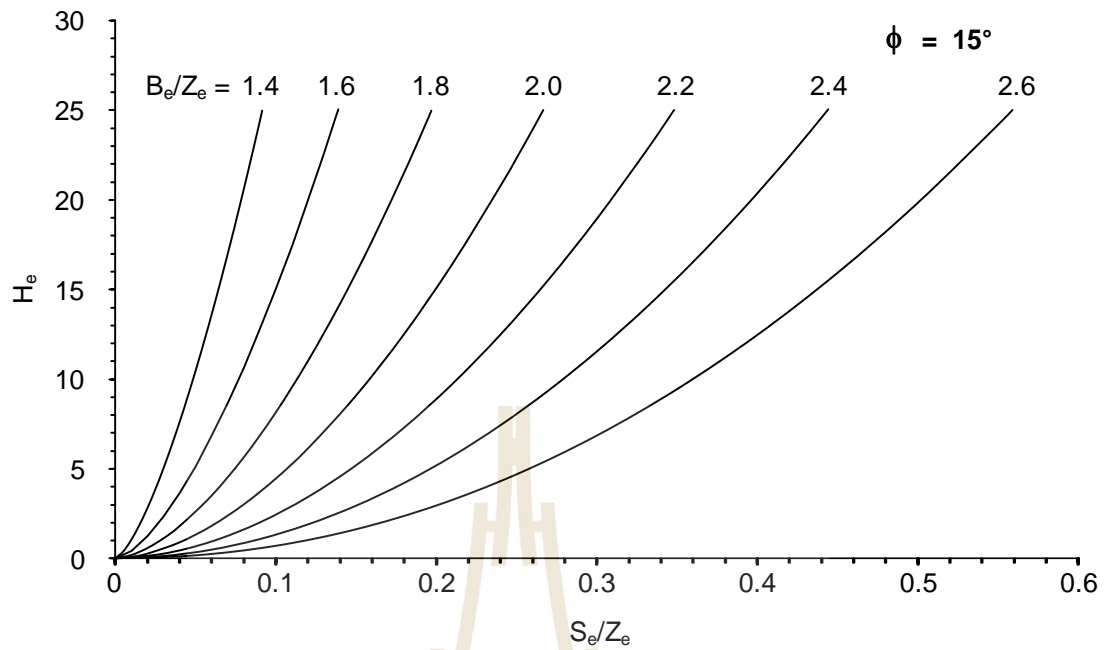
Figure 5.8 Curve fits for equivalent cavity height (H_e) with the computer simulations of friction angle 15 degrees.
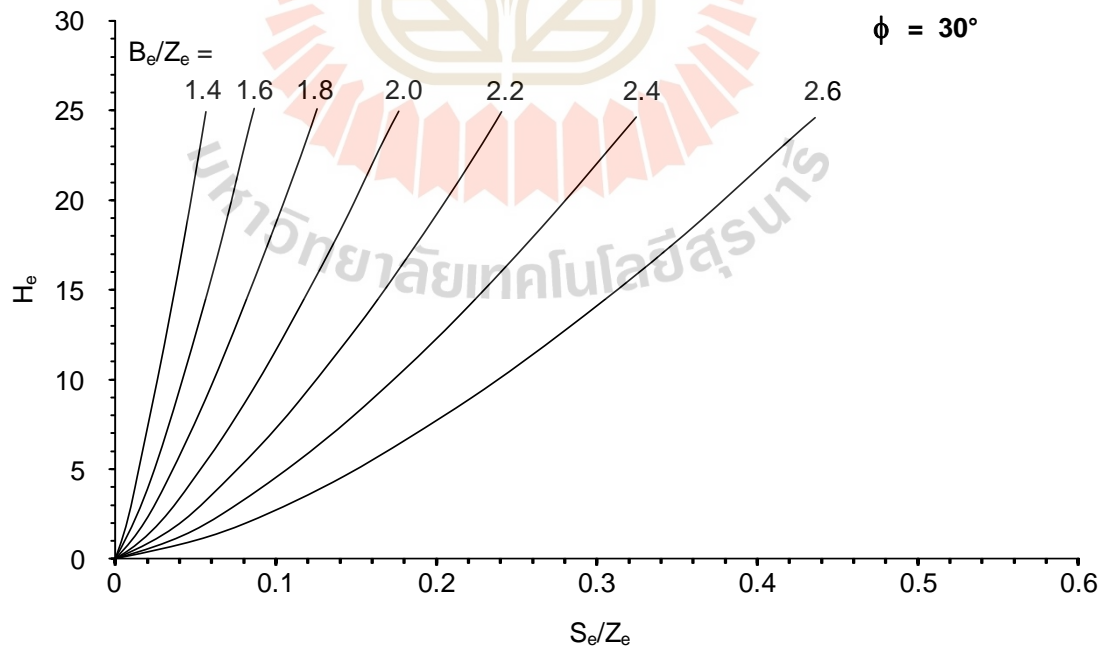
Figure 5.9 The fitting for equivalent cavity height (H_e) with the computer simulations of friction angle 30 degrees.
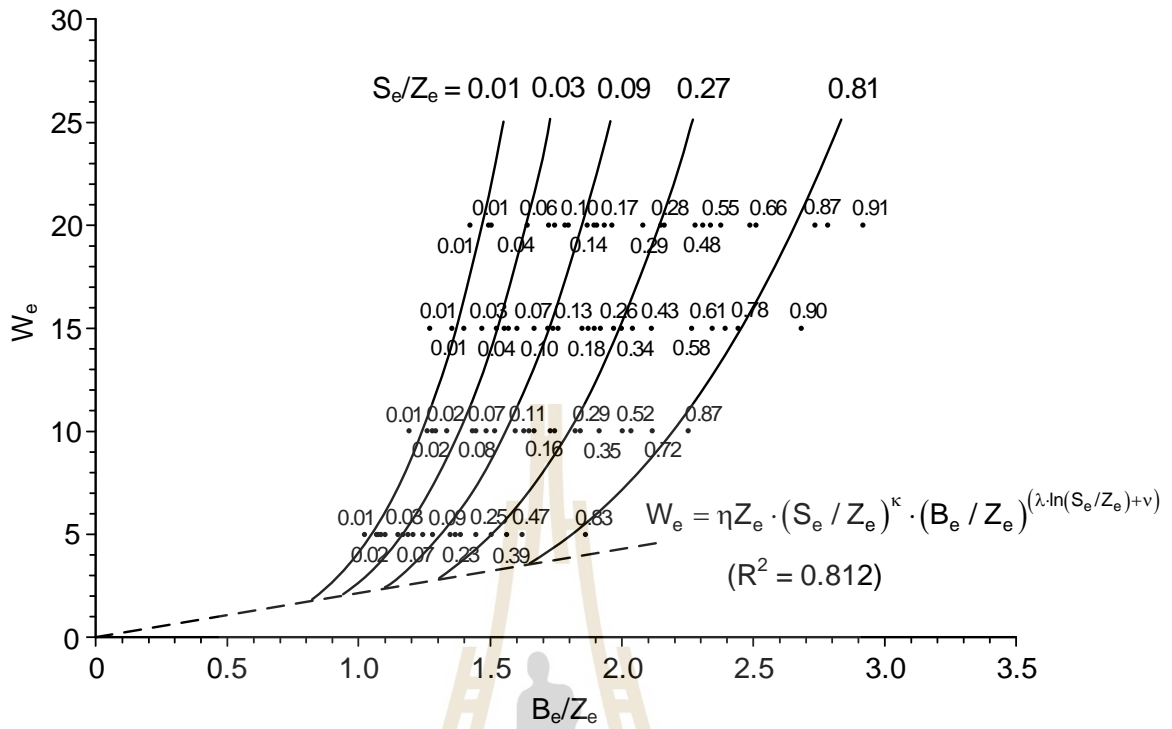
Figure 5.10 Curve fits for equivalent cavity width (W_e) compared with the computer simulations (point).

CHAPTER VI

DISCUSSIONS AND CONCLUSIONS

6.1 Discussions

This study has been focused on subsidence under super-critical condition. Physical and numerical models are performed to simulate subsidence induced by underground openings. Comparisons of the results and experimental findings from other researchers have been made.

The results from PFC^{2D} simulations closely agree well with the measurements from the physical modelling, suggesting that the test results are sufficiently reliable. The collapse of the cavern roof and overburden is dictated by the cavern height. The failure of the cavity roof can occur under the super-critical condition when the cavity height is however significantly greater than the critical roof deformation. The test results obtained here agree reasonably well with those of Thongprapha et al. (2015) and Saoanunt et al. (2019) who study the surface subsidence above void opening using clean gravel. The advantage of using ABS balls are that minimizes shape effect of gravel and it can reusable with unchanged properties. The maximum subsidence depends on the geometry of cavern and properties of overburden. For very narrow cavities at great depths, the maximum subsidence (S_{max}) is insensitive to height of the cavity. These results are consistent with McCay et al. (2018) and Singh and Yadav (1992) who suggest that the surface subsidence in controlled in part by the thickness of overburden. The trough width (B) is sensitive to the cavity depth (Z). This observation complies with the conclusion drawn by Singh (1992) that the extent of the settlement area increases with cavity width (W).

The results obtained from this study indicate that the friction angle affects the surface subsidence. Figures 4.6 - 4.8 show that for the same cavity geometry, higher friction angle of the overburden will result in a lower maximum subsidence on the ground surface. This agrees with the conclusion drawn by Thongprapha et al. (2015), Saoanunt et al. (2019), Bobet (2001), Al-Halbounil et al. (2018) and Zhang et al. (2018). The trough width tends to be independent of the overburden friction angle because the friction angle can affect cavern roof failure but does not control magnitude of trough width under supercritical condition. This postulation agrees with those of Singh (1992) that under super-critical condition, trough width is mainly governed by cavity width, not by the overburden properties.

Normalizing a series of lengths to size of particles ensures that there are not affected by scaling factors as absolute values are now converted to ratios. The equations are obtained from combining the physical models and numerical simulations (S_{max}, and B) to determine the mathematical relationships. All results are equivalented by size of ABS balls to isolate the effect of particle size (see equations 5.1-5.5) and normalized cavity depths. The normalization is also performed to isolate the particle size effect. The equivalent cavity height (H_e) and equivalent opening width (W_e) can be described by power equation. From equation (5.6), parameter B depends on the friction angle of the overburden, as shown in equations (5.12) and (5.13). This finding can be concluded that the friction angle is sensitive to the cavity height but not the cavity width. The proposed equations 5.6 and 5.9 can be used individually to estimate the cavity height and cavity width. H_e is largely governed by the maximum subsidence, while W_e is controlled by trough width (B), as suggested by the physical model results. The test results are considered reliable as evidenced by the strong correlation coefficients ($R^2 > 0.8$) obtained from the empirical equations.

Even though the effect of particle size has been not studied here because of limitation of material and device but by normalizing and equivalating methods allows us to compare

results from very different geometry size. Some discrepancies remain from of the H_e and W_e estimated by Saoanunt et al. (2019) . This is due to fact that their tested sand mass has cohesion of 15 kPa which has been incorporated into their analysis, while our ABS ball mass has zero cohesion.

Figure 5.10 shows the limit of the finding which is defined as dash line under the lowest W_e, No-bridging has been observed due to limitation of ABS ball and trapdoor device. Below this limit, the discrepancy could be minimized or eliminated if more test is available. However, for predicting actual salt cavity overlain by silty-sand layer, the W_e and B_e values are significantly larger than those used in the physical and numerical simulations. Even if minimizing the effect of angularity and roundness has provided satisfactory results. However, other issues such as particle size effect and cavity enlargement should be considered further to describe limitations of the equation, which is more related to the flowing characteristics of the particles above the cavity.

The proposed mathematical equations may be used for preliminary design of the cavern height and width of Maha Sarakham formation, based on the subsidence trough size and shape and the friction angle of the overburden materials in super-critical condition. However, given that geological conditions can vary from one site to another, the depth and particle sizes of the overlying soil should be known. This study may also assist to predict unseen cavities after sinkhole occurred. Subsequently, remedial measure may be implemented to minimize the impact and determine the restoration plan.

6.2   Conclusions

All objectives and requirements of this study have been met. This study focused on relationship between surface subsidence and various cavity configuration. The results of the physical models, numerical simulations and empirical equations can be concluded as follows:

- The close agreement is obtained between the physical models and numerical simulations. Both methods indicate that the increase of the maximum subsidence closely relates to the increase of cavity height (see Figure 4.4).

- The maximum subsidence increases with increasing cavity height and tends to approach a limit when the cavity depth to width ratio is 7.

- The magnitudes of trough width increase with increasing cavity width and depth (see Figure 4.5).

- Empirical equations defining the relationship between the cavity geometry and subsidence components with normalization by particle size are proposed by power relation (see equation (5.6) and (5.9)).

- The results obtained from the numerical simulations (PFC^{2D}) of the varied friction angles of overburden material from 15 to 35 degrees indicate that the surface subsidence magnitudes decrease with increasing the friction angle (see Figure 4.7(a)), while trough width tend to be insensitive to friction angle (see Figures 4.6 – 4.8)

- The effect of overburden friction angle can be observed from the numerical simulation. Their linear relation can be described as equations (5.12) and (5.13)

6.3   Recommendations for future studies

The uncertainties and adequacies of the study and results discussed above lead to the recommendations for future studies.

- The effect of topography and inclination of contact surface should also be studied.

- The effect of vertical and horizontal stresses on subsidence trough should be studied for each overburden thickness.

- The groundwater effect (buoyancy force) should be assessed by physical and numerical simulations. The density of the ABS balls should not be neglected.

- The overburden material with different friction angle should be tested to confirm the empirical equations proposed here.

- Different particles sizes should be used in the physical model to study the behavior of surface subsidence under various equivalent variables.

- Comparison of the predictions using the proposed equations with the actual in-situ conditions are desirable to enhance the applicability of the findings obtained here.

REFERENCES

Adachi, T., Kimura, M., and Kishida, K. (2003). Experimental study on the distribution of earth pressure and surface settlement through three-dimensional trapdoor tests. **Tunnelling and Underground Space Technology**. 18: 171-183.

Alejano, L R., Ramirez-Oyanguren, P., and Taboada, J. (1999). FDM predictive methodology for subsidence due to flat and inclined coal seam mining. **International Journal of Rock Mechanics and Mining Sciences**. 36: 475-491.

Al-Halbouni, D., Holohan, E., Taheri, A., Schöpfer, M., Emam, S., and Dahm, T. (2018). Geomechanical modelling of sinkhole development using Distinct Elements: Model verification for a single void space and application to the Dead Sea area. **Solid Earth.** 9:1341-1373

Asadi, A., Shahriar, K., Goshtasbi, K., and Najm, K. (2005). Development of new mathematical model for prediction of surface subsidence due to inclined coal-seam mining. **Journal of the Southern African Institute of Mining and Metallurgy.** 105(11): 15-20.

ASTM D3080/D3080M-11 (2011). **Standard Test Method for Direct Shear Test of Soils Under Consolidated Drained Conditions.** Annual Book of ASTM Standards, American Society for Testing and Materials, West Conshohocken, PA.

ASTM D422–63. (2007). **Standard Test Method for Particle-Size Analysis of Soils.** Annual Book of ASTM Standards, American Society for Testing and Materials, West Conshohocken, PA.

Atkinson, J. H. and Potts, D. (1977). Subsidence above shallow tunnels in soft ground. **Journal of the Geotechnical Engineering Division.** 103(4): 307-325.

Attewell, P. B. (1977). Ground movements caused by tunnelling in soil. Cardiff J.D. Geddes (Ed.), In **Proceedings of the first Conference on Large Ground Movements and Structures** (pp. 812–948). Pentech Press, London

Bahuguna, P. P., Srivastava, A. M. C., and Saxena N. C. (1991). A critical review of mine subsidence prediction methods. **Mining Science and Technology**. 15: 369-382.

Barton, N. R. (1974). **A Review of The Shear Strength of Filled Discontinuities in Rock.** Norwegian Geotechnology Institute of Oslo. pp. 105.

Bobet, A. (2001). Analytical solutions for shallow tunnels in saturated ground. **Journal of Engineering Mechanics.** 127(12): 1258-1266.

Caudron, M., Emeriault, F., Kastner, R., and Al Heib, M. (2006). Sinkhole and soil-structure interaction: Development of an experimental model. In **Proceedings of International Conference on Physical Modeling in Geotechnics** (pp. 1261-1267). Hong-Kong.

Chi, S.Y., Chern, J. C., and Lin, C. C. (2001). Optimized back-analysis for tunnelinginduced ground movement using equivalent ground loss model. **Tunnelling and Underground Space Technology**. 16(3): 159-165.

Chou, W. I. and Bobet, A. (2002). Predictions of ground deformations in shallow tunnels in clay. **Tunnelling and Underground Space Technology.** 17(1): 3-19.

Crosby, K. (2007). Integration of rock mechanics and geology when designing the Udon South sylvinite mine. In **Proceedings of the First Thailand Symposium on Rock Mechanics** (pp. 3-22). Nakhon Ratchasima: Suranaree University of Technology. Thailand.

Cundall, P.A. and Strack, O. D. L. (1979). A discrete numerical model for granular assemblies. **Geotechnique.** 29(1): 107-116.

Einstein, H.H. and Schwartz, C.W. (1979). Simplified analysis for tunnel supports. **Journal of the Geotechnical Engineering Division.** 105(4): 499-518.

Fuenkajorn, K. (2002). Design guideline for salt solution mining in Thailand. **Research and Development Journal of the Engineering Institute of Thailand.** 13(1): 1-8.

Fuenkajorn, K. and Aracheeploha, S. (2010). Prediction of cavern configurations from subsidence data. **Engineering Geology.** 110: 21-29.

Galli, G., Grimaldi, A., and Leonardi, A. (2004). Threedimensional modeling of tunnel excavation and lining. **Computers and Geotechnics.** 31: 171-183.

Ghabraie, B., Ren, G., Zhang, X., and Smith, J. (2015). Physical modelling of subsidence from sequential extraction of partially overlapping longwall panels and study of substrata movement characteristics. **International Journal of Coal Geology.** 140: 71-83.

Gonzales, C. and Sagesta, C. (2001). Patterns of soil deformation around tunnels. Application to the extension of the Madrid Metro. **Computers and Geotechnics.** 28: 445-468.

Grøneng, G., Nilsen, B., and Sandven, R. (2009). Shear strength estimation for Åknes sliding area in western Norway. **International Journal of Rock Mechanics and Mining Sciences.** 46(3): 479-488.

Guo, W., Zhao, G., Bai, E., Guo, M., and Wang, Y. (2021). Effect of overburden bending deformation and alluvium mechanical parameters on surface subsidence due to longwall mining. **Bulletin of Engineering Geology and the Environment.** 80(3): 2751-2764

Han, X. and Li, N., and Standing, J.R. (2007). An adaptability study of Gaussian equation applied to predicting ground settlements induced by tunneling in China. **Rock and Soil Mechanics.** 28: 23-28.

Hawkes, T. P. (2010). **A Simple Aprroach to Subsidence Prediction Above Longwall Mines.** Brigham Toung University. Utah, United States.

Helm, P. R., Davie, C.T., and Glendinning, S. (2013). Numerical modelling of shallow abandoned mine working subsidence affecting transport infrastructure. **Engineering Geology.** 154: 6-19.

Hood, M., Ewy, R.T., and Riddle, L.R. (1983). Empirical methods of subsidence prediction- a case study from Illinois. **International Journal of Rock Mechanics and Mining Sciences & Geomechanics.** 20(4): 153-170.

Itasca, (2008a), **PFC²ᴰ–Particle Flow Code in 2 Dimensions, Version 4.0**, User Manual, Itasca Consulting Group Inc., Minnespolis, MN, USA.

Itasca, (2008b), **User manual for PFC3D–Particle Flow Code in 3 Dimensions, Version 4.0**, Itasca Consulting Group Inc., Minnespolis, MN, USA.

Jenkunawat, P. (2005). Results of drilling to study occurrence of salt cavities and surface subsidence Ban Non Sabaeng and Ban Nong Kwang, Amphoe Ban Muang, Sakon Nakhon. **International Conference on Geology, Geotechnical and Mineral Resources of Indochina (GEOINDO 2005)** (pp. 259-267). Khon Kaen University. Thailand.

Ju, M., Li, X., Yao, Q., Liu, S., and Wang, X. (2007). Effect of sand grain size on simulated mining-induced overburden failure in physical model tests. **Engineering geology**. 226: 93-106.

Li, X. Q. and Zhu, C. C. (2007). Numerical Analysis on the Ground Settlement Induced by Shield Tunnel Construction. **Journal of Highway and Transportation Research and Development (English Edition).** 2(2): 73-79.

Li, Z. and Wang, J. (2011). Accident investigation of mine subsidence with application of particle flow code. **Procedia Engineering.** 26: 1698–1704.

Lisjak A. and Grasselli G., (2014). A review of discrete modelling techniques for fracturing process in discontinuous rock masses. **Journal of Rock Mechanics and Geotechnical Engineering.** 6: 301-314.

Liu, Y., Zhou, F., Liu, L., Liu, C., and Hu, S. (2011). An experimental and numerical investigation on the deformation of overlying coal seams above double-seam extraction for controlling coal mine methane emissions. **International Journal of Coal Geology.** 87: 139 – 149.

Loganathan, N., and Poulos, H. (1998). Analytical prediction for tunneling-induced ground movements in clays. **Journal of Geotechnical and Geoenvironmental Engineering.** 124(9): 846-856.

Lokhande, R.D., Murthy, V.M.S.R., and Singh, K.B. (2014). Predictive models for pot-hole depth in underground coal mining–some Indian experiences. **Arabian Journal of Geosciences.** 7(11): 4697–4705.

Mair, R. J., Taylor, R. N., and Bracegirdle, A. (1993). Subsurface settlement profiles above tunnels in clays. **Geotechnique.** 43(2): 315–320.

Meguid, M.A., Saada, O., Nunes, M.A., and Mattar, J. (2008). Physical modeling of tunnels in soft ground: A review. **Tunnelling and Underground Space Technology**. 23: 185-198.

McCay, A.T., Valyrakis, M., and Younger, P.L. (2018). A meta-analysis of coal mining induced subsidence data and implications for their use in the carbon industry. **International Journal of Coal Geology.** 192: 91-101.

McNearny, R.L. and Barker, K.A. (1998). Numerical modeling of large-scale block cave physical models using PFC2D. **Mining Engineering.** 50(2): 72-75.

National Coal Board (1975). **Subsidence Engineer's Handbook Mining Dep.**, National Coal Board, London, 111 pp.

Nieland, J. D. (1991). **SALT_SUBSID: A PC-Based Subsidence Model.** Solution Mining Research Institute, Report No. 1991-2-SMRI, California, USA, 67pp.

New, B.M. and O'Reilly, M.P. (1991). Tunnelling induced ground movements: predicting their magnitude and effects. In **Proceedings of the Fourth International Conference on Ground Movements and Structures** (pp. 671–697). Cardiff, Wales, Pentech Press.

O'Reilly, M.P. and New, B. M. (1982). Settlements above tunnels in the United Kingdom - their magnitude and prediction. In **Proceeding of the Tunnelling 82, The Institution of Mining and Metallurgy** (pp. 55–64). London.

Parise, M. and Lollino, P., (2011). A preliminary analysis of failure mechanisms in karst and man-made underground caves in Southern Italy. **Geomorphology.** pp.132–143.

Park, D. and Li, J. (2004). Subsidence Simulation Using Laser Optical Triangulation Distance Measurement Devices. In **Proceeding of the Gulf Rocks 2004, the Sixth North America Rock Mechanics Symposium (NARMS)** Houston, Texas.

Peck, R. B. (1969). Deep excavations and tunneling in soft ground. In **Proceedings of the Seventh international conference on soil mechanics and foundation engineering, State of the art.** Sociedad Mexicana de Mecánica de Suelos (pp. 225–290).

Peng, S. S. (1992). **Surface Subsidence Engineering**. New York: Society of Mining Engineers.

Powers, M.C. (1953). A new roundness scale for sedimentary particles. **Journal of Sedimentary Research.** 23(2): 117–119.

Rawal, K., Hu, L., and Wang, Z. (2017). Numerical Investigation of the Geomechanics of Sinkhole Formation and Subsidence. In **Proceeding of Geotechnical Frontiers 2017** (pp. 480-487). Orlando, Florida.

Sagaseta, C. (1987). Analysis of undraind soil deformation due to ground loss. **Géotechnique**. 37(3): 301-320.

Saoanunt, N., Chanpen, S., Khamrat, S., Thongprapha, T., and Fuenkajorn, K. (2019). Prediction of shallow salt cavity geometry from surface subsidence configurations. **Arabian Journal of Geosciences.** 12(24) :795.

Saoanunt, N. and Fuenkajorn, K. (2015). Physical model simulations of super critical subsidence as affected by mining sequence and excavation rate. In **Proceedings of the Ninth South East Asia Technical University Consortium Symposium (SEATUC).** Suranaree University of Technology, Thailand.

Sartkeaw, S., Khamrat, S., and Fuenkajorn, K. (2019). Physical model simulation of surface subsidence under sub-critical condition. **Research and Development International Journal of Physical Modelling in Geotechnics.** 19(5) :234-246**.**

Satarugsa, P., Youngmee, W., and Meesawat, S. (2005). New regional boundary of MahaSarakham Formation in the Northeastern Thailand: results from 2D seismic mapping. In **Proceedings on International Conference on Geology, Geotechnology and Mineral Resources of Indochina (GEOINDO 2005)** (pp. 212-220). Khon Kaen University. Thailand.

Satarugsa, P., Youngmee, W., and Meesawat, S., (2011). The Lessons Learnt from Geophysical Investigation of Sinkholes in Rock Salt in Thailand. **International Conference on Geology, Geotechnology and Mineral Resources of Indochina (GEOINDO 2011).** (pp. 445-455). Khon Kaen University, Thailand.

Shahriar, K., Amoushahi, S., and Arabzadeh, M. (2009). Prediction of surface subsidence due to inclined very shallow coal seam mining using FDM. In **Proceedings of the Coal Operators Conference** (pp. 130-139). University of Wollongong, Dubai, United Arab Emirates.

Singh, M. M. (1992). Mine subsidence. In: Hartman, H.L. (Ed), **SME Mining Engineering Handbook (**pp. 938-971). Society for Mining Metallurgy and Exploration, Inc., Littleton, Colorado.

Singh, K. B. and Dhar, B. B. (1997). Sinkhole subsidence due to mining. **Geotechnical & Geological Engineering**. 15(4): 327-341.

Singh, R.P., and Yadav, R.N. (1995). Prediction of subsidence due to coal mining in Raniganj coalfield, West Bengal, India. **Engineering Geology.** 39(1-2): 103-111.

Suwanich, P. (1986). **Potash and Rock Salt in Thailand: Nonmetallic Minerals Bulletin No.2,** Economic Geology Division, Department of Mineral Resources, Bangkok, Thailand.

Tao, X., Ye, M., Wang, X., Wang, D., Castro, R., and Zhao, J. (2015). Experimental and numerical investigation of sinkhole development and collapse in central florida. In **Proceedings of the Fourteenth Multidisciplinary Conference on Sinkholes and the Engineering and Environmental Impacts of Karst** (pp. 501–506). University of South Florida Tampa.

Terzaghi, K. (1936). Stress distribution in dry and in saturated sand above a yielding trapdoor. In **Proceeding of the International Conference on Soil Mechanics** (pp. 307-311). Cambridge.

Thongprapha, T., Fuenkajorn, K., and Daemen, J. J. K. (2015). Study of surface subsidence above an underground opening using a trap door apparatus. **Tunnelling and Underground Space Technology.** 46: 94–103.

Unlu, T., Akcin, H., and Yilmaz, O. (2013). An integrated approach for the prediction of subsidence for coal mining basins. **Engineering Geology**: 166, 186–203.

Vattanasak, H. (2006). Salt Reserve Estimation for Solution Mining in the Korat basin, Master Thesis, Nakhon Ratchasima: Suranaree University of Technology.

Waltham, T., Bell, F. G., and Culshaw, M. G. (2005). **Sinkholes and Subsidence: Karst and Cavernous Rocks in Engineering and Construction**, Springer, Chichester, 382 pp.

Wang, J. G., Leung, C. F., and Chow Y. K. (2003). Numerical solutions for flow in porous media. **International Journal for Numerical and Analytical Methods in Geomechanics.** 27(7): 565-583

Wannakao, L. and Walsri, C. (2007). Subsidence models in salt production area. In **Proceedings of the First Thailand Symposium on Rock Mechanics** (pp. 311-321). Nakhon Ratchasima: Suranaree University of Technology.

Wannakao, L., Munjai, D., and Janyakorn, S. (2005). Geotechnical investigation of surface subsidence at Ban Non Sabaeng salt production area, Sakon Nakhon, Thailand. In **Proceedings of the International Conference on Geology, Geotechnical and Mineral Resources of Indochina (GEOINDO 2005).** Khon Kaen University, Thailand.

Warren, J. (1999). **Evaporites: Their Evolution and Economics.** 4th ed. Blackwell Science, Oxford, 438p.

Whittaker, B. N. and Reddish, D. J. (1989). **Subsidence Occurrence, Prediction and Control.** Elsevier, Amsterdam, 541p.

Zhang, W., HL, L., Xiang Y., Chu, J., Dong, Z., and Xiao, Yang. (2018). Application of transparent soil model test and DEM simulation in study of tunnel failure mechanism. **Tunnelling and Underground Space Technology.** 74: 178-184.

BIOGRAPHY

Mr. Chanodom Lertsuriyakul was born on January 22, 1988 in Nakhon Ratchasima province, Thailand. He received his Bachelor's degree in Engineering (Geotechnology) from Suranaree University of Technology in 2009. For his post- graduate, he continued to study with a Master's degree in Geological Engineering Program, Institute of Engineering, Suranaree university of Technology. During graduation, 2010-2012, he was a part time worker in position of Research assistant at the Geomechanics Research Unit, Institute of Engineering, Suranaree university of Technology. He achieved his Master's degree in Engineering (Geotechnology) in 2012. He had then worked as a Site Engineering at Ch. Karnchang (Lao) Company Limited for 2 years, involving Xayaburi Hydroelectric Power Project, Lao PDR.